General Disclaimer

One or more of the Following Statements may affect this Document

- This document has been reproduced from the best copy furnished by the organizational source. It is being released in the interest of making available as much information as possible.

- This document may contain data, which exceeds the sheet parameters. It was furnished in this condition by the organizational source and is the best copy available.

- This document may contain tone-on-tone or color graphs, charts and/or pictures, which have been reproduced in black and white.

- This document is paginated as submitted by the original source.

- Portions of this document are not fully legible due to the historical nature of some of the material. However, it is the best reproduction available from the original submission.

NASA Contractor Report 172123

Graphite / LARC-160 Technology Demonstration Segment Test Results

W.H. Morita and S.R. Graves

Rockwell International Corporation
Los Angeles, CA 90009

NASA

National Aeronautics and
Space Administration

Langley Research Center
Hampton, Virginia 23665

FOREWORD

This final report presents results of a test pro-
gram performed by Rockwell International for the NASA/
Langley Research Center under contract NAS1-15371,
Development and Demonstration of Manufacturing Processes
for Fabricating Graphite/LARC-160 Polyimide Structure
Elements. This report is a follow on to NASA CR-165809,
which describes graphite/polyimide process development,
subelement fabrication, and fabrication of the graphite/
polyimide technology demonstration segment (TDS). The
TDS is a full-scale quarter-segment of the Space Shuttle
orbiter body flap. The objective of the test program
was to verify the feasibility of large bonded graphite/
polyimide structure through test of the TDS. Results
of the test program indicate this verification was
achieved.

The technical monitor for this program was H.B.
Dexter of the NASA/LaRC Materials Division. This report
was prepared by the Advanced Engineering Department of
Rockwell's Shuttle Orbiter Division. The following con-
tributed to the report:

> W.H. Morita, S.R. Graves, M.A. Morrow,
> W.T. Appleberry, P.E. Kimball, I. Bouton, and
> M. Shareef of Advanced Engineering; D.H. Wykes,
> R.K. Frost, H.E. Flanery, K.C. Hong, B.D. Bhombal,
> J. Brooks, J.S. Jones, and J.D. Reed of Labora-
> tories and Test; and P.J. Hodgetts of Quality
> Control.

CONTENTS

PRECEDING PAGE BLANK NOT FILMED

ILLUSTRATIONS

TABLES

1. INTRODUCTION

Early Shuttle orbiter studies identified several structural items for which application of advanced composites could save significant orbiter weight. Several of these structural components were part of the baseline design, including the graphite/epoxy payload bay doors and the boron/epoxy-reinforced titanium main engine thrust structure. Other components, such as the body flap, elevons, and vertical tail, were identified for advanced high-temperature graphite/polyimide (Gr/PI) composite application. A complex Gr/PI technology demonstration segment (TDS) was designed, fabricated, and tested to confirm the structural performance of Celion/LARC-160 Gr/PI. The test results reported herein verified this advanced structure concept.

In 1975, NASA selected the orbiter body flap (Figure 1-1) as a demonstration component for the Composites for Advanced Space Transportation Systems (CASTS) program. Since that time, studies of orbiter composite structures have emphasized the body flap. In 1976, a preliminary design concept for a composite body flap was established. Adhesive bonding of joints was used throughout, thus eliminating stress-concentration and fatigue problems commonly associated with mechanical fasteners. In 1977 through 1980, the design data base for Gr/PI structure was expanded through an extensive test program of subelements related to the body flap (Reference 1).

The TDS was conceived to demonstrate the state of the art of Celion/LARC-160 Gr/PI composite technology through the design, fabrication, and test of a large, complex, all-bonded structure. The TDS was designed to simulate a section of the orbiter composite body flap incorporating three ribs and extending from the forward cove back to the rear spar. The TDS design is composed of three stability ribs, instead of two stability ribs and a hinge rib, and does not include the full-depth honeycomb core trailing edge. The TDS assembly is illustrated in Figure 1-2.

The objectives of this Gr/PI technology development program were (a) verify the advanced composite design/analysis techniques, (b) develop manufacturing techniques for complex Gr/PI structure, and (c) demonstrate the integrity of Gr/PI structure (all-bonded) to sustain orbiter mechanical load and thermal environments. The technology readiness of this advanced structural concept was demonstrated when the TDS was successfully subjected to the following simulated orbiter loads and thermal extremes:

- Ultimate (140% design limit) mechanical load applied at room temperature

- Ultimate mechanical load applied at 260°C (500°F)

- 400 cycles (four lifetimes) of limit load applied at 260°C (500°F)

- 125 thermal cycles between -170 and 315°C (-160 and 600°F)

- Ultimate load applied at 260°C (500°F)

1

Results of the tests, preceded by discussions on the TDS design concept and test setup, are presented in this report.

Use of commercial products or names of manufacturers in this report does not constitute official endorsement of such products or manufacturers, either expressed or implied, by the National Aeronautics and Space Administration.

A801125 B-3
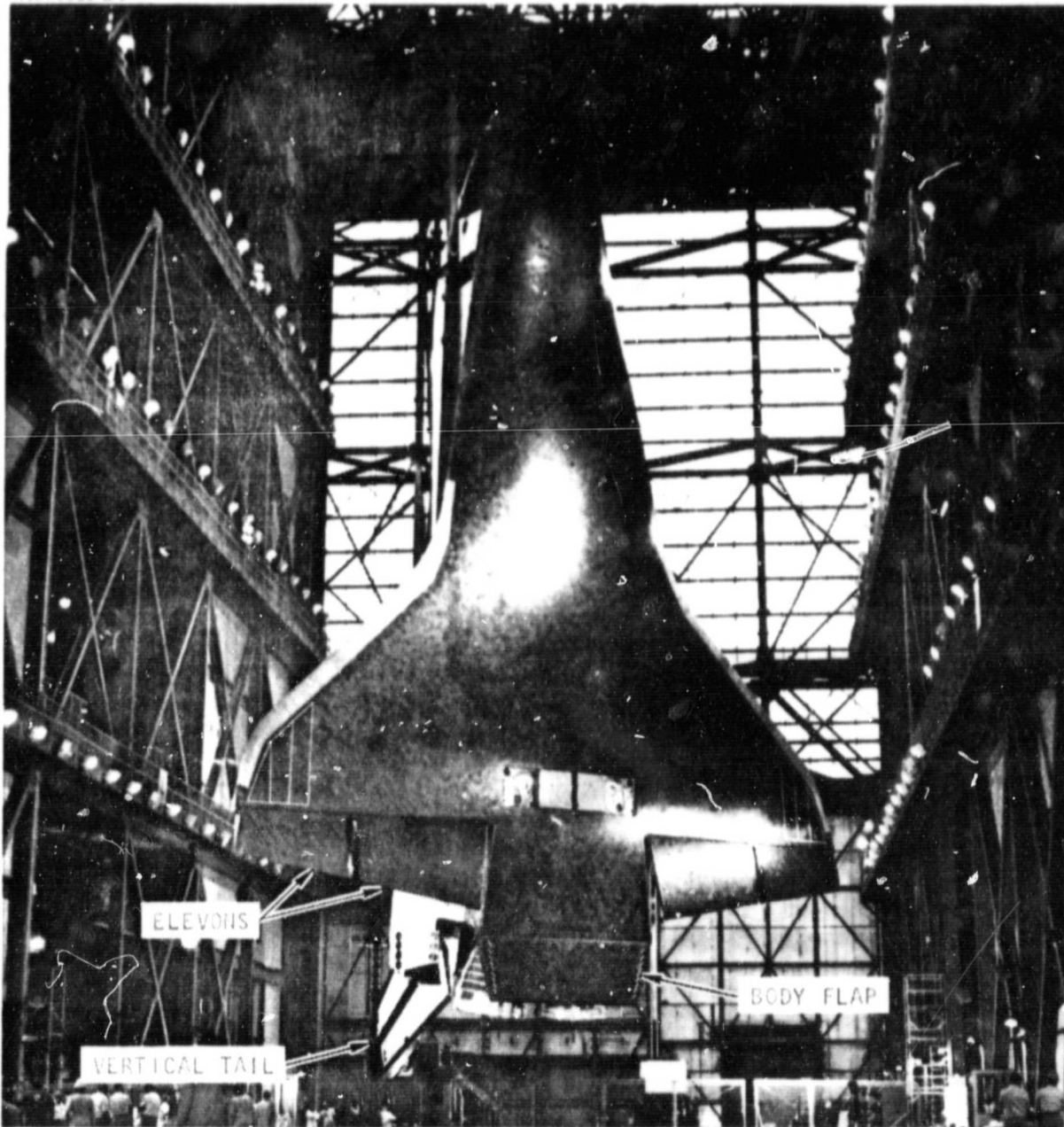
Figure 1-1. Space Shuttle Orbiter Columbia

2

A810826 F-2
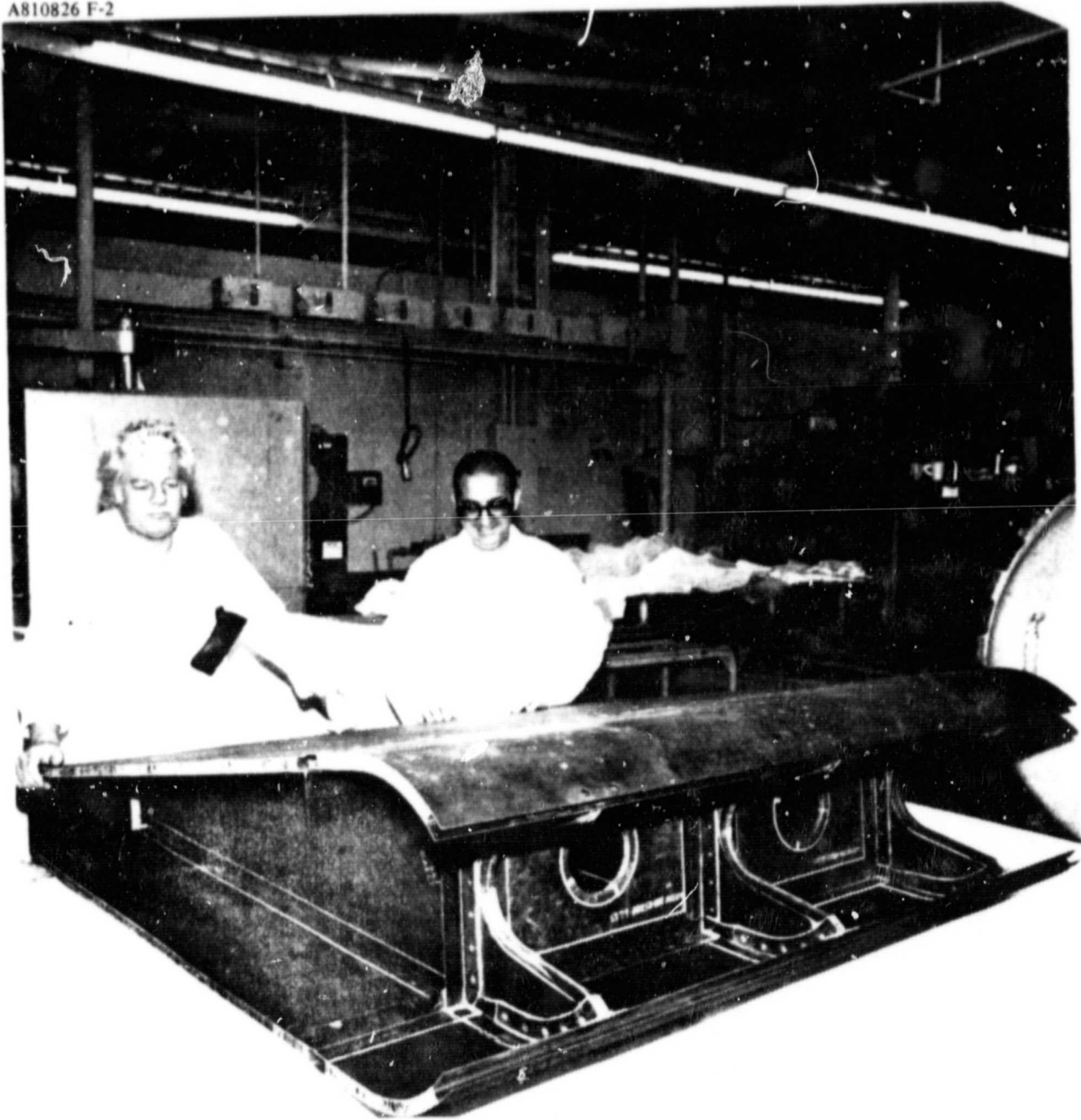
Figure 1-2.   Gr/PI Technology Demonstration Segment

2. TECHNOLOGY DEMONSTRATION SEGMENT DESIGN CONCEPT AND TEST APPROACH

Structural weight reduction and orbiter performance gain can be realized by taking advantage of the large strength-to-weight and stiffness-to-weight ratios of advanced composites. Savings of 25 percent of the total weight of the structure/thermal protection system (TPS) weight can be realized where 315°C (600°F) structural allowable Gr/PI is used. In comparison with the baseline aluminum structure, 177°C (350°F) structural allowable, Gr/PI allows reduced TPS requirements; and the TPS tiles can be bonded directly to the Gr/PI substrate because of the thermal compatibility and stiffness of the components. The direct-bond concept and its advantages are illustrated in Figure 2-1, and discussed in Reference 2.

The body flap was chosen as the demonstration component for graphite/polyimide technology because it is a relatively large, retrofittable structure. Also, it is subjected to extreme acoustic, aerodynamic, and thermal environments. The flight environment would thus thoroughly test the advanced structural concepts and demonstrate feasibility of application to other orbiter structures and future space vehicles.

The body flap structure is attached to the orbiter lower aft fuselage by four rotary actuators. This assembly, with its aerodynamic and thermal seals, provides the Shuttle pitch trim control and shields the main engines from the high temperatures of reentry. The body flap is approximately 2.1 m (7 ft) wide, 6.4 m (21 ft) long, and 0.46 m (1.5 ft) thick. Except for the front spar access panels, which are mechanically fastened, the composite body flap design concept is an all-bonded Gr/PI sandwich structure (Figure 2-2). The composite body flap design consists of upper and lower honeycomb sandwich cover panels, eight stability ribs, two closeout ribs, four actuator ribs, a full-depth honeycomb trailing edge, front and rear spars, and leading-edge access panels. The material used in this concept is Celion/LARC-160 Gr/PI prepreg tape 0.0064 cm (0.0025 in.) per ply. The honeycomb core is fiberglass polyimide composite with a nominal density of 48 kg/m^3 (3.0 lbm/ft^3).

Table 2-1 compares the projected weight of the composite body flap with direct-bond TPS tiles to the orbiter baseline configuration. The composite body flap, including the thermal protection system, is projected to weigh 216 kg (477 lbm) or 31.8 percent less than the aluminum baseline (Reference 3).

The Gr/PI composite body flap design concept is discussed in detail in Reference 4. The body flap analysis and structural loads are presented in Appendix A.

PRECEDING PAGE BLANK NOT FILMED

Figure 2-1. Advanced Thermal Structure Concept
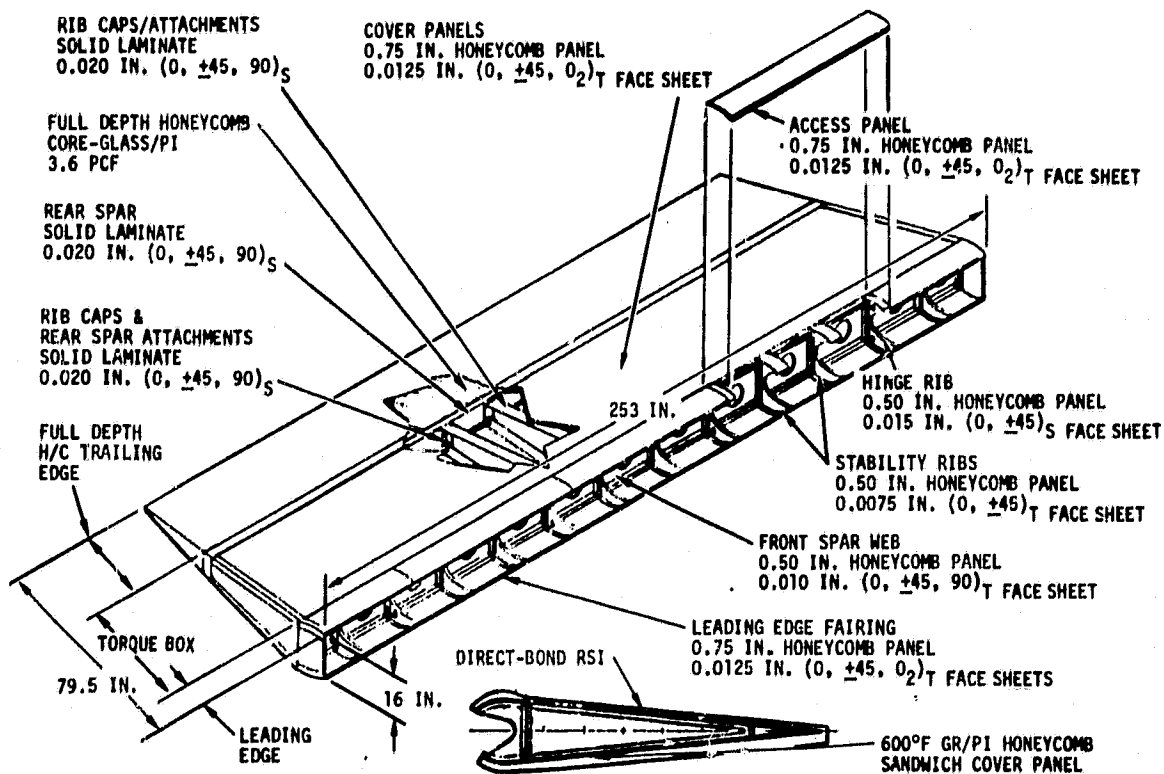
Figure 2-2. Composite Body Flap Design Concept

Table 2-1. Composite Body Flap Potential Weight Savings

Configuration	Body Flap Weight-kg (lbm)		
	Structure	TPS	Totals
Baseline	211 (465)	469 (1,034)	680 (1,499)
Composite	162 (357)	302 (665)	463 (1,022)
Weight saved	49 (108)	167 (369)	216 (477)

2.1 Gr/PI TECHNOLOGY DEMONSTRATION SEGMENT DESIGN CONCEPT

The progress made between 1977 and 1980 in design and analysis methodology, fabrication techniques, subelement testing, and nondestructive evaluation (NDE) was integrated into the graphite/polyimide (Gr/PI) technology demonstration segment (TDS). The TDS was designed to simulate a section of the orbiter composite body flap incorporating three ribs and extending from the forward cove back to the rear spar (Figure 2-3). The TDS design is composed of three stability ribs instead of the body flap design of two stability ribs and a hinge rib. Also the TDS is without the full-depth honeycomb core trailing edge. The TDS measures 137 by 152 cm (54 by 60 in.), is 43 cm (17 in.) high at the front spar, and 18 cm (7 in.) high at the rear spar.

The TDS design illustrated in Figure 2-4 is all bonded except for the front spar and upper leading edge, which are mechanically fastened to allow access to the torque box interior. A bonded structure was chosen because of its adaptability to composite structures. The relatively low bearing strength of composites often necessitates increased thicknesses and edge distances which results in decreased structural efficiency. Adhesive bonding offers a means of assembly that transfers the loads by shear in a manner similar to the resins' normal means of load transfer and thereby utilizes the best characteristics of the composites. Localized stress concentrations and their associated fatigue problems are also alleviated.

Honeycomb construction was chosen as the primary structural system because of the relatively low projected structural loads and high stiffness requirements for the acoustic environment (165 dB) and direct-bond TPS. Meeting the minimum weight requirement with these structural requirements dictates the use of minimum material gauges. This is most easily accomplished through the use of honeycomb sandwich construction. The skins on the honeycomb sandwich are unbalanced lay-ups; that is, they are not symmetrical about their respective centerlines, but the sandwich becomes symmetrical about the core centerline when the unbalanced face sheets are bonded in place.
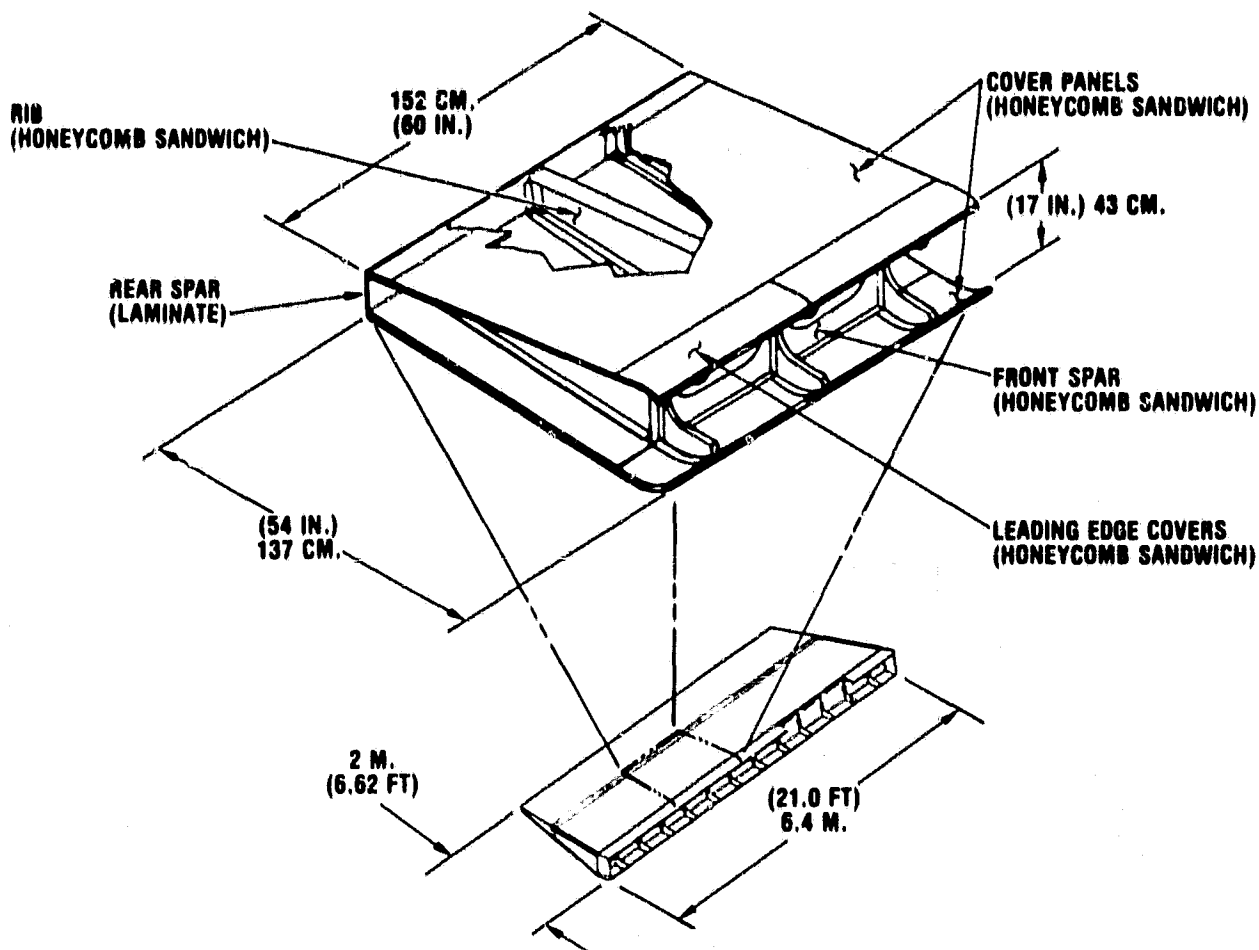
Figure 2-3. Gr/PI Body Flap Concept and Technology
Demonstration Segment (TDS)

The TDS was fabricated from the following materials:

1. Celion/LARC-160 graphite/polyimide 0.00635-cm (0.0025-in.)
    undirectional tape in most laminates.

2. Celion/LARC-160 graphite/polyimide 0.0165-cm (0.0065-in.) 35 x 34
    satin harness weave fabric in the 0/90 layers of the rib caps.
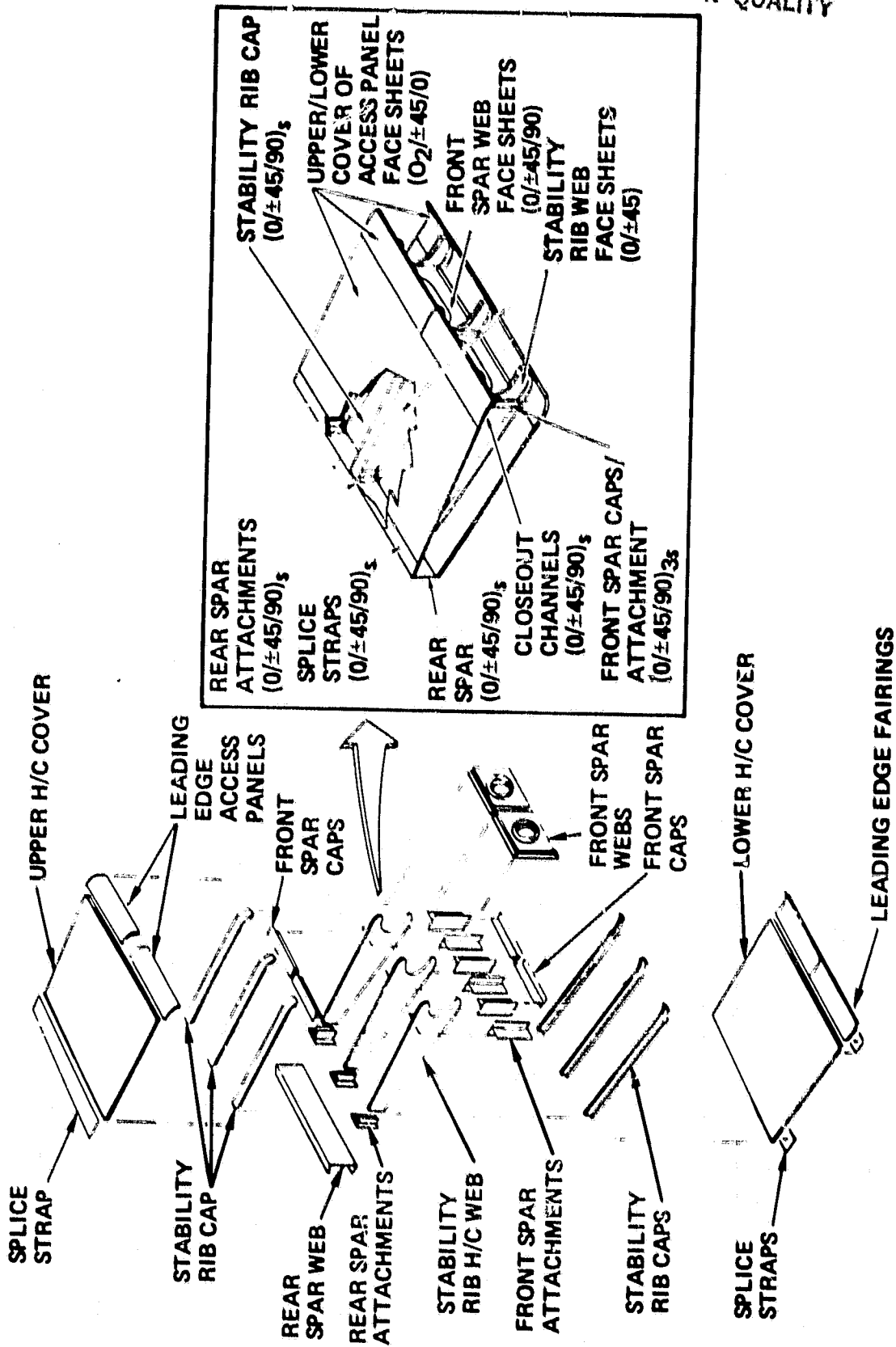
Figure 2-4. Gr/PI Demonstration Segment Design

STABILITY RIB CAP
(0/±45/90)s

UPPER/LOWER
COVER OF
ACCESS PANEL
FACE SHEETS
(O2/±45/0)

FRONT
SPAR WEB
FACE SHEETS
(0/±45/90)

STABILITY
RIB WEB
FACE SHEETS
(0/±45)

REAR SPAR
ATTACHMENTS
(0/±45/90)s

SPLICE
STRAPS
(0/±45/90)s

REAR
SPAR
(0/±45/90)s

CLOSEOUT
CHANNELS
(0/±45/90)s

FRONT SPAR CAPS/
ATTACHMENT
(0/±45/90)3s

UPPER H/C COVER

LEADING
EDGE
ACCESS
PANELS

FRONT
SPAR
CAPS

FRONT SPAR
WEBS

FRONT SPAR
CAPS

LOWER H/C COVER

LEADING EDGE FAIRINGS

SPLICE
STRAP

STABILITY
RIB CAP

REAR
SPAR WEB

REAR SPAR
ATTACHMENTS

STABILITY
RIB H/C WEB

FRONT SPAR
ATTACHMENTS

STABILITY
RIB CAPS

SPLICE
STRAPS

9

3. HRH-327-3/16-3.0 glass/polyimide honeycomb core with a density of 48.06 kg/m^3 (3.0 lbm/ft^3). The core thickness was 1.91 cm (0.75 in.) in the cover panels and 1.27 cm (0.5 in.) in the stability ribs

4. FM-34 polyimide adhesive for bonding the components into an integral structure

The TDS cover panel assembly is a honeycomb sandwich structure with five-ply $(0_2/\pm45/0)$ skins. The individual skin laminates are unsymmetrical and warp by themselves. However, the sandwich becomes symmetrical about the core centerline when the face sheets are bonded in place. The panels are closed out fore and aft by an eight-ply $(0/\pm45/90)_s$ channel.

The stability rib web is a sandwich structure with unsymmetrical three-ply $(0/\pm45)$ face sheets. The rib is closed out in the forward section by an external eight-ply $(0/\pm45/90)_s$ channel. The rib cap has a quasi-isotropic lay-up that is nominally 0.051 cm (0.02 in.) thick, except in the forward section where it has been built-up to 0.368 cm (0.145 in.) to accept mechanical loads.

The front spar is a sandwich structure with four-ply $(0/\pm45/90)$ skins on 1.27-cm (0.5-in.) honeycomb core. The spar has a 12.7-cm-diameter (5-in.) opening in the center to allow access to the torque box interior. The spar is closed out by "h" sections that allow the spar to be bolted to the "T" attachments on the cover panels and stability ribs. The spar opening is closed out by a four-piece circular ring channel fabricated from three layers of Gr/PI fabric.

The rear spar is an eight-ply $(0/\pm45/90)_s$ solid laminate channel. The spar is bonded to the cover panel through the legs of the channel and to the stability ribs with small attachments similar to the rib caps.

The curved leading edge panel construction, identical to that of the cover panels, curves to an outside radius of 21.9 cm (8.622 in.) and is closed out by channels fore and aft. The upper access panel is mechanically attached; the lower panel is adhesively bonded.

The methods used in fabrication of the TDS are described in References 5 and 6. The completed TDS is shown in Figure 1-2.

2.2 TDS TEST PROVISIONS

The TDS was designed to withstand structural loads representative of the aft body flap. Because the TDS was designed without an actuator rib, the stability ribs had to be modified forward of the front spar to interface with the test support structure through mechanical fasteners. Provisions were added at the rear spar for applying test loads.

The following changes were made in the forward load interface area. The forward section of the rib caps were beefed up, doublers were added to the front spar vertical attachment ("T" members), and the entire forward area was shimmed and machined to a level surface (Figure 2-5). To this area, large Gr/PI plates were attached to interface with the steel test fixture (Figure 2-6).

The original aft test provisions shown in Figure 2-7 were damaged and required modification. When the TDS was being mated with the test fixture, the center load introduction attachment separated from the rear spar (Figure 2-8). Visual inspection also revealed adhesive bond separation at the internal rib/rear spar attachment at each rib (Figure 2-9). Cause of the bond failure could not be determined since nondestructive inspections after component assembly had indicated no anomalies.

To repair the rib/spar shear tie, a Gr/PI doubler plate was blind-riveted and bonded to the rear spar and rib attachments as shown in Figure 2-10. The interface for the test loads applied at the rear spar was modified to react the loads through the cover panels. As shown in Figure 2-10, Gr/PI load pads and steel clevis members were attached to the cover panels. The load pads were bonded with RTV-560 adhesive and pinned with steel pins, as shown in Figure 2-11. The honeycomb core in the cover panels was locally potted to preclude core crushing under the load pads.

2.3 TECHNOLOGY DEMONSTRATION SEGMENT TEST APPROACH

The test program for the graphite/polyimide (Gr/PI) technology demonstration segment (TDS) is outlined below. The test objectives were to verify the structural adequacy of a typical composite body flap section to sustain mechanical and thermal load cycles representative of 100 Space Shuttle missions and to develop confidence in large bonded Gr/PI structures. The TDS test program and test loads are summarized in Figure 2-12. The test program involved ultimate load at room temperature and 260°C (500°F), 400 cycles (four lifetimes) of limit load at 260°C (500°F), and 125 thermal cycles between -107 and 315°C (-160 and 600°F).

The 260°C (500°F) maximum structural load temperature is based on orbiter entry and TAEM* environment. The 315°C (600°F) condition occurs due to heat soak back after the orbiter has landed (see Appendix A). The body flap is loaded and supported through four hinge ribs. However, lack of a hinge rib on the TDS precludes actual body flap loads. Test conditions to simulate the stress state in the region of the body flap stability ribs were determined from a TDS NASTRAN finite element model. The TDS NASTRAN model is described in detail in Appendix B. Rationale, loads, and results for each of the tests are presented in subsequent sections.

---

*TAEM--Terminal Area Energy Management (Shuttle orbiter maneuver in preparation for landing).

11

A810824 A-1

FORWARD LOAD ATTACHMENT AREA
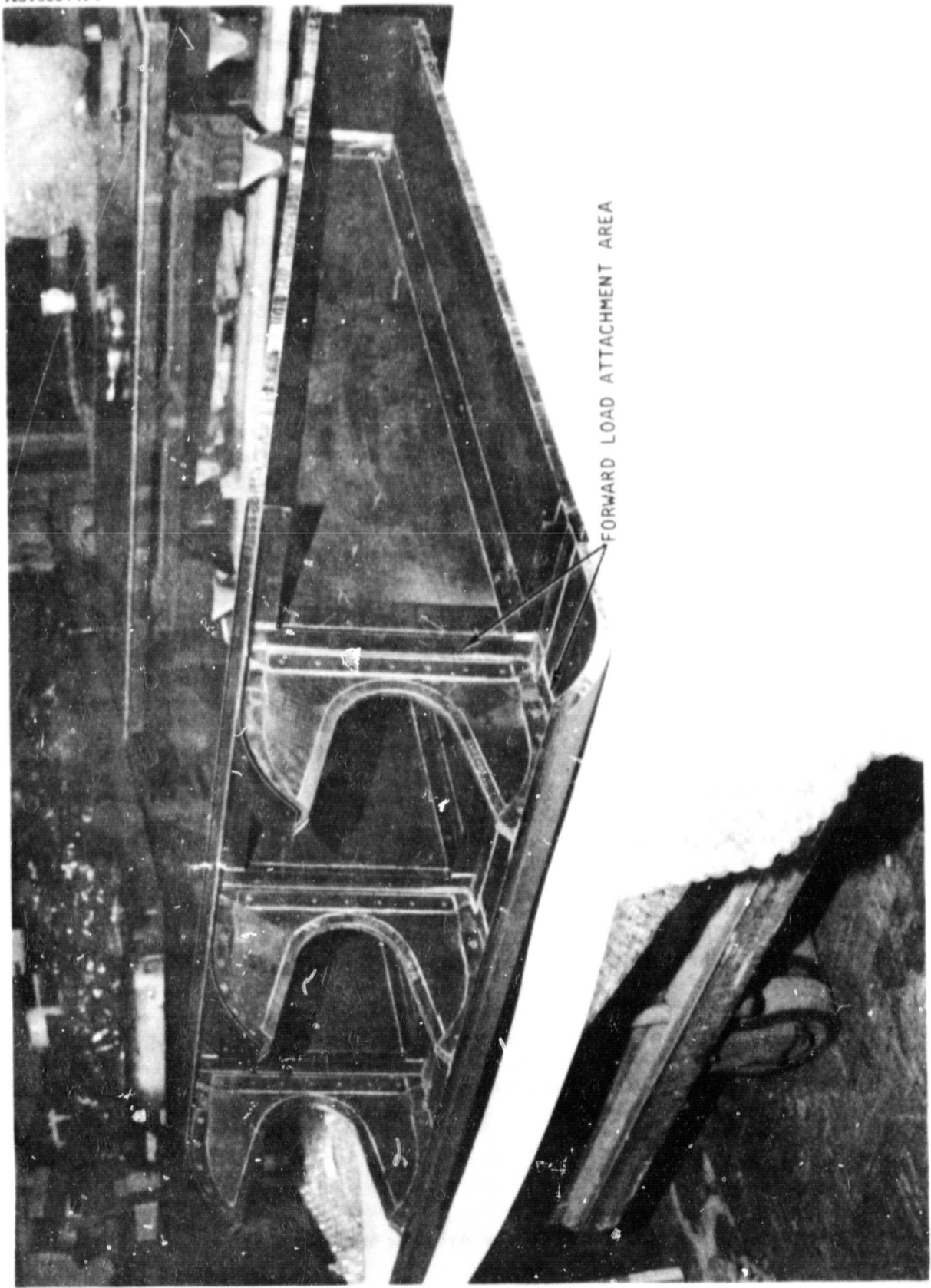
Figure 2-5. TDS Forward Load Attachment Area

0.051 CM (0.020 IN.) PI
CAP THICKNESS INCREASED
TO 0.368 CM (0.145 IN.)
FORWARD OF THE FRONT SPAR

TOP LEFT SIDE VIEW
1/4 SCALE

PI-CAP
SHIM

T-SECTION
SHIM

SYMMETRICAL ABOUT ℄

LEVELING SHIMS

MOUNTING PLATE
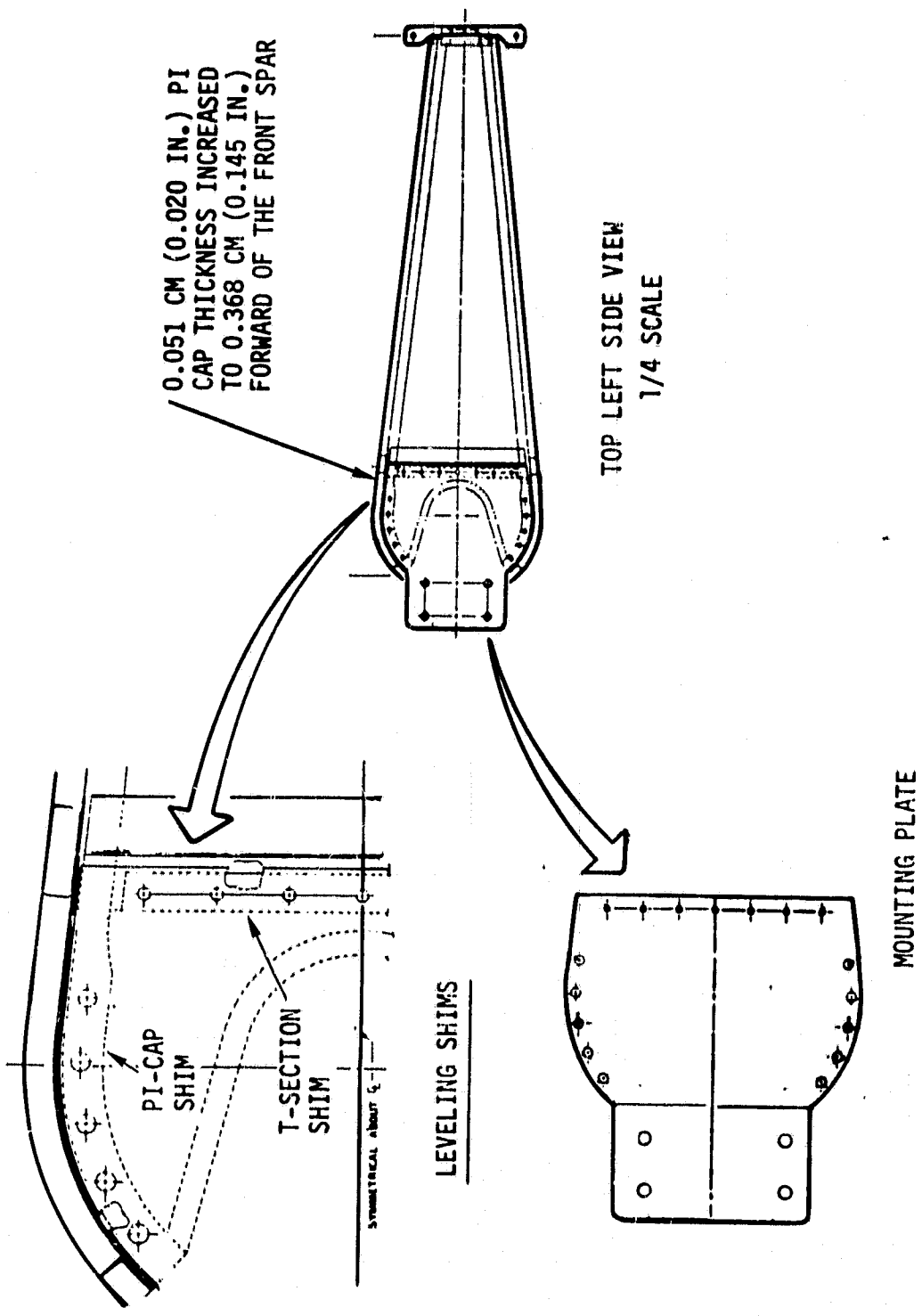
Figure 2-6. TDS Test Provisions - Forward Section

13
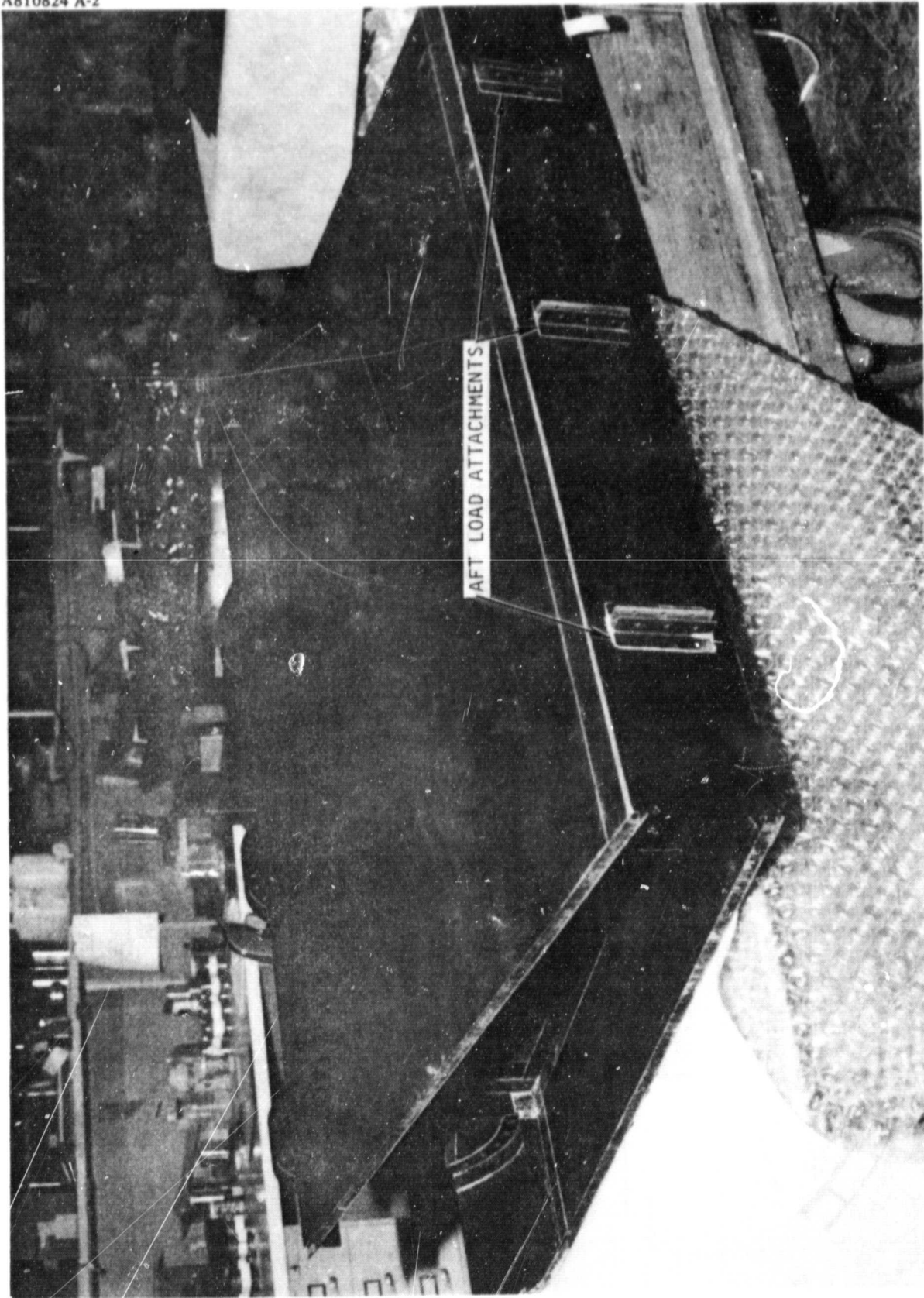
Figure 2-7. Original TDS Aft Load Attachment Area

A811014 G-7

REAR SPAR DELAMINATION

SEPARATED AFT LOAD ATTACHMENT
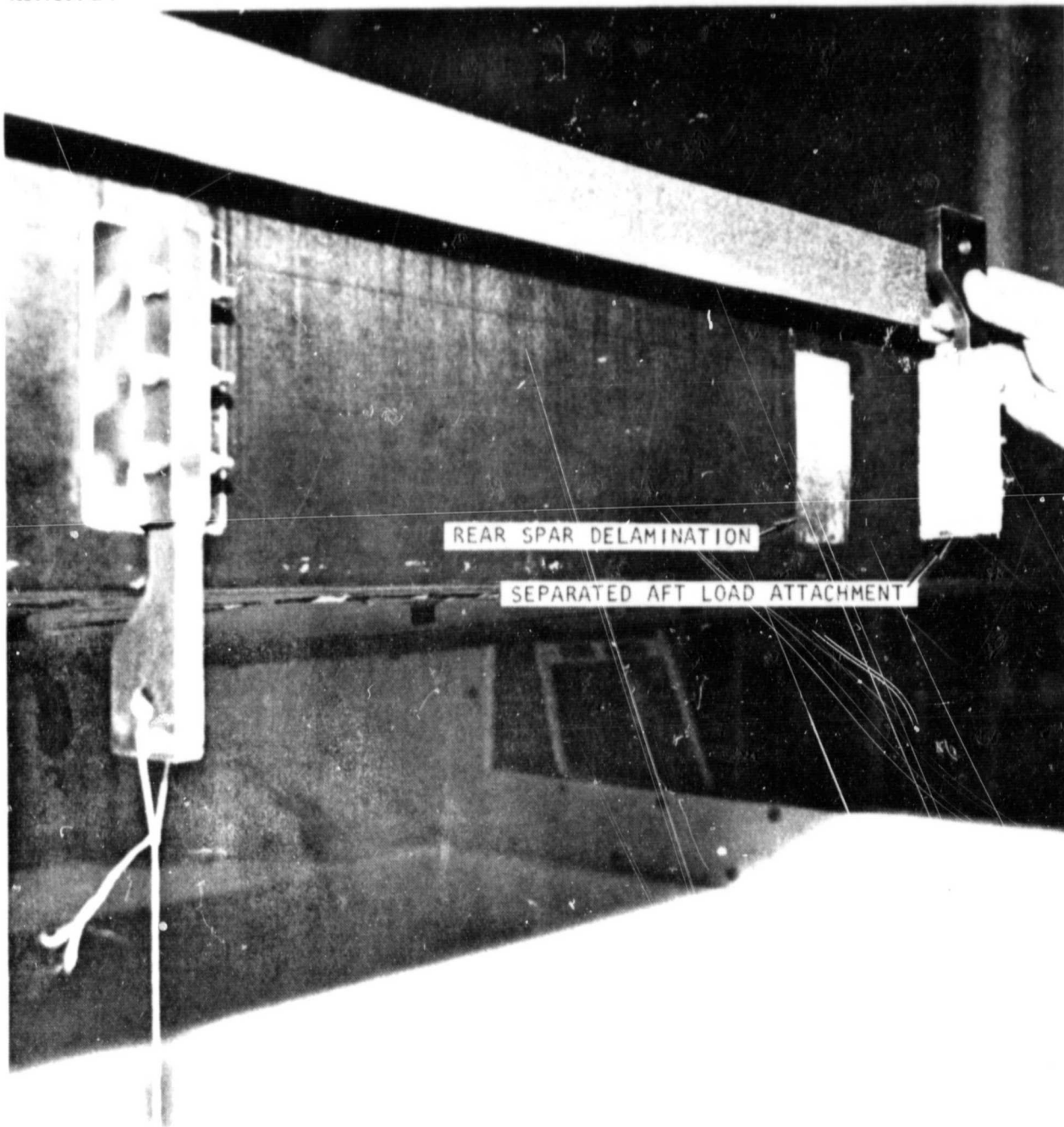
Figure 2-8. Separation of Aft Load Attachment Member

15

A811014 G-10
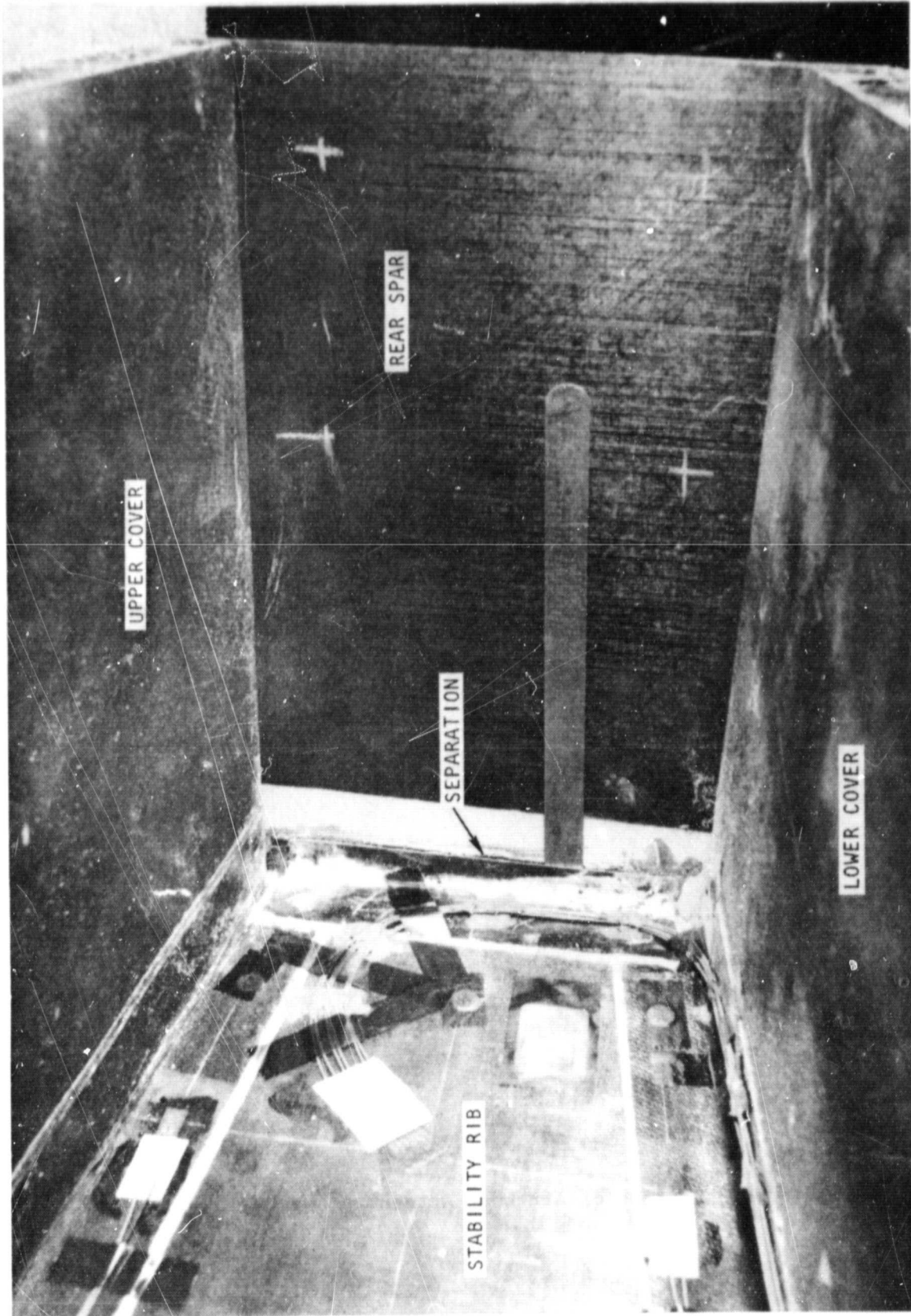
Figure 2-9. Separation of Aft Rib-to-Rear-Spar Bond
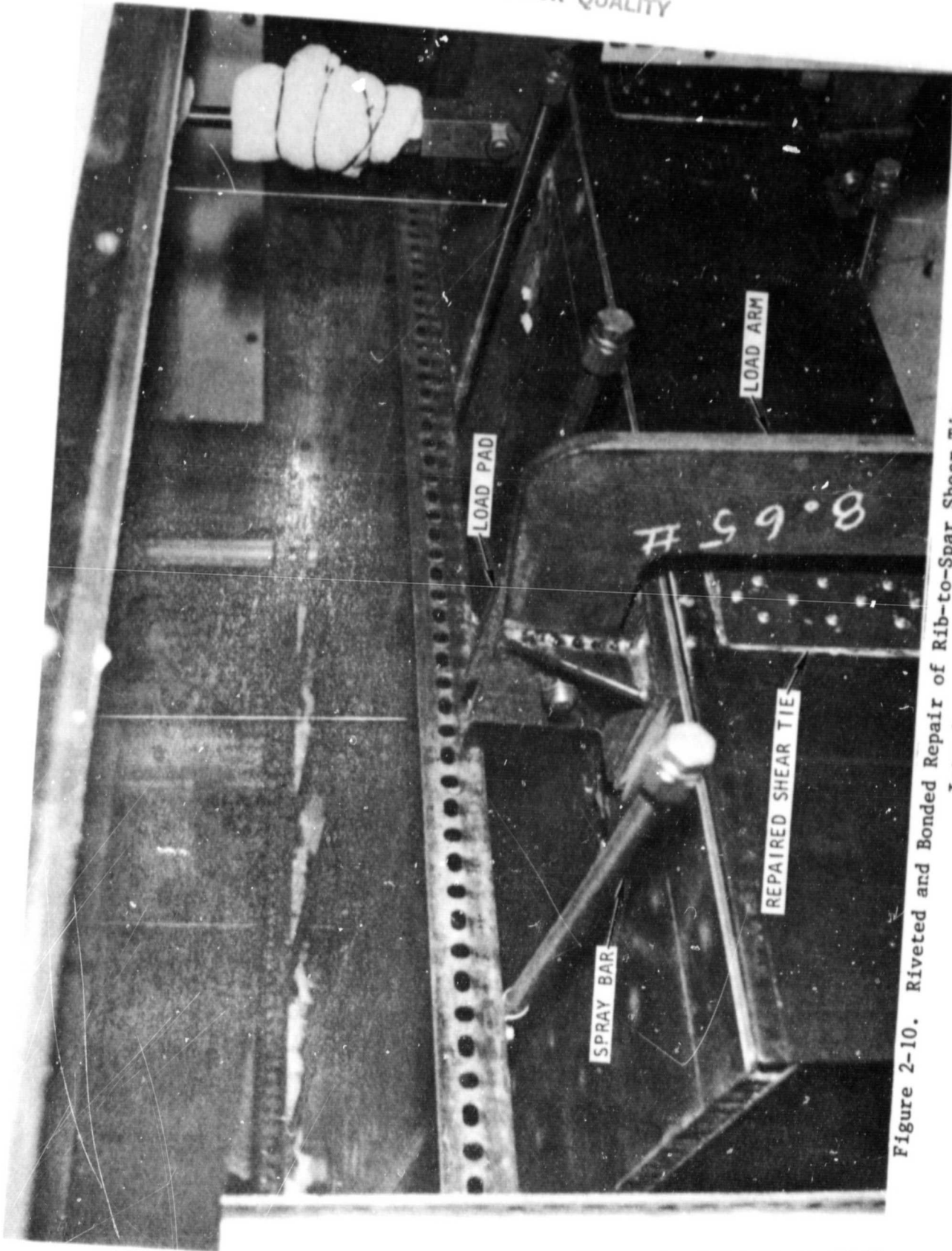
Figure 2-10. Riveted and Bonded Repair of Rib-to-Spar Shear Tie, and New Aft Load Introduction Method

A811216 C-1

HONEYCOMB CORE POTTED
UNDER LOAD PAD

STEEL CLEVIS

STEEL PIN

RTV BOND
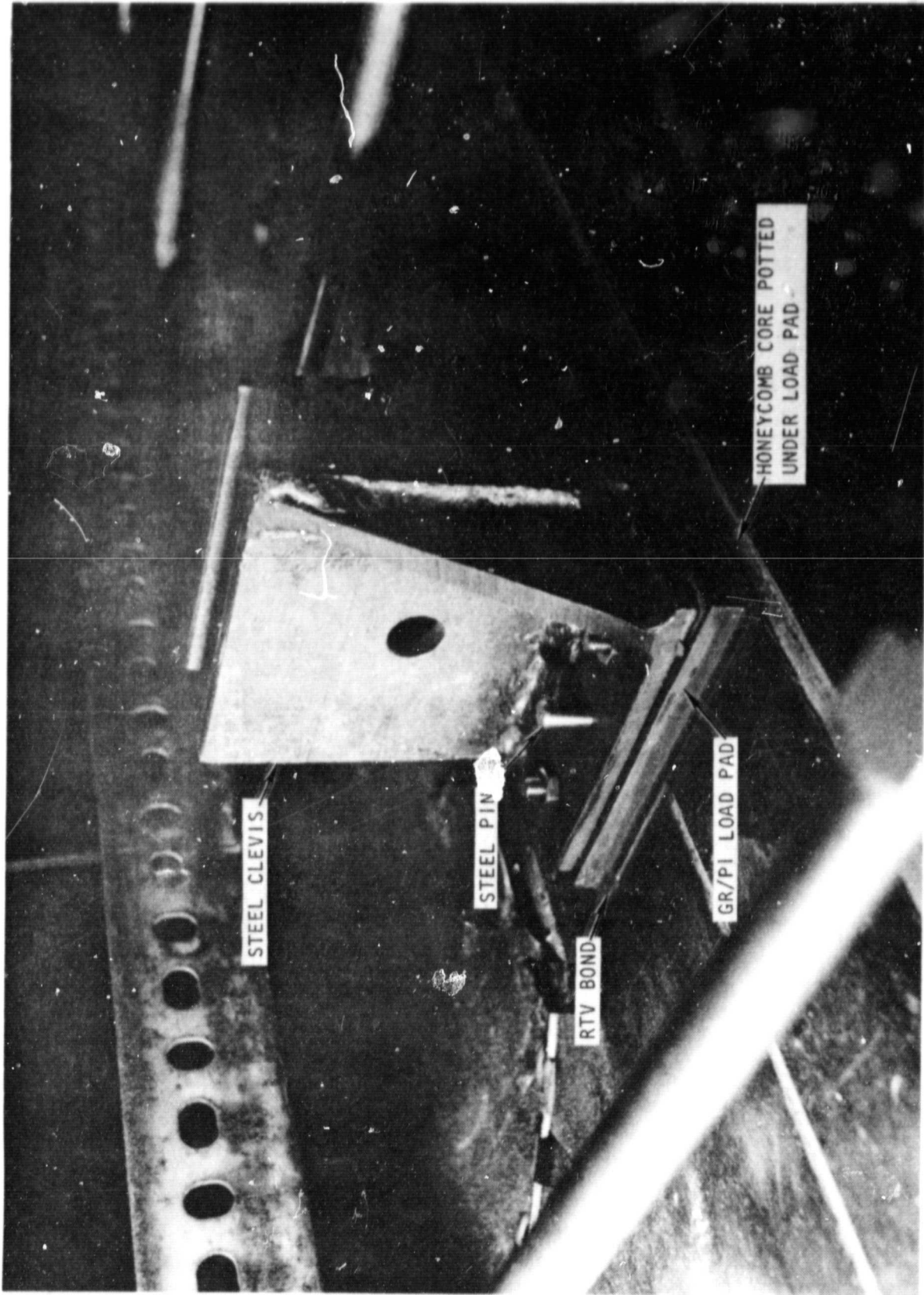
GR/PI LOAD PAD

Figure 2-11. New Load Pad for Aft Load Introduction

18

1. TEST OBJECTIVES

- DEVELOP CONFIDENCE IN LARGE ALL-BONDED GR/PI STRUCTURE
- VERIFY STRUCTURAL ADEQUACY OF A TYPICAL COMPOSITE BODY FLAP SEGMENT TO SUSTAIN LOADS REPRESENTING 100 ORBITER MISSIONS
- SIMULATE BODY FLAP STRESS STATE

2. TEST PROGRAM

- ULTIMATE (140% DESIGN LIMIT) MECHANICAL LOAD APPLIED AT ROOM TEMPERATURE
- ULTIMATE MECHANICAL LOAD APPLIED AT 260°C (500°F)
- 400 CYCLES (FOUR LIFETIMES) LIMIT LOAD APPLIED AT 260°C (500°F)
- 125 THERMAL CYCLES BETWEEN −107 & 315°C (−160 & 600°F)
- ULTIMATE LOAD APPLIED AT 260°C (500°F)

ULTIMATE MECHANICAL LOADS APPLIED AT ROOM TEMPERATURE & 260°C (500°F)

ANCHOR (TEST FIXTURE)

11.21 KN (2,520 LBF)

2.49 KN (560 LBF)

9.963 KN (2,240 LBF)

14.7 KN (3,324 LBF)
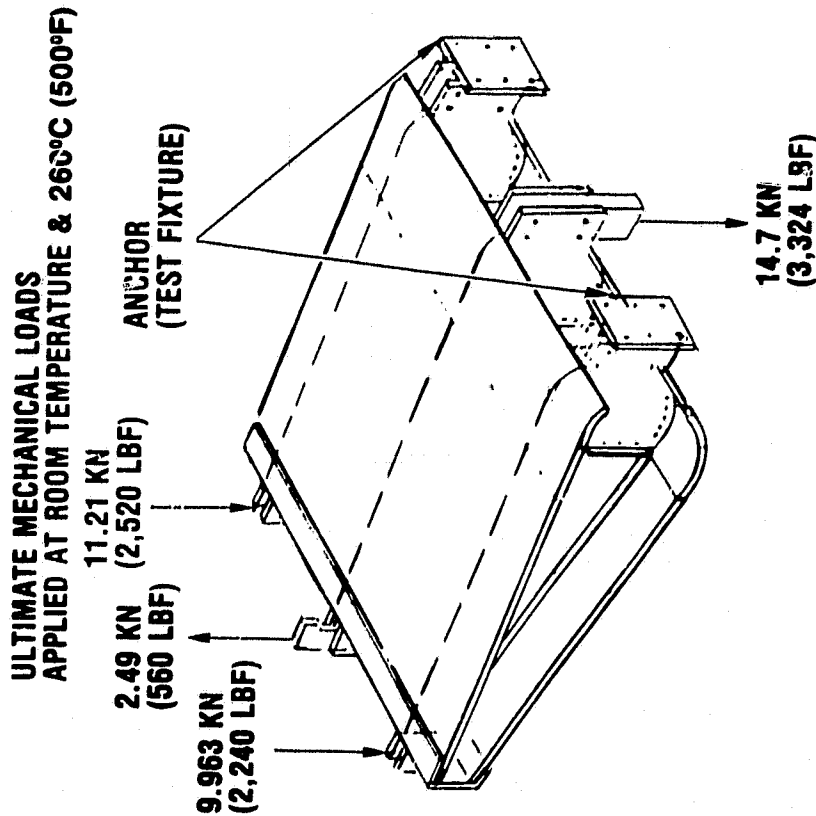
Figure 2-12. Gr/PI Technology Demonstration Segment Test Program

19

3. TEST COMPONENT INSTRUMENTATION AND TEST SETUP

3.1 TEST COMPONENT INSTRUMENTATION

Test component instrumentation consisted of strain gages, deflectometers, thermocouples, and the Laboratory Data System (LDS). Locations and symbols of the instrumentation are presented in Figures 3-1 through 3-9. Photographs of the instrumentation installation are presented in Figures 3-10 through 3-12.

3.1.1 Strain Gages

Fifteen axial strain gages and eight three-leg strain rosettes were bonded to the TDS. The axial strain gage designation type is WK-06-125AD-350, while the rosette strain gage designation type is WK-06-125RA-350. The high-temperature strain gages performed well at 260°C (500°F). However, few gages survived the extended 315°C (600°F) exposure during the thermal cycling test.

Strain gages were placed to give adequate coverage of the TDS response in high-strain areas with a minimum number of gages. Much of the instrumentation was located along the rib subjected to the highest load (RIB No. 1). Because of access difficulties, few gages were placed inside the structure. No gages were placed on the front spar since the panels had to be readily removed for inspections, and no strain gages were placed on the rear spar.

DEFLECTION TRANSDUCER (D)
MOUNTING TAB LOCATION
(20 REQUIRED)

UNI-AXIAL STRAIN GAGE (A)
(15 REQUIRED)

ROSETTE STRAIN GAGE (R)
(8 REQUIRED)

THERMOCOUPLE (T)
(33 REQUIRED)
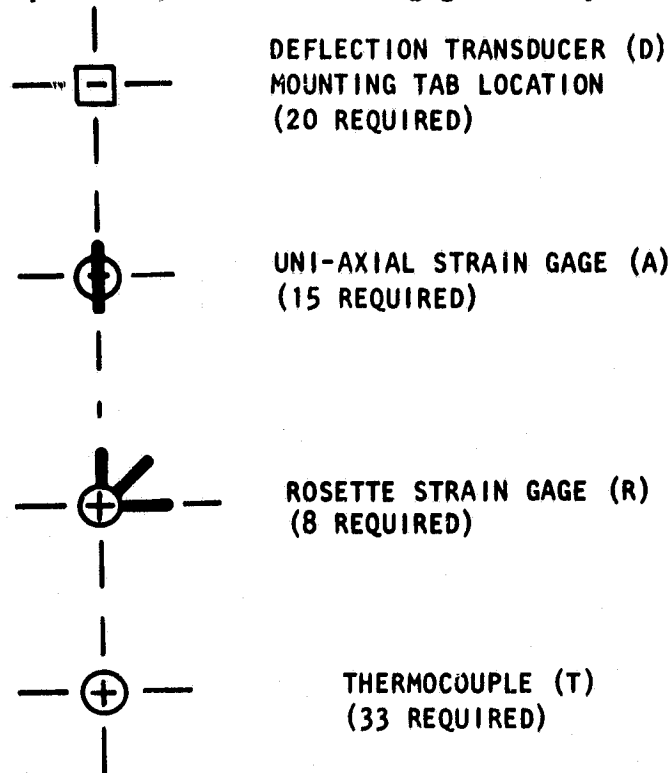
Figure 3-1. Instrumentation Symbols
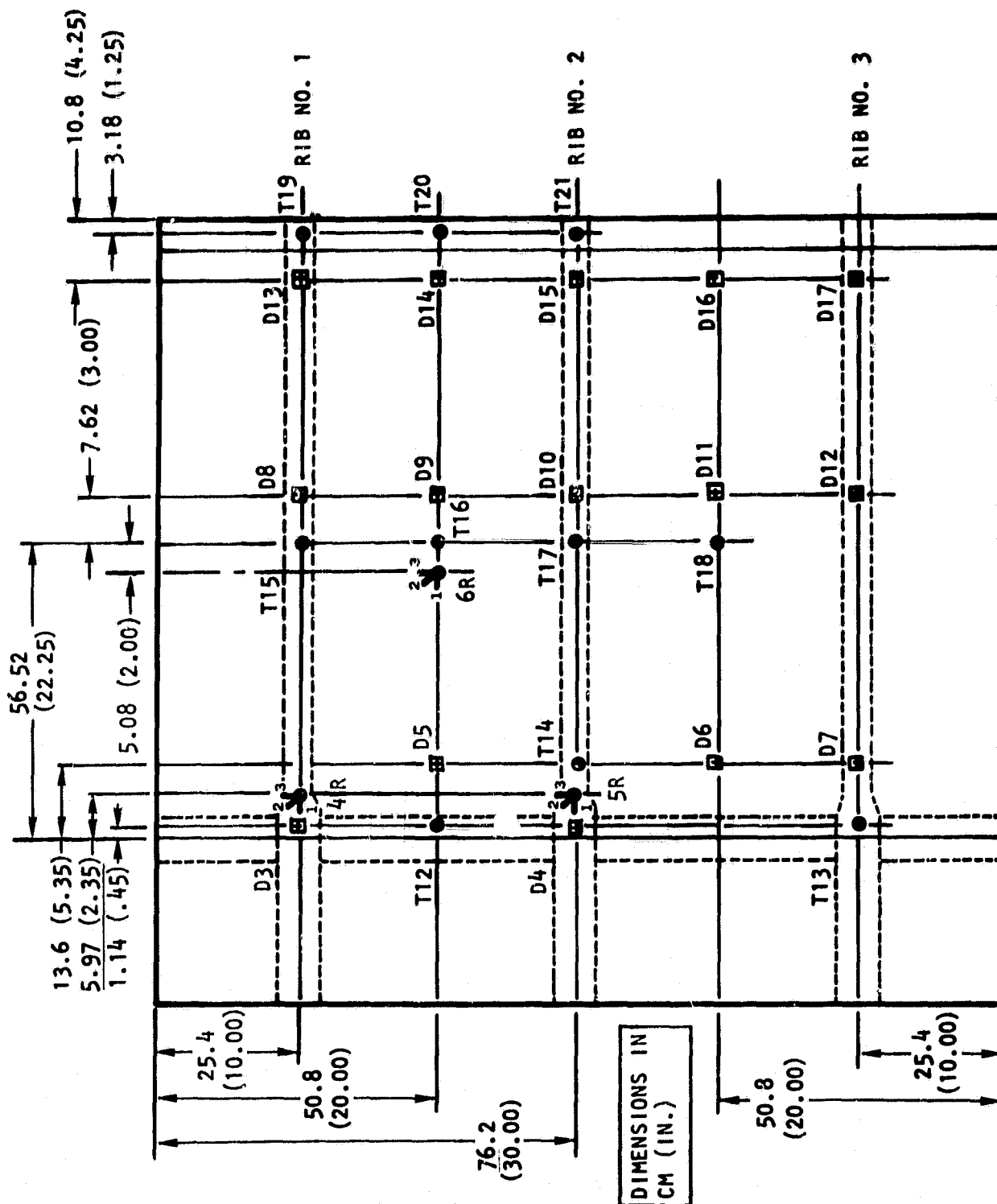
Figure 3-2. Outer Surface of Lower Honeycomb Cover Panel
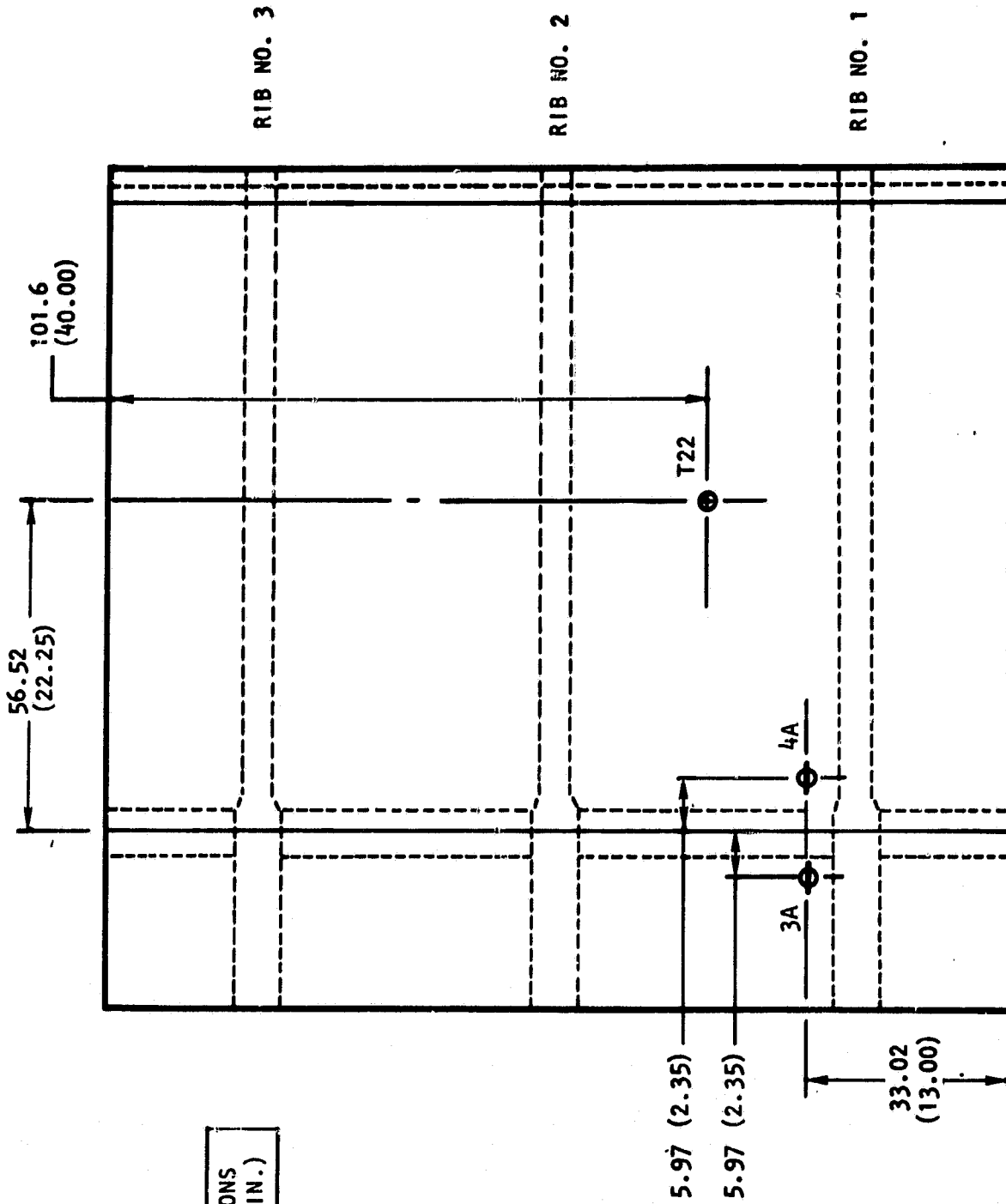
Figure 3-3. Inner Surface of Lower Honeycomb Cover Panel

Figure 3-4. Outer Surface of Upper Honeycomb Cover Panel

24
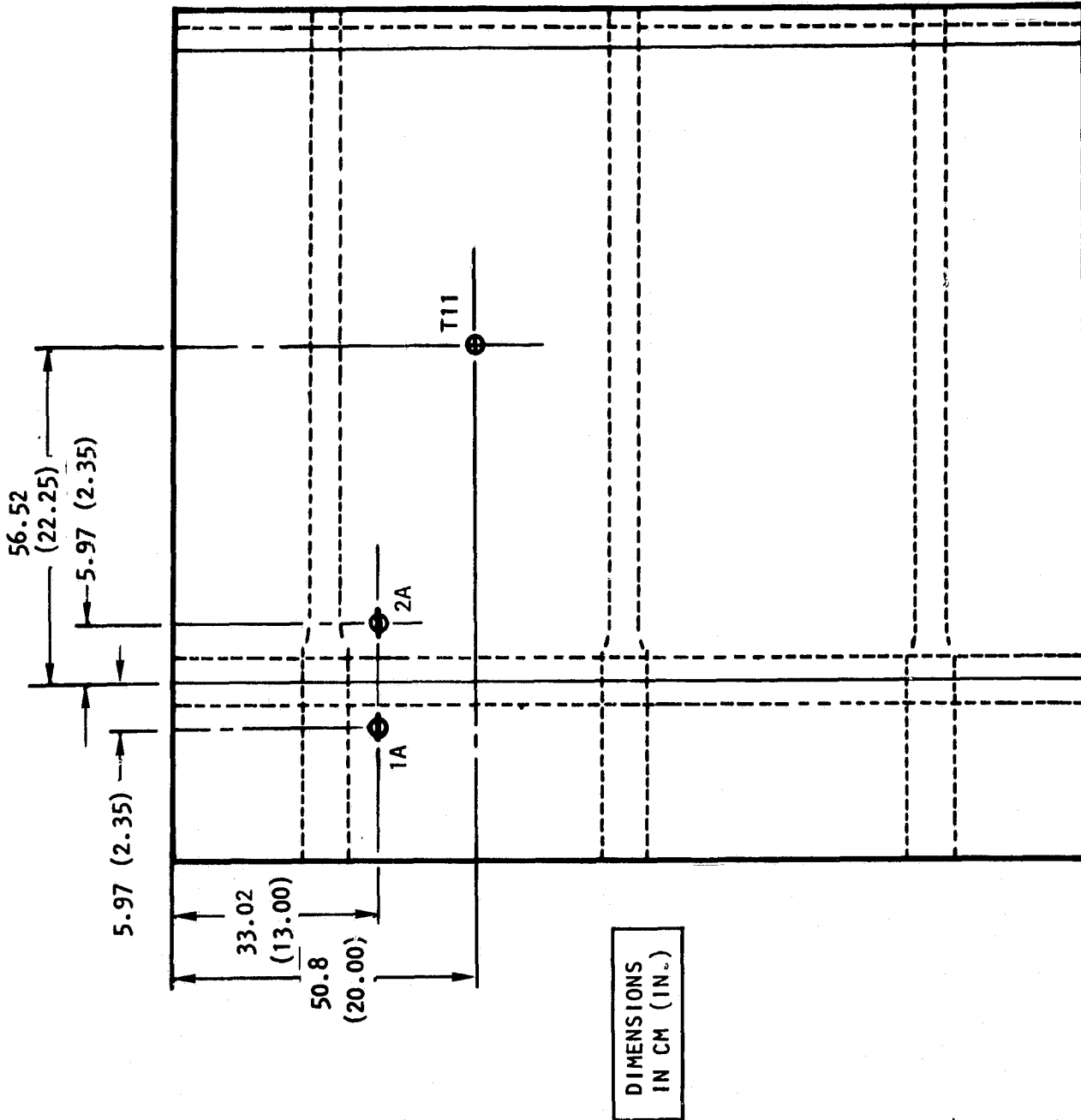
Figure 3-5. Inner Surface of Upper Honeycomb Cover Panel
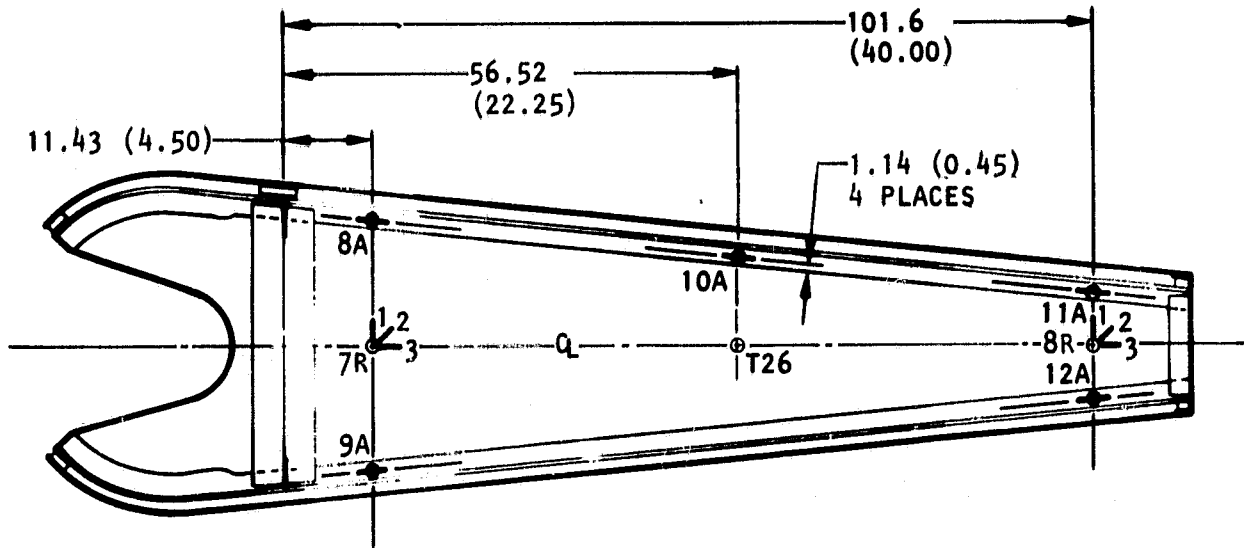
LEFT-SIDE VIEW
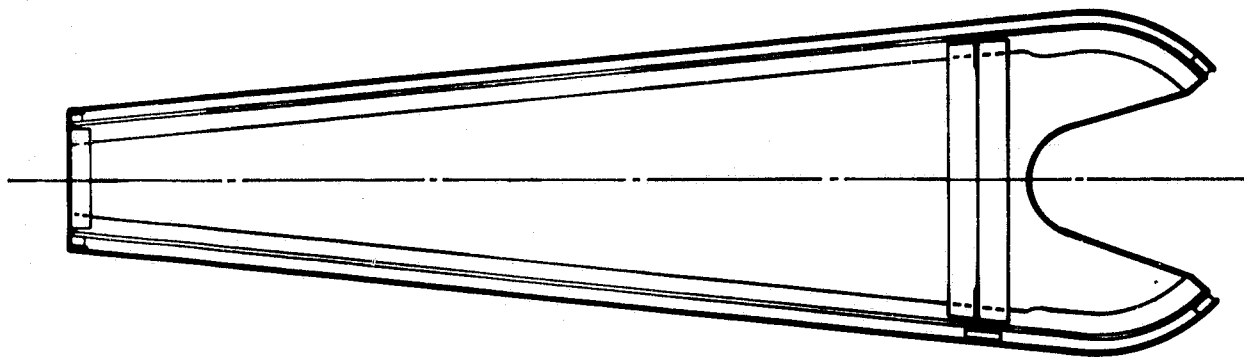
DIMENSIONS
IN CM (IN.)

RIGHT-SIDE VIEW

Figure 3-6. Rib No. 1

26
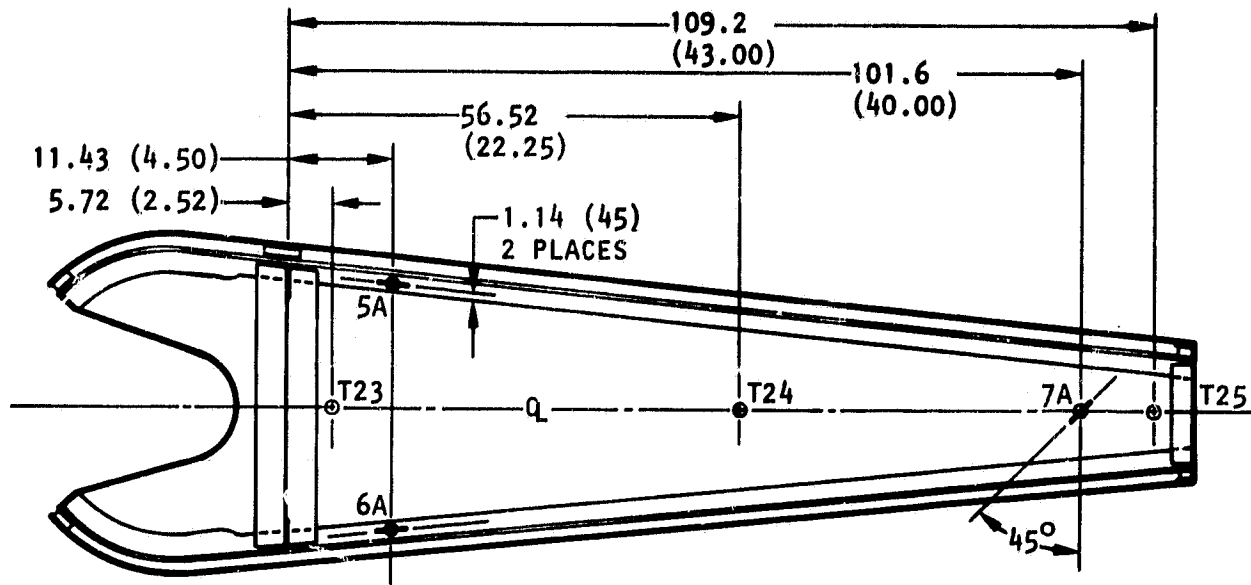
LEFT-SIDE VIEW
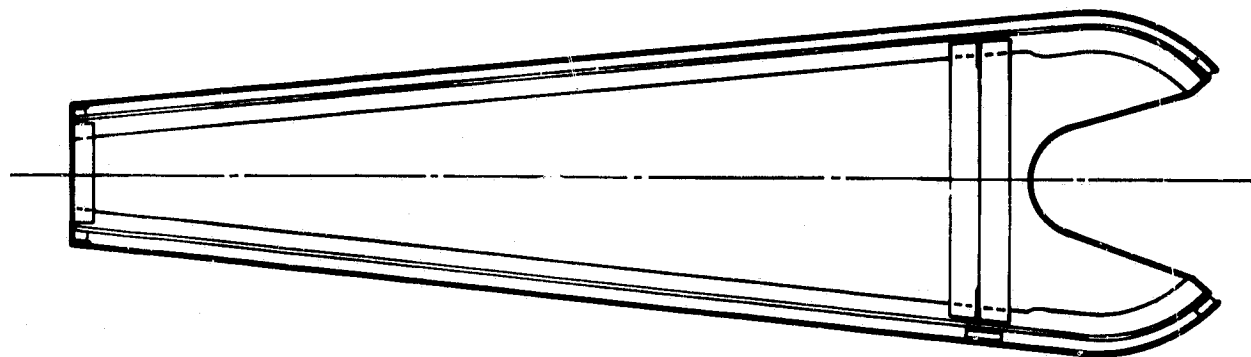
DIMENSIONS
IN CM (IN.)

RIGHT-SIDE VIEW

Figure 3-7. Rib No. 2

27

LEFT-SIDE VIEW

DIMENSIONS
IN CM (IN.)

RIGHT-SIDE VIEW

Figure 3-8.   Rib No. 3

(a) RIGHT SIDE VIEW, RIB NO. 1

DIMENSIONS
IN CM (IN.)

(b) FRONT SPAR WEBS, VIEW LOOKING FORWARD

(c) REAR SPAR, VIEW LOOKING AFT
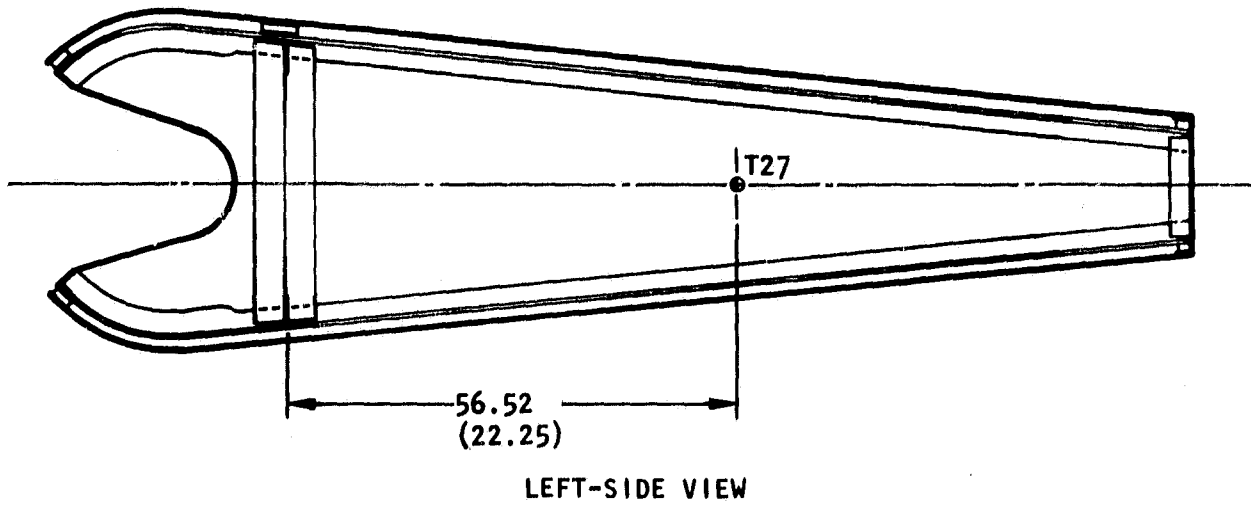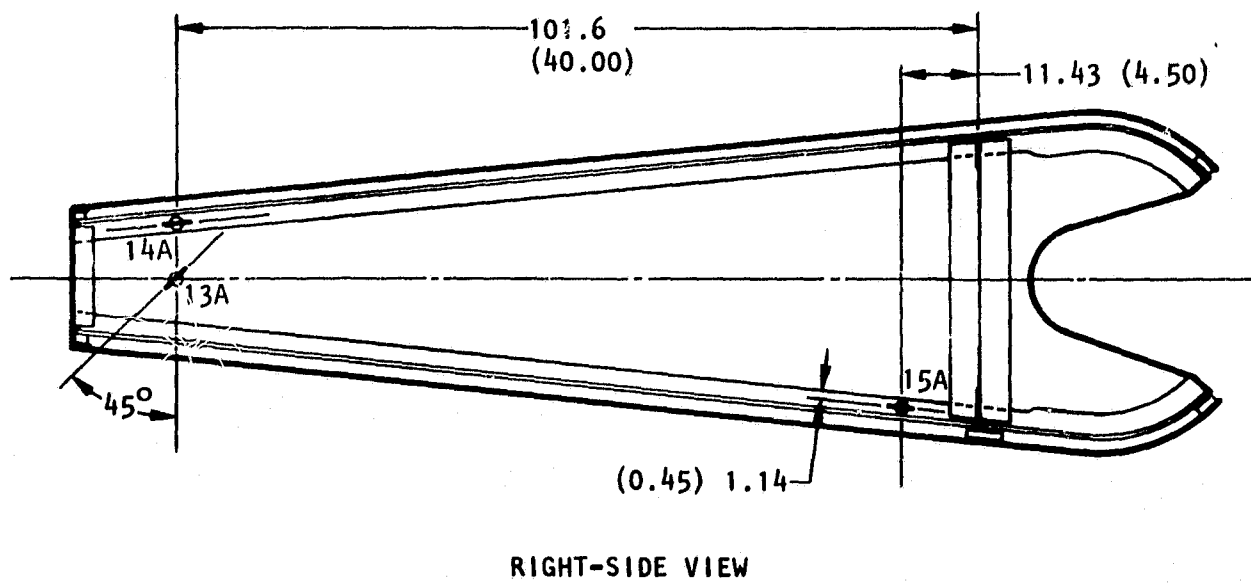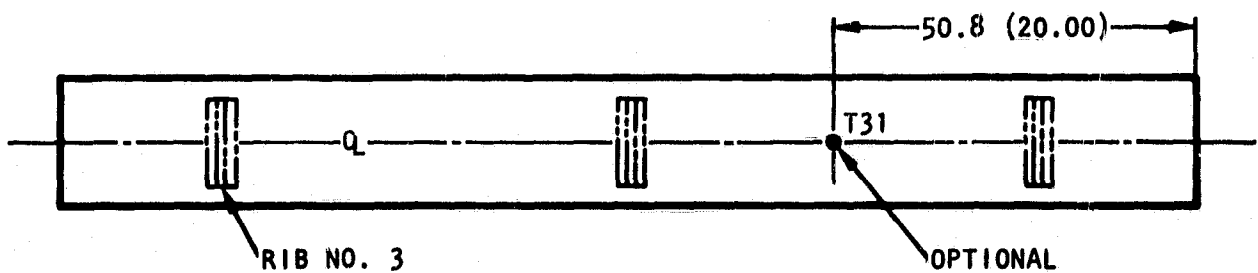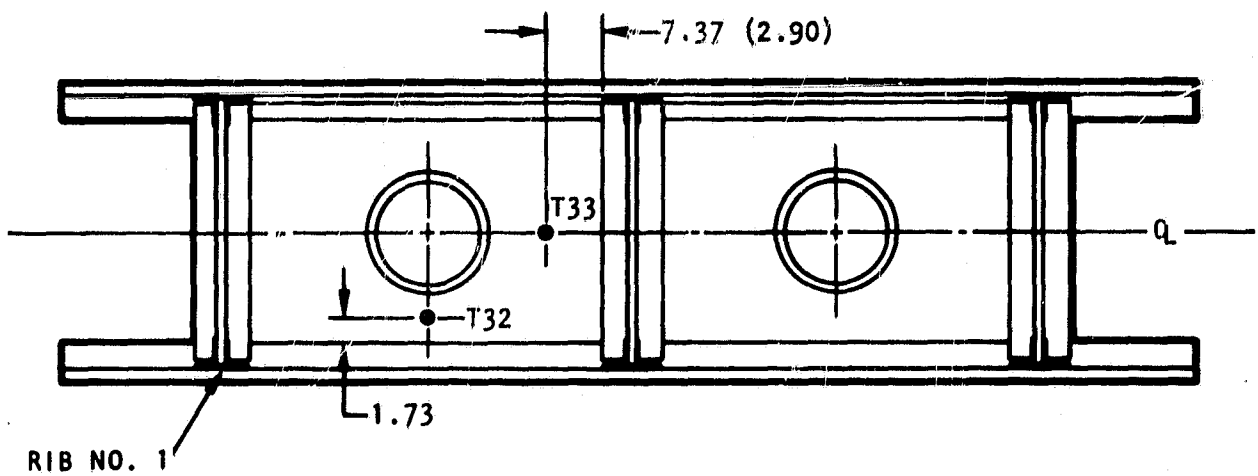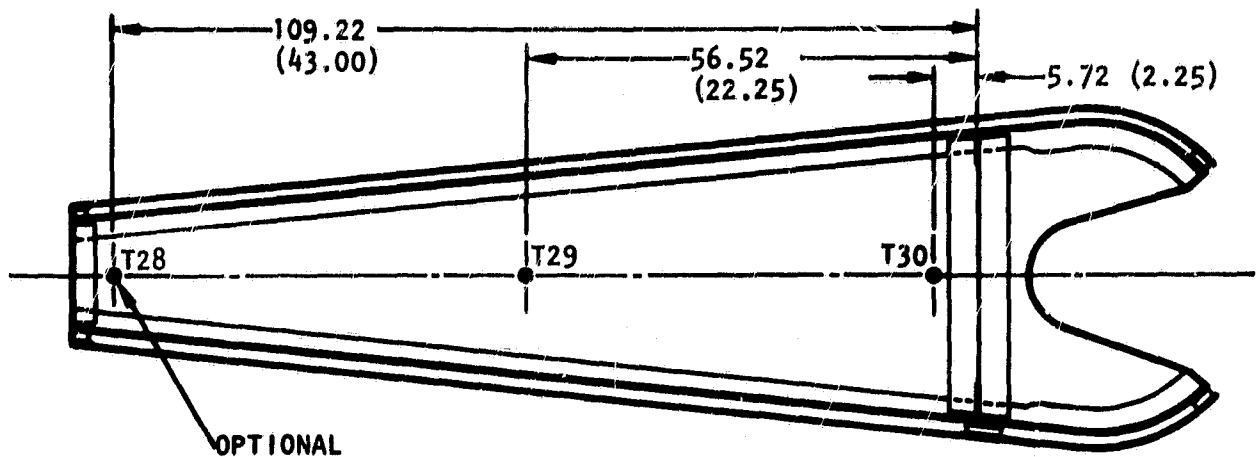
Figure 3-9.   Thermocouple Locations on Spars and Rib No. 1

A810930 G-13C

Figure 3-10.   Strain Gage, Thermocouples, and Deflection
Mounting Tabs - Lower Honeycomb Cover Panel

A811207 A-6
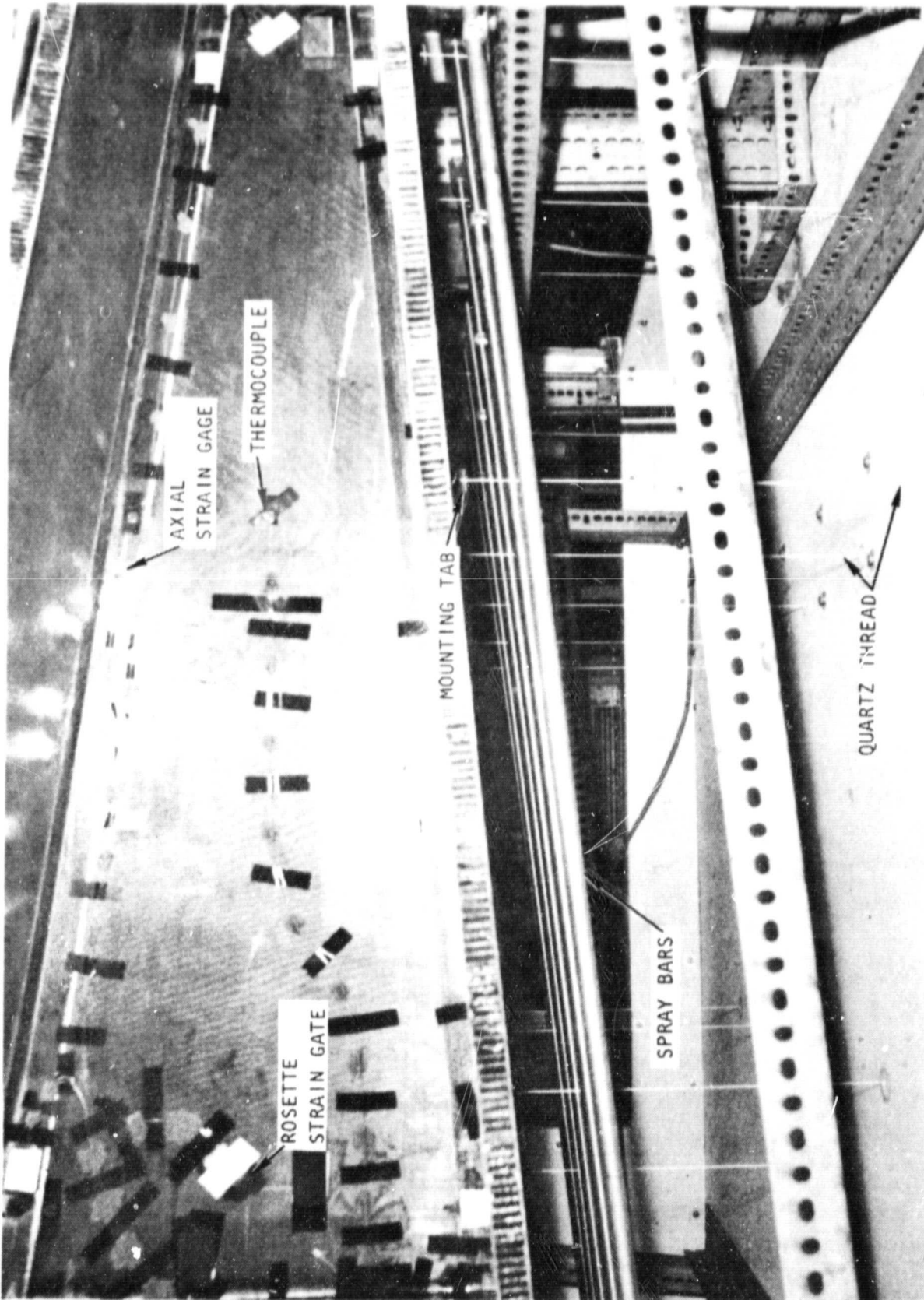
Figure 3-11. Quartz Thread and Gr/PI Mounting Tabs for
Deflection Measurement

A811207 A-8
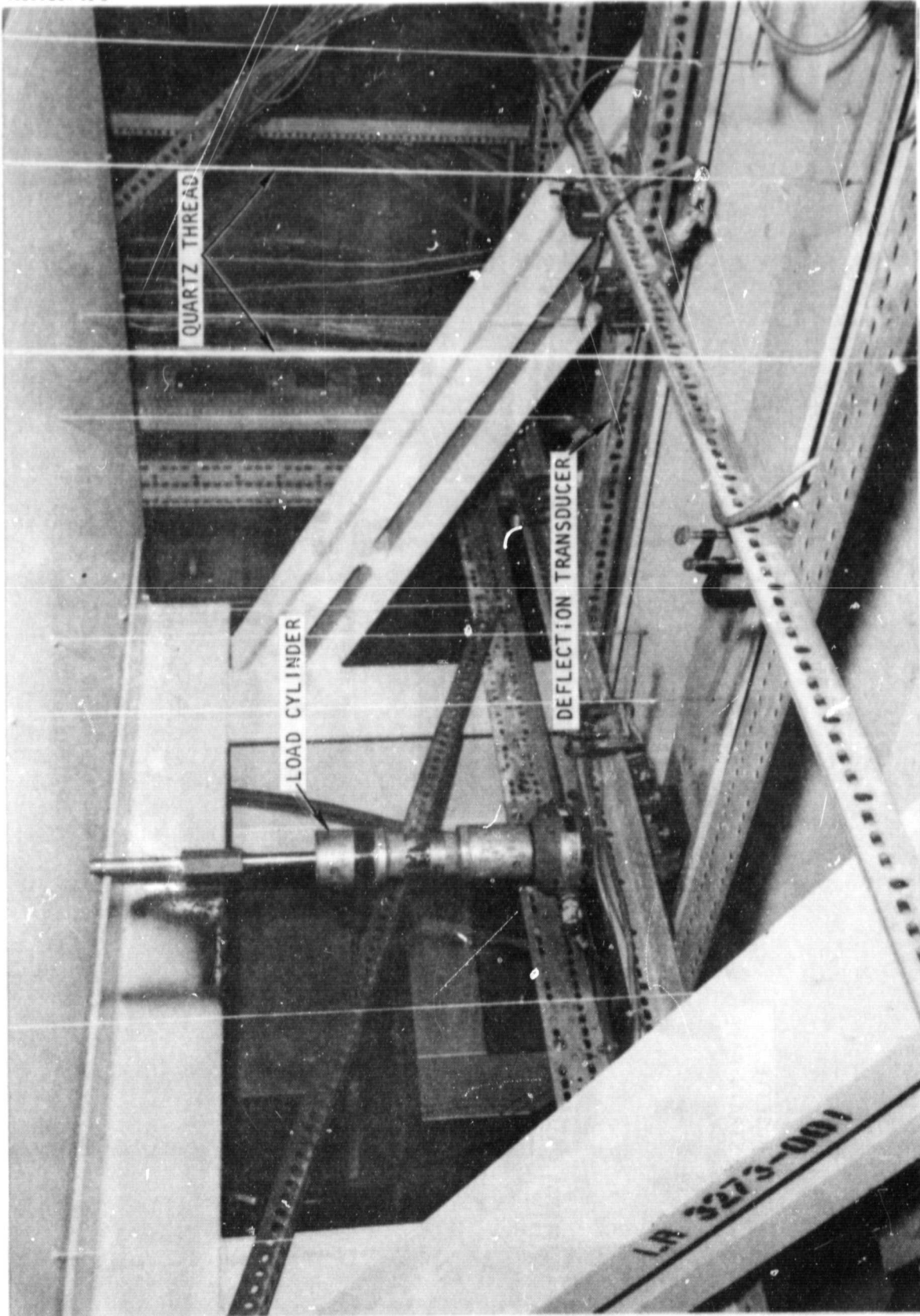
Figure 3-12. Quartz Thread Attached to Bending Beam
Deflection Tranducers and Forward Cylinder

3.1.2 Deflectometers

Twenty deflectometers were installed; seventeen were located on the TDS, two on the TDS/fixture interface attachments, and one on the center rib forward load point attachment. Gr/PI mounting tabs (Figure 3-11) were bonded to the TDS and connected to calibrated bending beam deflection transducers located outside of the thermal enclosure. Quartz thread (Figures 3-11 and 3-12) was used to make the attachment between the TDS mounting tabs and the transducers to minimize thermally induced error in the deflection readings. Quartz, in the pure form, has a thermal expansion coefficient in the order of 0.54 parts per million per degree Centigrade (0.3 parts per million per degree Fahrenheit).

3.1.3 Thermocouples

Thirty-three data thermocouples (T/C's), plus additionals for thermal control, were bonded to the structure with commercially available graphite cement. The T/C's were fabricated from 24-gauge copper-constantan wire.

3.1.4 Laboratory Data System (LDS)

The test data were acquired and processed by the LDS, which is a computer-based digital data system capable of variable rates of data sampling. It provided the following functions:

a. Signal conditioning for all sensors

b. Data multiplexing and analog/digital conversion for acquisition

c. Processor conversion of all data into engineering units

d. Core, magnetic tape, or disc memory storage

e. Line printer for data printout

f. Burroughs digital display units to provide continuous monitoring of up to 14 data channels per unit

g. Tektronix hard copy graphics terminal and necessary software to reduce test data to X-Y plots in a matter of minutes after the test.

3.2 TEST SETUP

The graphite/polyimide technology demonstration segment (TDS) test article is cantilever-supported at the forward end of the outer ribs, while test loads are applied at the rear spar and forward center rib (Figure 2-12). Tests were conducted at room temperature and 260°C (500°F), and the test article was thermal-cycled from -107 to 315°C (-160 to 600°F). The overall test setup is shown in Figure 3-13. Note the thermal enclosure in the open position for the ambient temperature test. The thermal enclosure was closed for the elevated temperature tests.

33

A811207 A-3C
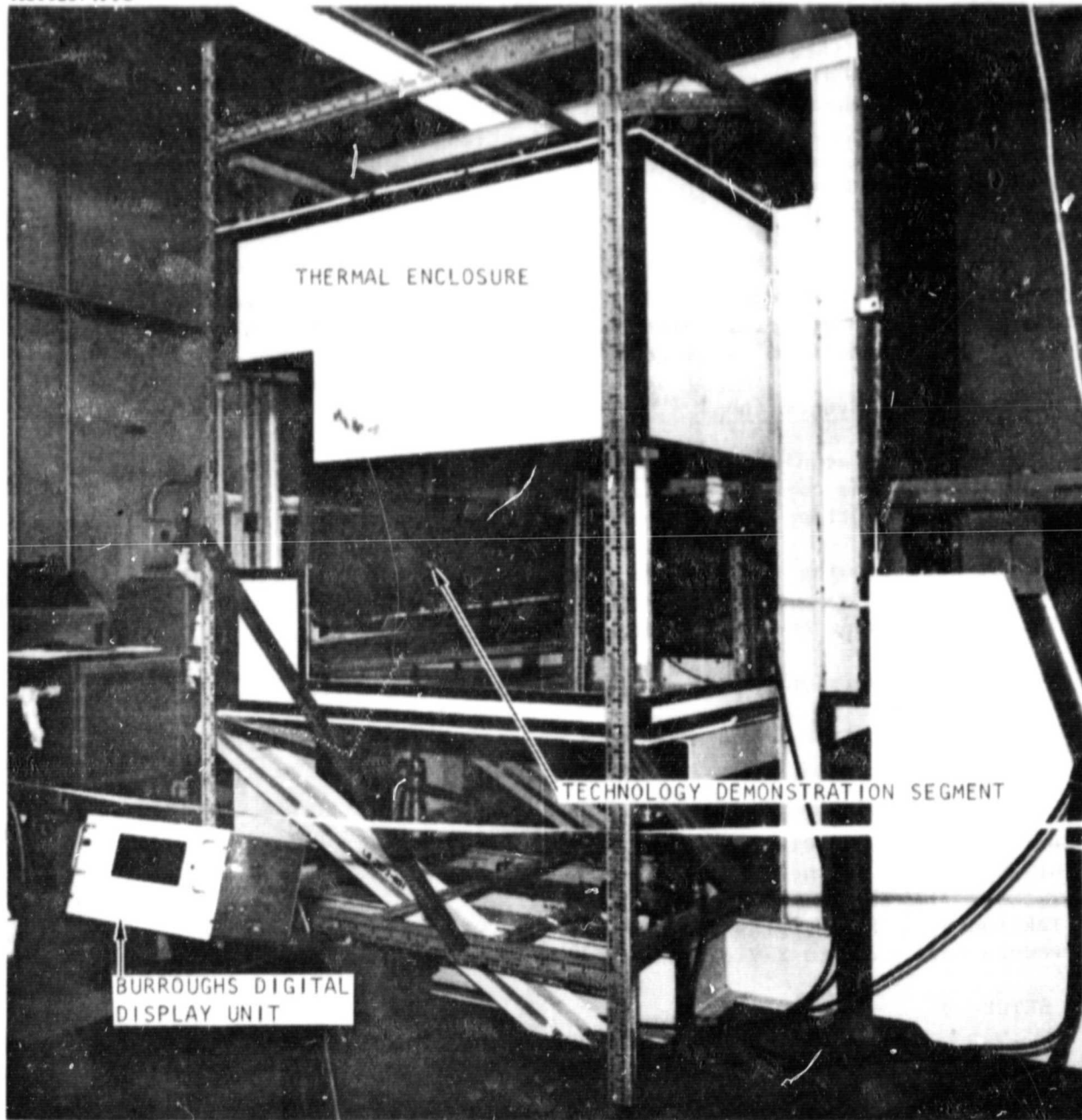
Figure 3-13. Overall Test Setup – Thermal Enclosure in Open Position

3.2.1 Load Support Interfaces and Load Cylinders

The TDS was provided with 0.69-cm-thick (0.27-in.) Gr/PI attachment fittings or mounting plates (Figures 3-14 and 3-15) to interface with the steel test fixture as depicted in Figure 2-6. Four hydraulic cylinders, each with its own load cell, were used to apply the test loads (Figures 3-12 and 3-16). The cylinders were simultaneously and proportionally loaded with an Edison cyclic load maintainer. The load cells provided load read-out for the data system. The forward load cylinder was attached to the test article through the mounting plates shown in Figure 3-15. The aft load cylinders were attached to the test article at the rear spar through the steel arms and load pads as shown in Figure 3-17.

3.2.2 Thermal Control System

The thermal control system had 12 stainless steel spray bars (Figures 2-10, 3-11, and 3-14) located approximately 7.62 cm (3.0 in.) above and below the TDS. Nitrogen gas was piped through the spray-bar assembly to cool the structure to -107°C (-160°F) during the thermal cycling test. Hot air was piped through the spray bars to heat the structure to 260°C (500°F) during the mechanical load test. The upper and lower spray-bar temperatures could be independently controlled. The 125-cycle thermal cycle test required a temperature of 315°C (600°F). The heating was accelerated by twelve 63.5-cm-long (25-in.) quartz radiant heat lamps located on the underside of the TDS to augment the heating system. Two radiant heat lamps were located below and in line with each spray bar (Figure 3-14). The thermal enclosure surrounding the TDS was fabricated from commercially available asbestos-free insulation board bolted to an angle iron frame.

A820126 D-12

SPRAY BAR

QUARTZ THREAD FOR
DEFLECTION MEASUREMENT

FORWARD SUPPORT INTERFACE AND
GR/PI LOAD PLATE

SPRAY BAR

QUARTZ LAMP
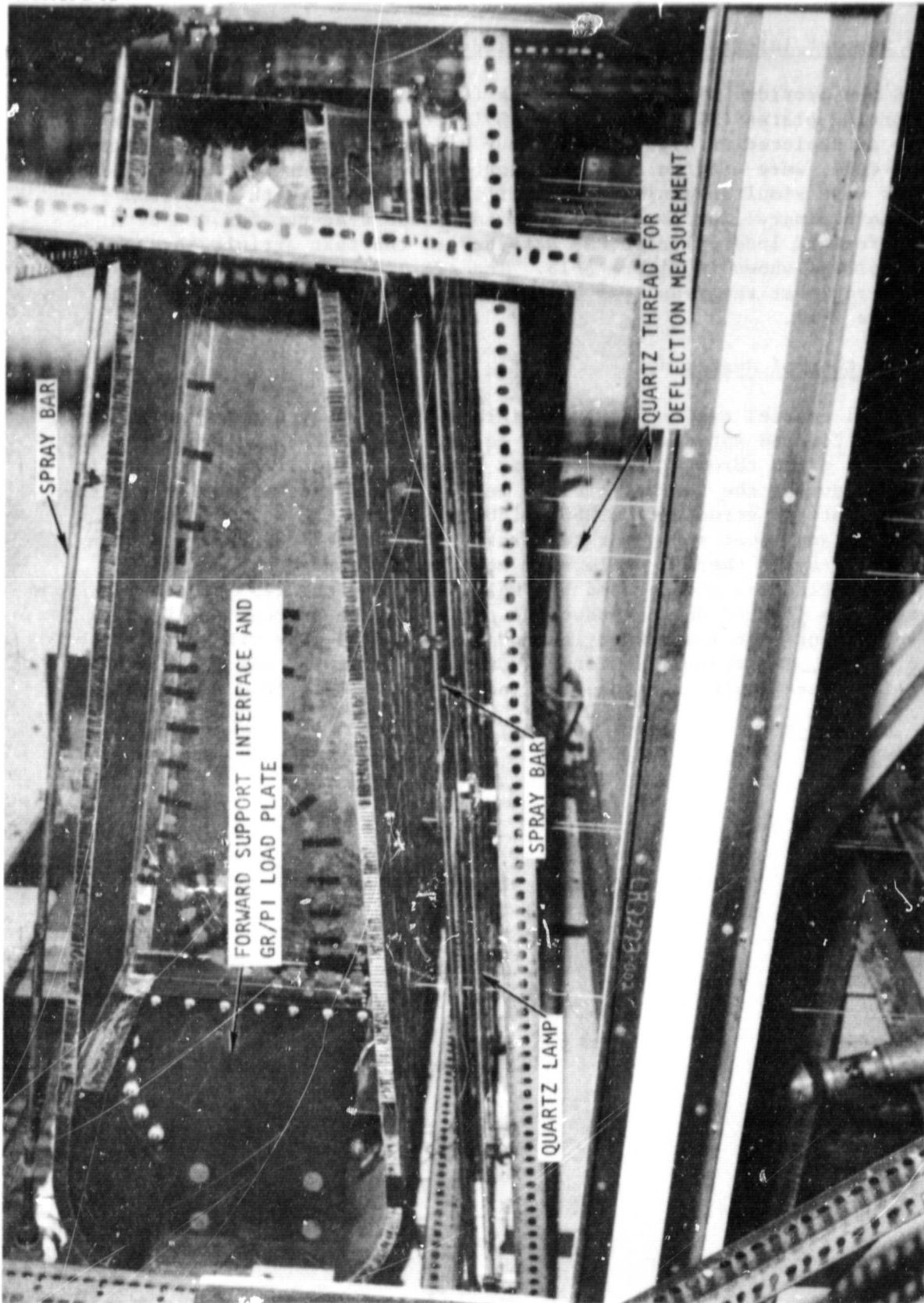
Figure 3-14. Forward Support Interface, Deflection Instrumentation,
Combination of Gas Spray Bars and Quartz Radiant
Heat Lamps for 600°F Thermal Cycles

A811207 A-10
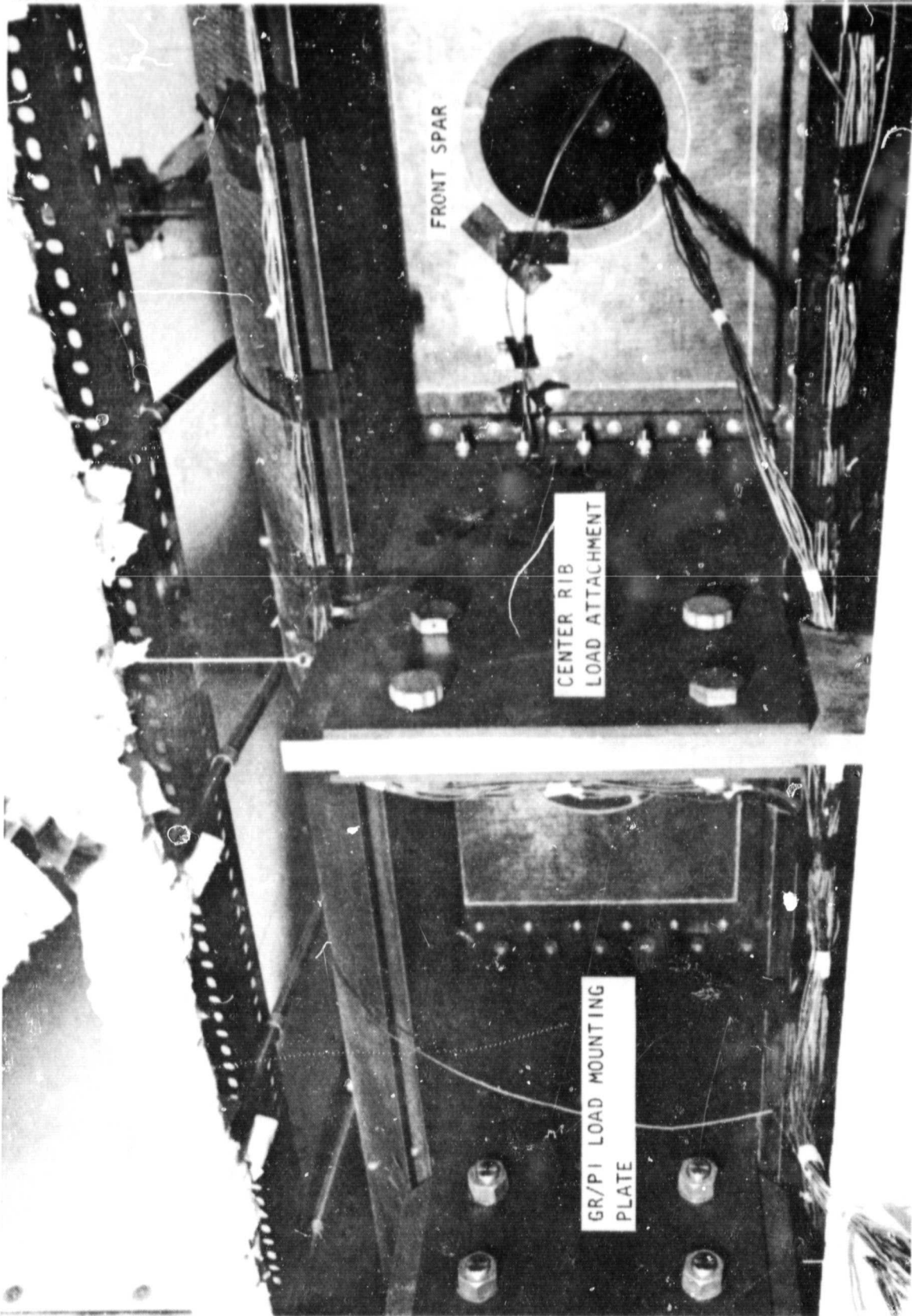
Figure 3-15. Loading Attachment at Forward End of Rib No. 2
and Fixture Attachment at Rib No. 3

A811207 A-7C

LOAD CYLINDER

DEFLECTION TRANSDUCER
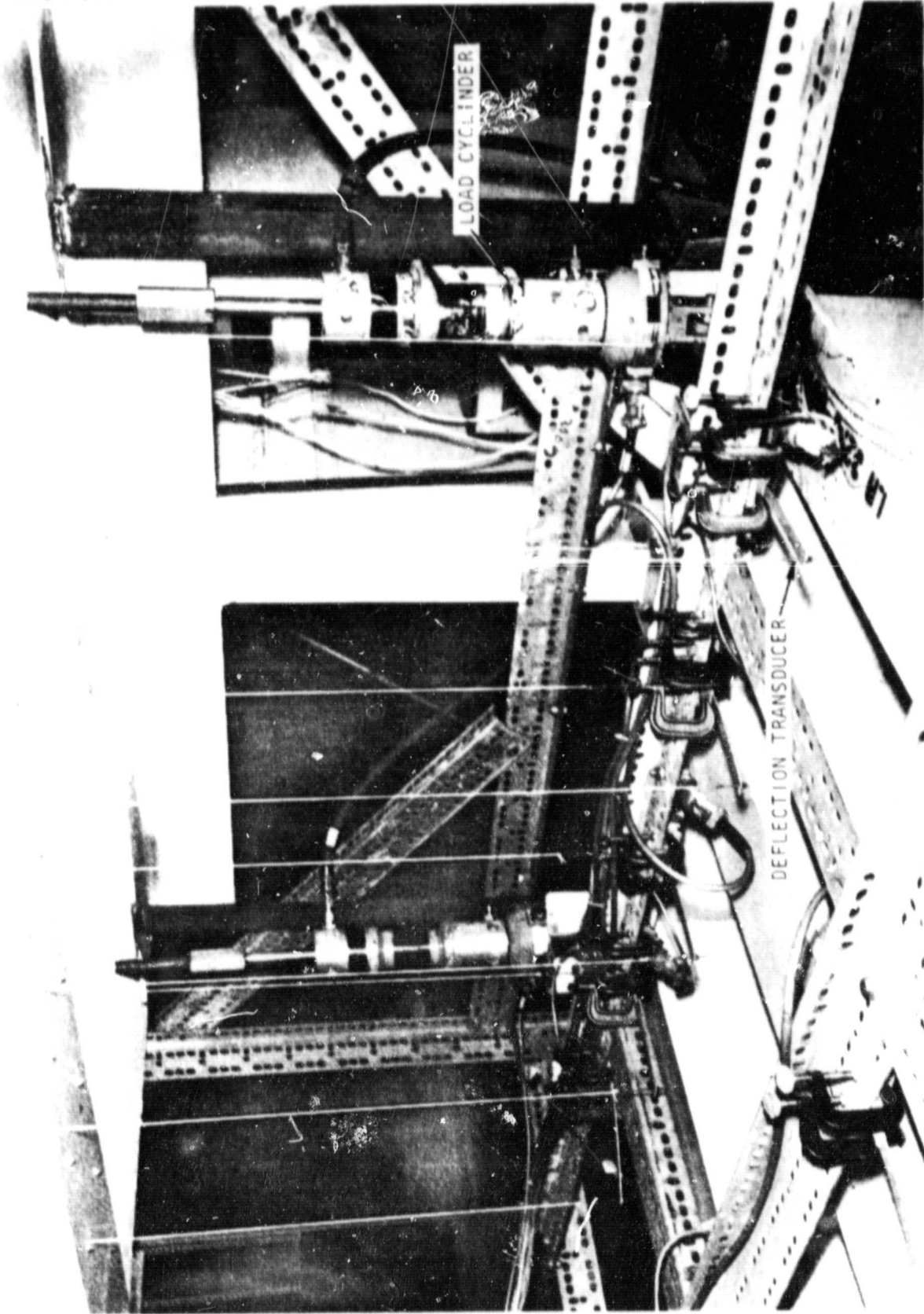
Figure 3-16. Hydraulic Load Cylinders (Rear Spar), Calibrated Bending Beam Deflection Transducers, and Quartz thread Connections

38

A811207 A-5C
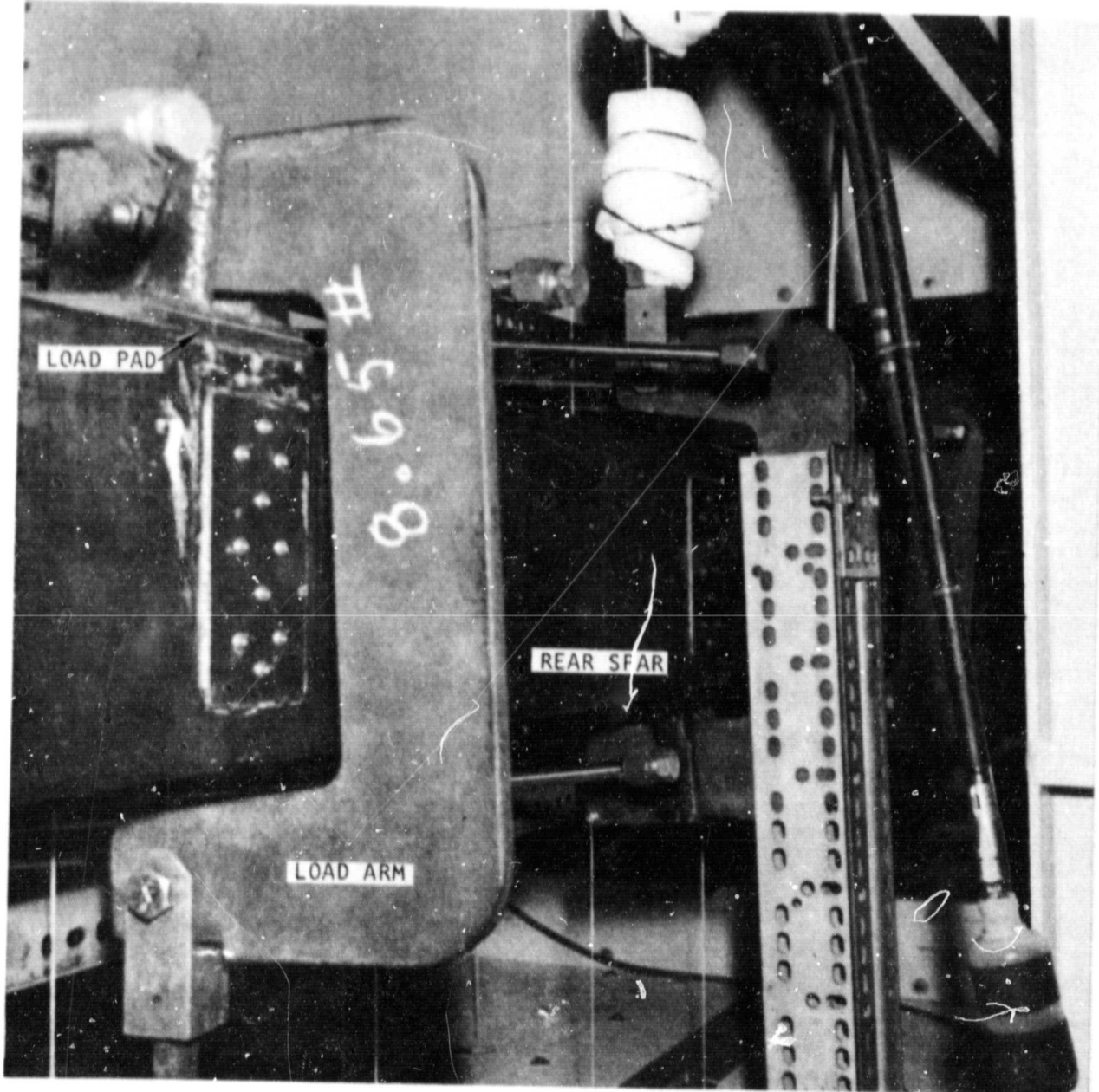
Figure 3-17. Rear Spar Load Fixtures

4. ROOM TEMPERATURE ULTIMATE MECHANICAL LOAD TEST

The graphite/polyimide (Gr/PI) technology demonstration segment (TDS) was successfully subjected to simulated ultimate mechanical load at room temperature. Test program objectives were (1) to simulate the body flap stress state in the vicinity of the stability ribs, (2) to verify the TDS structural integrity under orbiter ultimate static stress levels, and (3) to verify the analytically predicted mechanical response.

As shown in Figure 4-1, the TDS was cantilever-supported at the outer ribs, the middle rib was loaded to stress the front spar, and concentrated loads were applied at the trailing edge, which caused a twisting downward moment and flexed the rear spar. These loads simulated the body flap ultimate load case. The initial analytical predictions for the TDS mechanical response did not agree well with the test data. However, good correlation of the test data was achieved after refinement of the finite element model. Thus, the first and third objectives were achieved: i.e., the body flap stress state was simulated, and the TDS analytical response was verified. Also, the second test objective was achieved; a thorough NDE inspection of the TDS revealed no anomalies resulting from the ultimate load test.

4.1 ROOM TEMPERATURE ULTIMATE MECHANICAL LOAD TEST PROCEDURE

The test loads shown in Figure 4-1 were applied incrementally (10 percent), with data readings taken after each increment. The test instrumentation and test setup are described in Section 3.

The first test run to ultimate load was stopped at 110 percent of limit when the steel load arm fitting at the rear spar Rib No. 1 location separated from the Gr/PI load pad. The load pads were then pinned and bonded in place, as described in Figure 2-11. Subsequently, the test article was successfully loaded to ultimate load without evidence of failure.

4.2 ROOM TEMPERATURE ULTIMATE LOAD TEST RESULTS AND DATA CORRELATION

A NASTRAN finite element analysis (described in Appendix B) was used to predict the TDS response. The analytical predictions made prior to the test did not agree with the test data. The original NASTRAN model was quite simple, having less than 350 nodes. This NASTRAN model was reviewed, and several changes were made as discussed in Appendix B. The final version of the model was quite complex, having over 1,000 nodes, and good data correlation was achieved, as indicated in the following paragraphs.

TEST OBJECTIVES

• SIMULATE BODY FLAP STRESS STATE & VERIFY
GR/PI STRUCTURAL INTEGRITY UNDER ORBITER
ULTIMATE STATIC STRESS LEVELS

• VERIFY ANALYTICALLY PREDICTED STRAIN
LEVELS

TEST CONSTRAINTS

• LACK OF A HINGE RIB PRECLUDES ACTUAL
BODY FLAP LOADS — LOCAL STRESS FIELDS
IN THE VICINITY OF THE BODY FLAP
STABILITY RIBS SIMULATED

APPROACH

• LOADING CONDITIONS DEFINED TO REPRODUCE
THE BODY FLAP STRESS LEVELS AS DETERMINED
FROM TDS NASTRAN MODEL

• APPLY CONCENTRATED LOADS AT TDS
TRAILING EDGE
• DISPLACE CENTER SUPPORT
• CANTILEVER FROM OUTER RIBS
LEADING EDGE

ANCHOR
(TEST FIXTURE)

APPLIED AT ROOM TEMPERATURE

11.21 KN (2520 LBF)

2.49 KN (560 LBF)

9.963 KN
(2240 LBF)

14.7 KN
(3324 LBF)
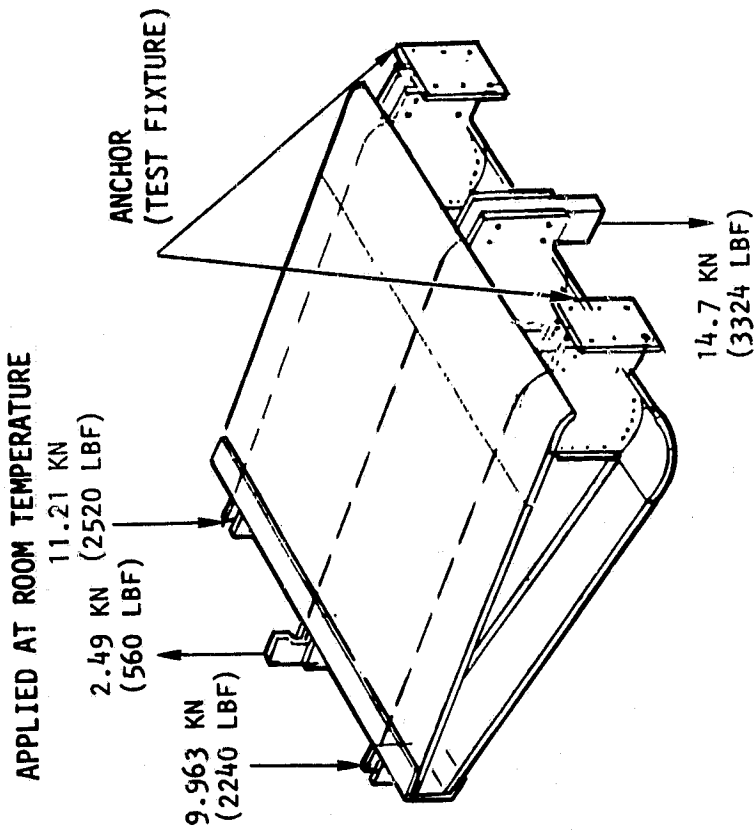
Figure 4-1. Room Temperature Mechanical Load Test

4.2.1 Deflections

The TDS deflected shape is illustrated in Figure 4-2. The deflected shape of the TDS during test correlated well with the NASTRAN prediction. The deflection test data are tabulated with the test predictions in Table 4-1. These data are plotted in Figures 4-3 through 4-5, which show the deflected shape along each rib. Deflection transducers or deflectometers are noted by the symbol Ⓓ. Nearly two-thirds of the total deflection is due to a rigid body rotation about the forward supports. While this rotation is less than 0.5 degrees, it accounts for 1.14 cm (0.45 in.) of deflection at the rear spar. In general, the predicted deflections differed from the actual deflections by less than 5 percent, with a maximum difference of 26 percent at transducer D19.

Table 4-1. TDS Deflections Under Ultimate Load
at Room Temperature

Transducer No.	Prediction		Test Results	
	Centimeters	Inches	Centimeters	Inches
D1	-1.66	(-0.653)	-1.60	(-0.628)
D2	-1.16	(-0.455)	-1.12	(-0.440)
D3	-0.37	(-0.144)	-0.36	(-0.140)
D4	-0.47	(-0.186)	-0.42	(-0.167)
D5	-0.54	(-0.213)	-0.57	(-0.226)
D6	-0.55	(-0.216)	-0.55	(-0.218)
D7	-0.47	(-0.184)	-0.48	(-0.190)
D8	-1.16	(-0.455)	-1.19	(-0.470)
D9	-1.16	(-0.455)	-1.18	(-0.464)
D10	-1.13	(-0.446)	-1.14	(-0.448)
D11	-1.12	(-0.442)	-1.13	(-0.443)
D12	-1.10	(-0.435)	-1.12	(-0.442)
D13	-1.81	(-0.713)	-1.80	(-0.707)
D14	-1.75	(-0.688)	-1.69	(-0.665)
D15	-1.66	(-0.652)	-1.62	(-0.638)
D16	-1.68	(-0.660)	-1.62	(-0.638)
D17	-1.73	(-0.680)	-1.68	(-0.660)
D18	-0.08	(-0.032)	-0.08	(-0.033)
D19	-0.23	(-0.091)	-0.18	(-0.072)
D20	-0.08	(-0.031)	-0.11	(-0.042)

4.2.2 Axial Strain Gage Response

The location of the axial strain gages was presented in Section 3. The response of the axial strain gages is compared to the predicted response in Table 4-2. These data are plotted for typical gages in Figures 4-6 through 4-8. Figure 4-6 presents the strain distribution along the length of the upper and lower caps of Rib No. 1. Gages A8 and A9 agree within three percent of the predicted values. Gages A11 and A12 are not as close on a percentage basis,

RIB NO. 1
(2520 LBF)
11.21 KN

RIB NO. 2
(560 LBF)
249 KN

RIB NO. 3
(2240 LBF)
9.963 KN

14.7 KN
(3324 LBF)

FRONT SPAR

REAR SPAR
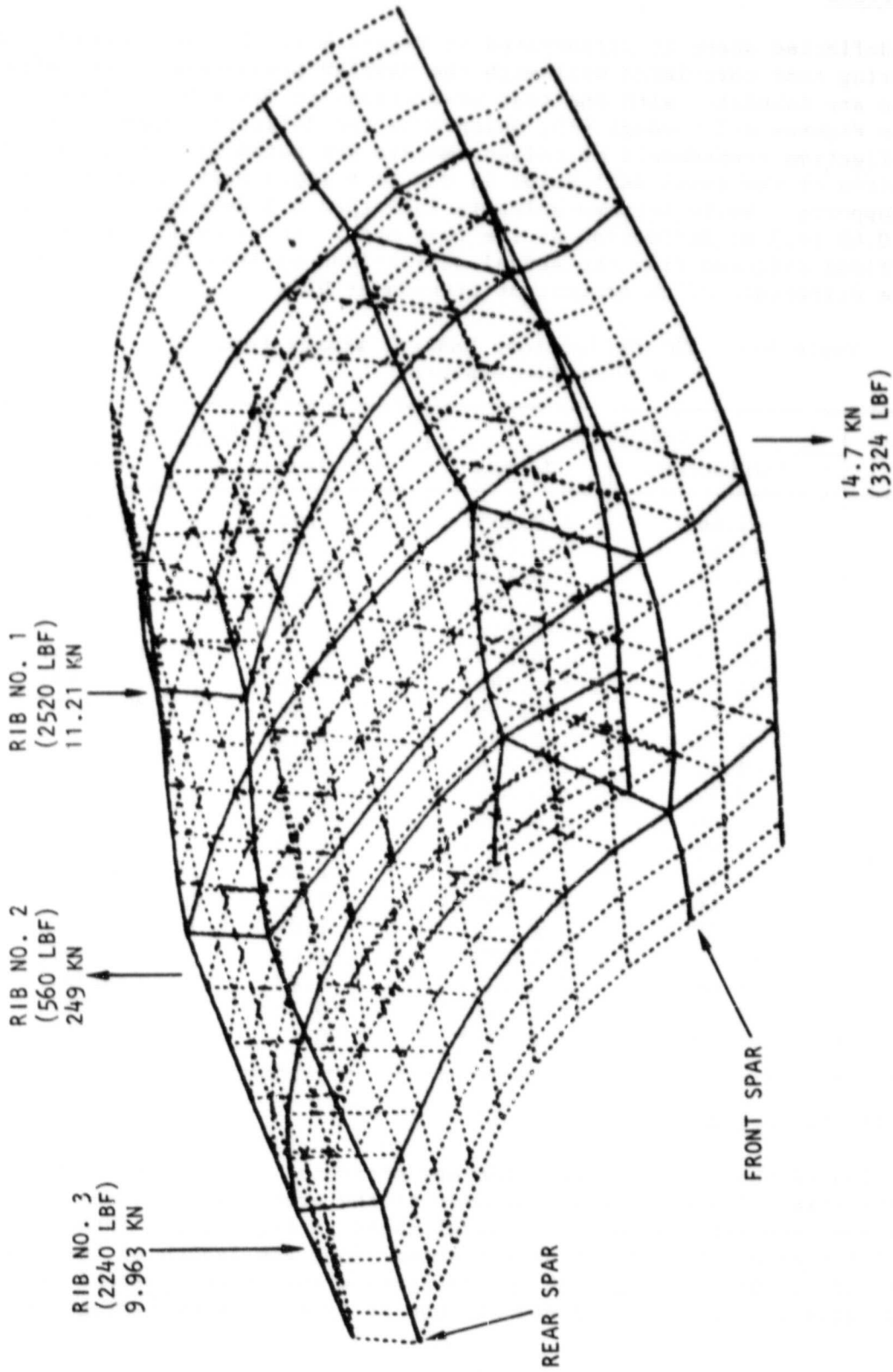
Figure 4-2. Deflected Shape of TDS During Room Temperature Ultimate Load Test
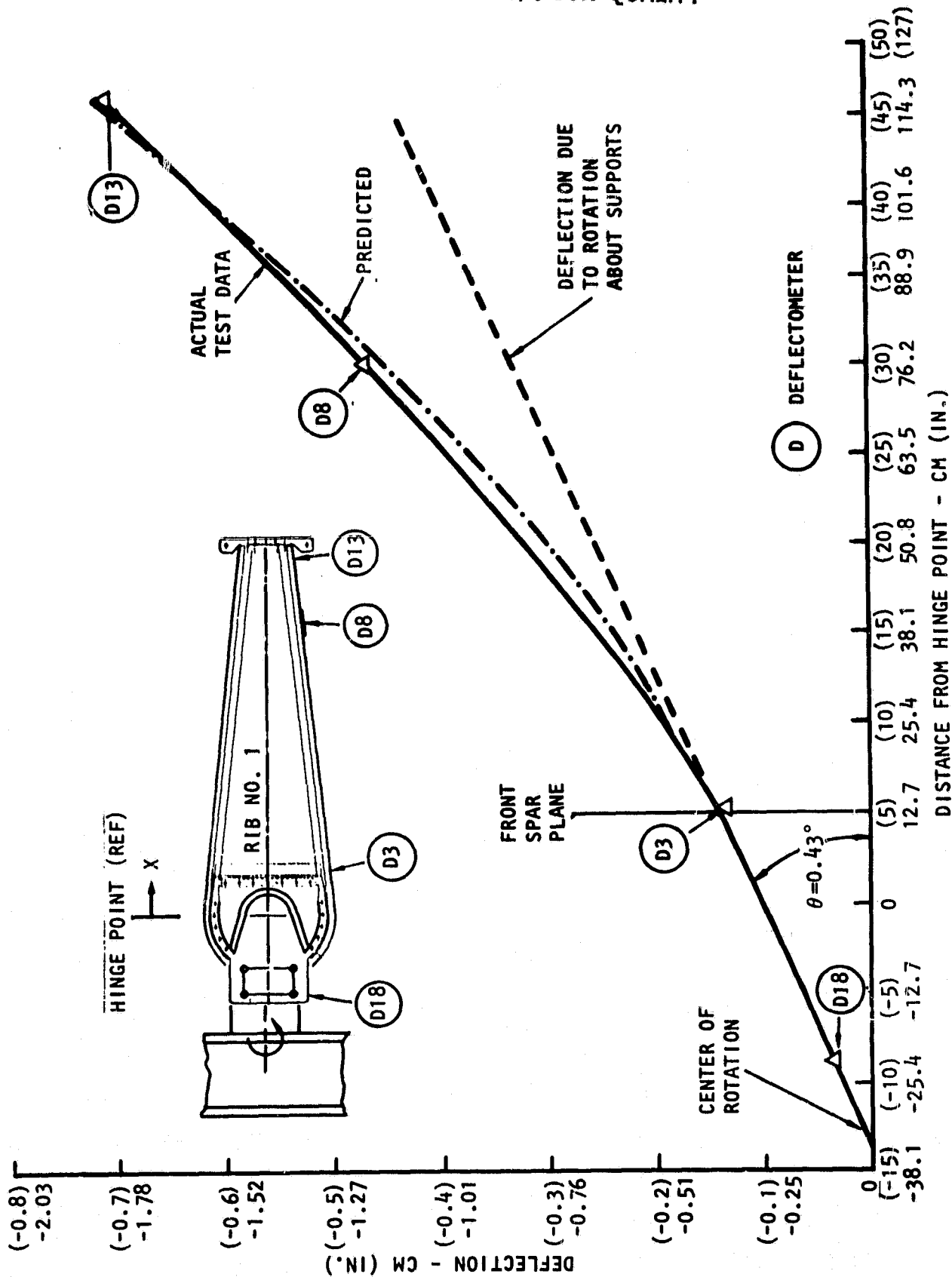
Figure 4-3. Deflected Shape Along Rib No. 1, Room Temperature Ultimate Load Test
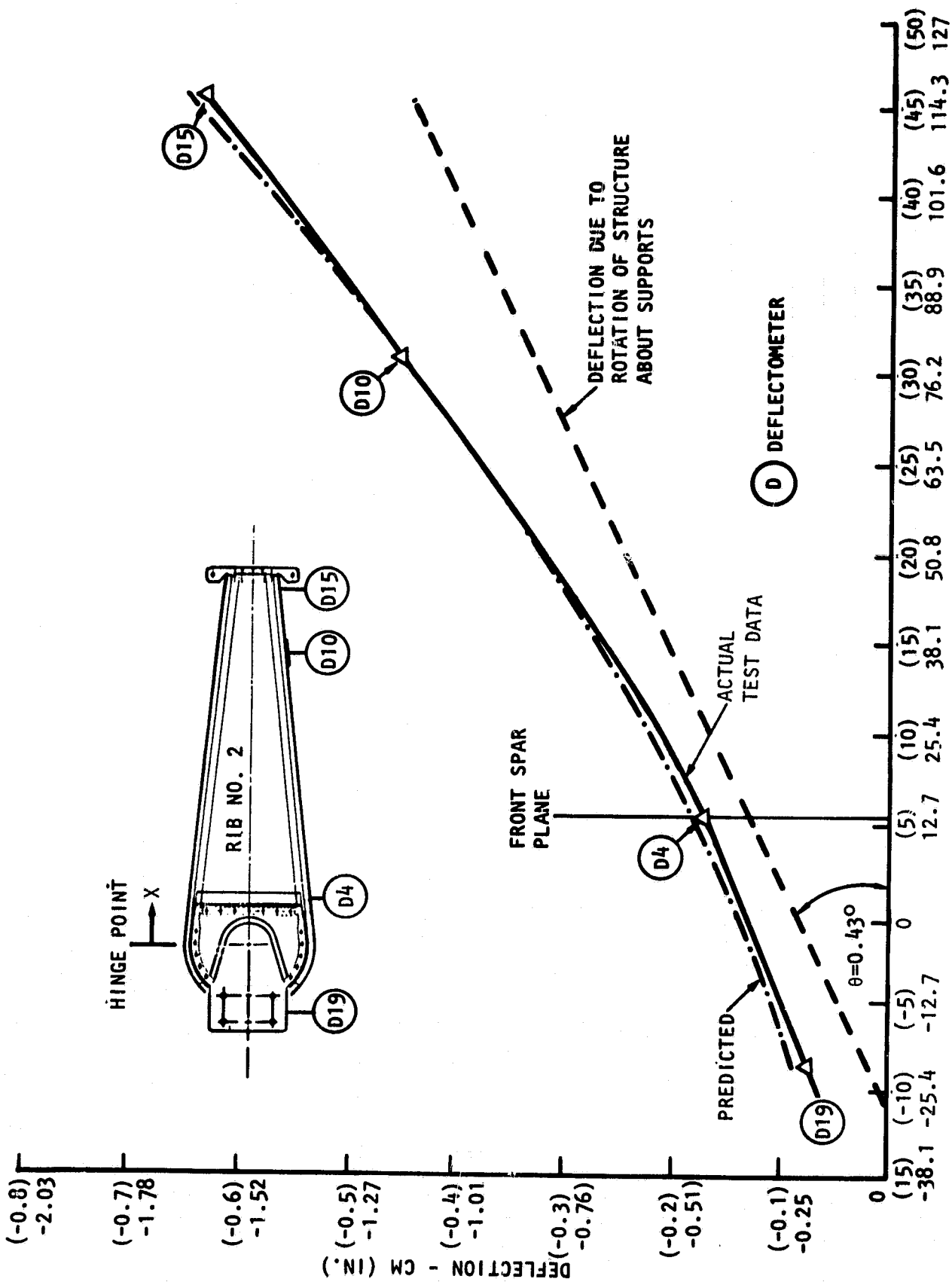
Figure 4-4. Deflected Shape Along Rib No. 2, Room Temperature Ultimate Load Test

46
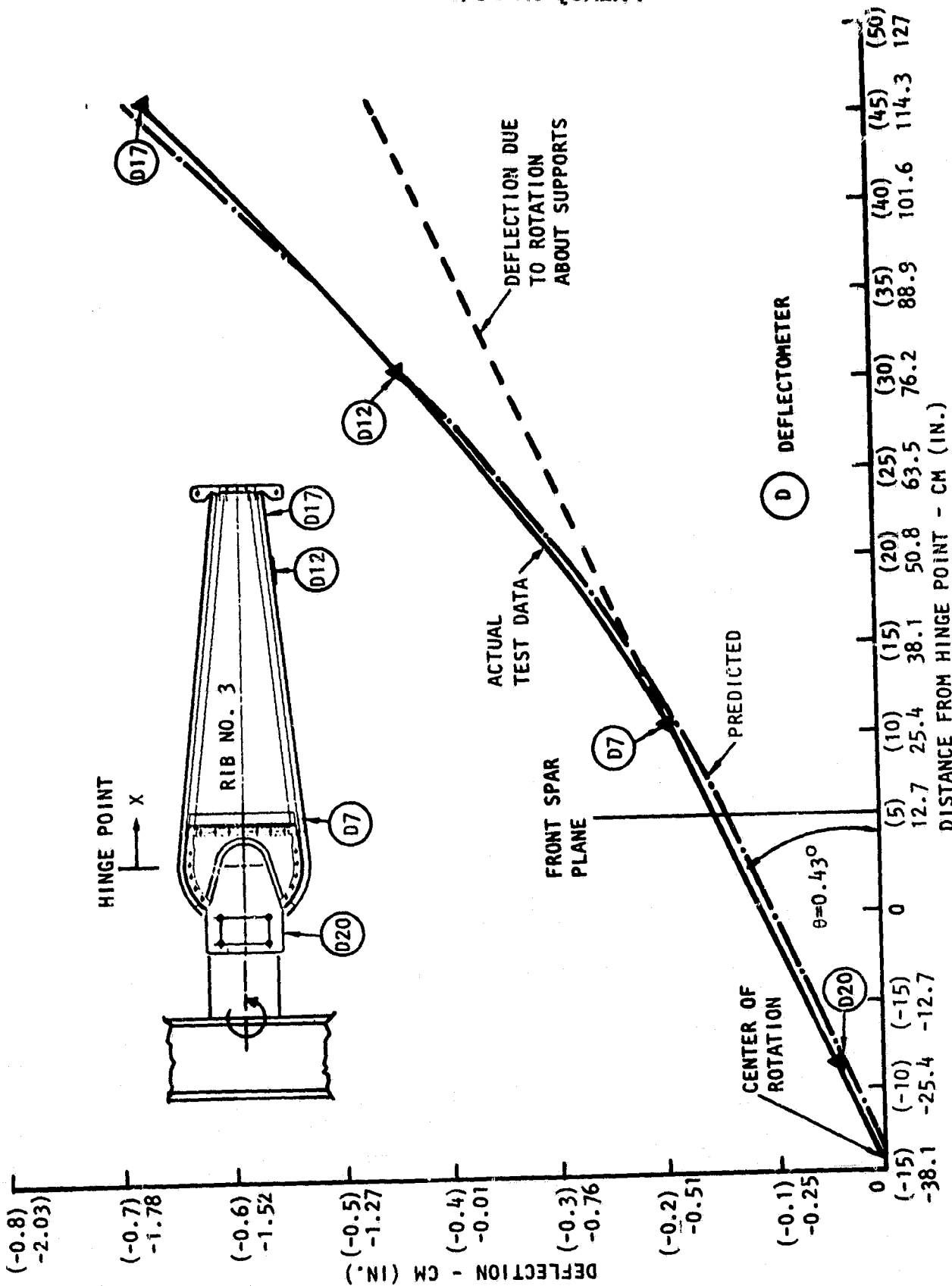
Figure 4-5. Deflected Shape Along Rib No. 3, Room Temperature Ultimate Load Test
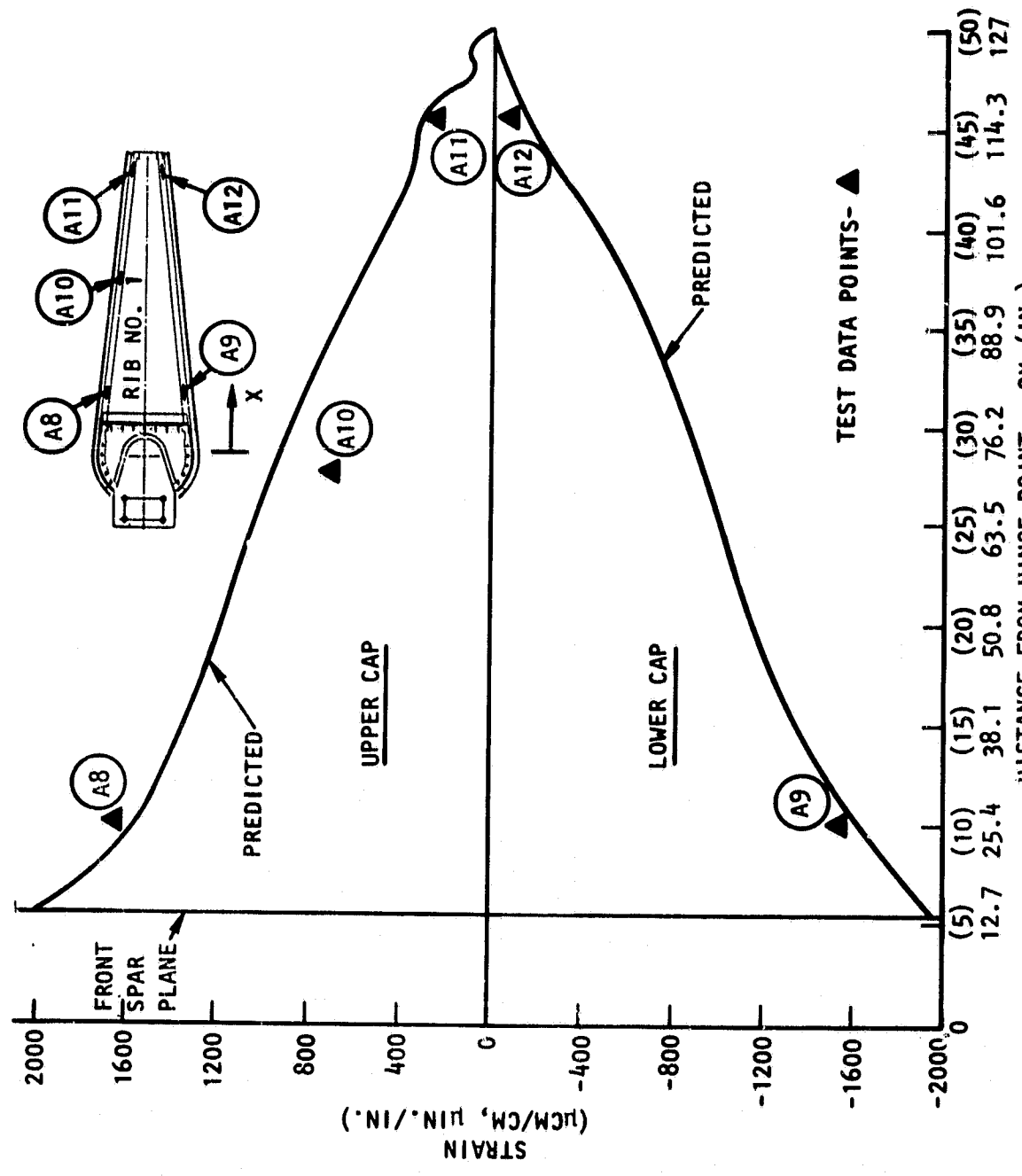
Figure 4-6. Strain Distribution Along RIB No. 1 Caps, Room Temperature
Ultimate Load Test

Table 4-2. Axial Strain Gage Response During Room
Temperature Ultimate Load Test

Gage No.	Test Results Strain (µ in./in.)	Prediction Strain (µ in./in.)	Prediction Stress (psi)	Test Results Strain (µcm/cm)	Prediction Strain (µcm/cm)	Prediction Stress (MPa)
A1	521	484	1,259	521	484	8.68
A2	1,864	1,492	4,759	1,864	1,492	32.81
A3	-921	-499	-1,315	-921	-499	-9.07
A4	-1,416	-1,355	-4,265	-1,416	-1,355	-29.40
A5	1,024	1,211	9,565	1,024	1,211	65.95
A6	-1,055	-1,198	-10,184	-1,055	-1,198	-70.21
A7[1]	-	-	-	-	-	-
A8	1,664	1,614	12,753	1,664	1,614	87.92
A9	-1,562	-1,612	-13,702	-1,562	-1,612	-94.47
A10	707	970	7,660	707	970	52.81
A11	263	310	2,449	263	310	16.88
A12	-82	-145	-1,235	-82	-145	-8.51
A13	1,608	1,499	-	1,608	1,499	-
A14	355	368	2,905	355	368	20.03
A15	-1,557	-1,635	-13,896	-1,557	-1,635	-95.80

[1]Not installed

but the magnitude of the error is small. Also, the load is applied in the vicinity of these gages, making accurate modeling difficult. It was anticipated that gage A10 would have good correlation, being removed from the end effects. However, gage A10 was in error by 37 percent, which could be a testing anomaly. As shown in Figures 4-7 and 4-8, the gages on Ribs 2 and 3 had good to excellent correlation between the test data and analytical predictions.

Axial strain gages A1, A2, A3, and A4 were placed on the cover panels to measure the load transfer across the split between the leading edge access panels and main box covers (Figures 3-3 and 3-5). The area was difficult to model accurately (Appendix B), but fair data correlation was achieved. Gages A1 and A3 were predicted to have the same order magnitude strain response, as were gages A2 and A4. However, the strain response of gage A3 was nearly double that of gage A1. The reason for this discrepancy is not readily apparent. The test response for gages A1, A2, and A4 varied from the predicted response by 7, 20, and 4 percent, respectively.

49
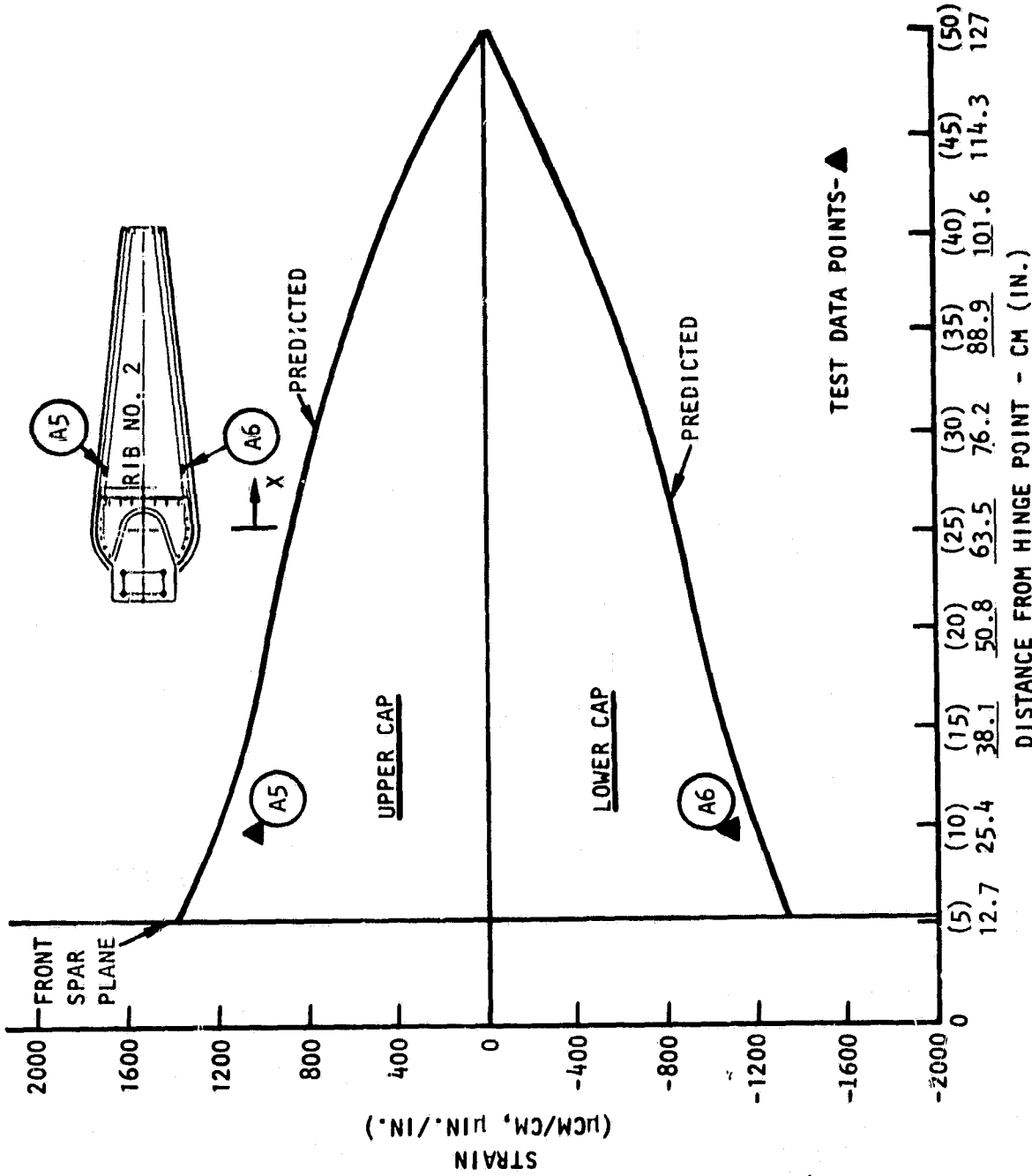
Figure 4-7. Strain Distribution Along RIB No. 2 Caps, Room Temperature
Ultimate Load Test
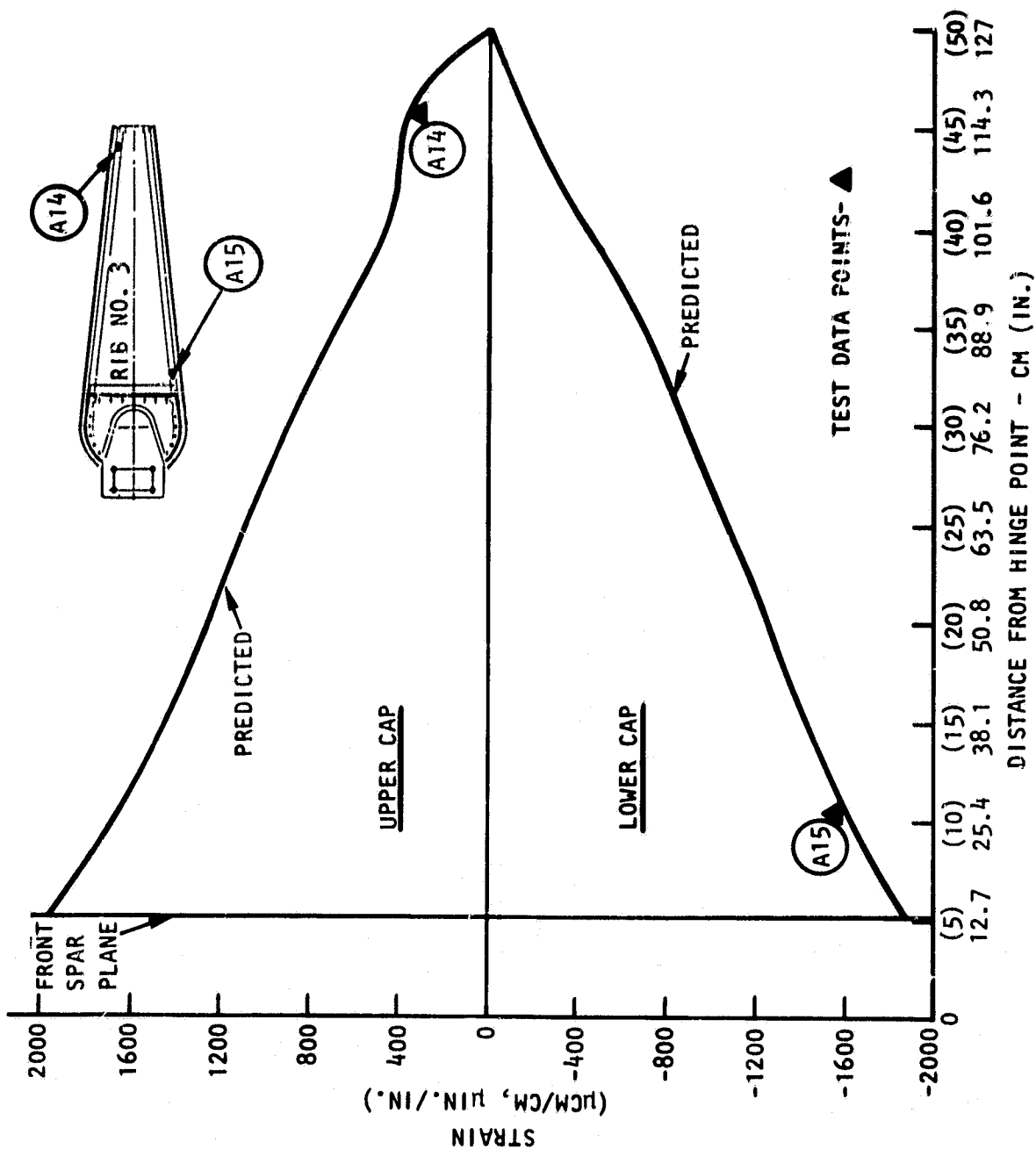
Figure 4-8. Strain Distribution Along RIB No. 3 Caps, Room Temperature
Ultimate Load Test

Table 4-3. Rosette Response During Room Temperature Ultimate Load Test

Gage No.	Test Strains(1) (μ cm/cm, μ in./in.)			Predicted Strains (μ cm/cm, μ in./in.)				Predicted Stress (psi)			Predicted Stress (mpa)		
	ε_1	ε_2	ε_3	ε_1	ε_2	ε_3	γ_{xy}	σ_x	σ_y	τ_{xy}	σ_x	σ_y	τ_{xy}
R1	622	370	-44	1,623	655	-199	113	5,300	789	295	36.5	5.4	2.0
R2	519	61	-440	1,300	509	-455	173	3,653	-3,744	450	25.2	-25.8	3.1
R3	809	662	-132	1,081	677	-144	418	3,506	354	1,087	24.2	2.4	7.5
R4	-668	-241	97	-1,903	-771	228	-133	-6,226	-1,004	-347	-42.9	-6.9	-2.4
R5	-630	-65	453	-1,276	-331	449	-164	-3,578	3,721	-427	-26.7	25.6	-2.9
R6	-881	-144	143	-1,064	-252	145	-415	-3,445	-305	-1,078	-23.7	-2.1	-7.4
R7	-107	-875	40	23	-834	-28	-1,667	275	90	-5,334	1.9	0.6	-36.8
R8	-932	-2,460	384	-1,011	-2,249	660	-4,146	-9,595	-274	-13,268	-66.2	-1.9	-91.5

(1)

$\varepsilon_x = \varepsilon_1$

$\varepsilon_y = \varepsilon_3$
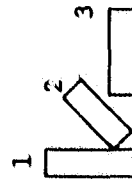
$\gamma_{xy} = (2\varepsilon_2 - \varepsilon_1 - \varepsilon_3)$

4.2.3 Rosette Strain Gage Response

The response of the rosette strain gages is presented in Table 4-3. The location of these gages was illustrated in Section 3. Gages R1, R2, R4, and R5 did not agree well with the predicted values. However, these gages are located near the split in the cover panels at the front spar. The NASTRAN model attempted to model this area, but the stress state is complex, and good correlation was not anticipated. Also, the strains in these gages are relatively small, and small change in magnitude results in a large percentage error. Gages R3 and R6 are located in the center of the cover panels away from the end effects and show good correlation between the test data and analytical predictions.

The rosettes on the Rib No. 1 web (R7 and R8) provided exellent correlation between the test response and the predictions, as shown in Figure 4-9. The predicted shear strain varied from the actual shear strain by less than three percent. Further evidence for accurate modeling of the webs is given by axial strain gage A13 (Table 4-2). This gage is located on Rib No.3 web and oriented at 45 degrees. The actual and predicted values for this gage differed by only 6.8 percent.

4.3 NDE RESULTS AFTER ROOM TEMPERATURE ULTIMATE LOAD TEST

The techniques described in Appendix C, were used to subject the TDS test article to a thorough NDE inspection after the room temperature ultimate mechanical load test. The inspection found no evidence of blistering, cracks, delamination, skin-to-core debond, or other forms of damage.

4.4 CONCLUSIONS

All objectives of the room temperature ultimate mechanical load test were achieved. The technology demonstration segment, weighing approximately 22.7 kg (50 lbm), sustained over 1,900 kg (4 kips) load while cantilever-supported on a 152-cm (60-in.) moment arm. There was no evidence of failure. The analytical predictions were in good agreement with the experimental test results. In the high strain areas of the rib caps and webs, the test data and predictions varied by less than five percent.
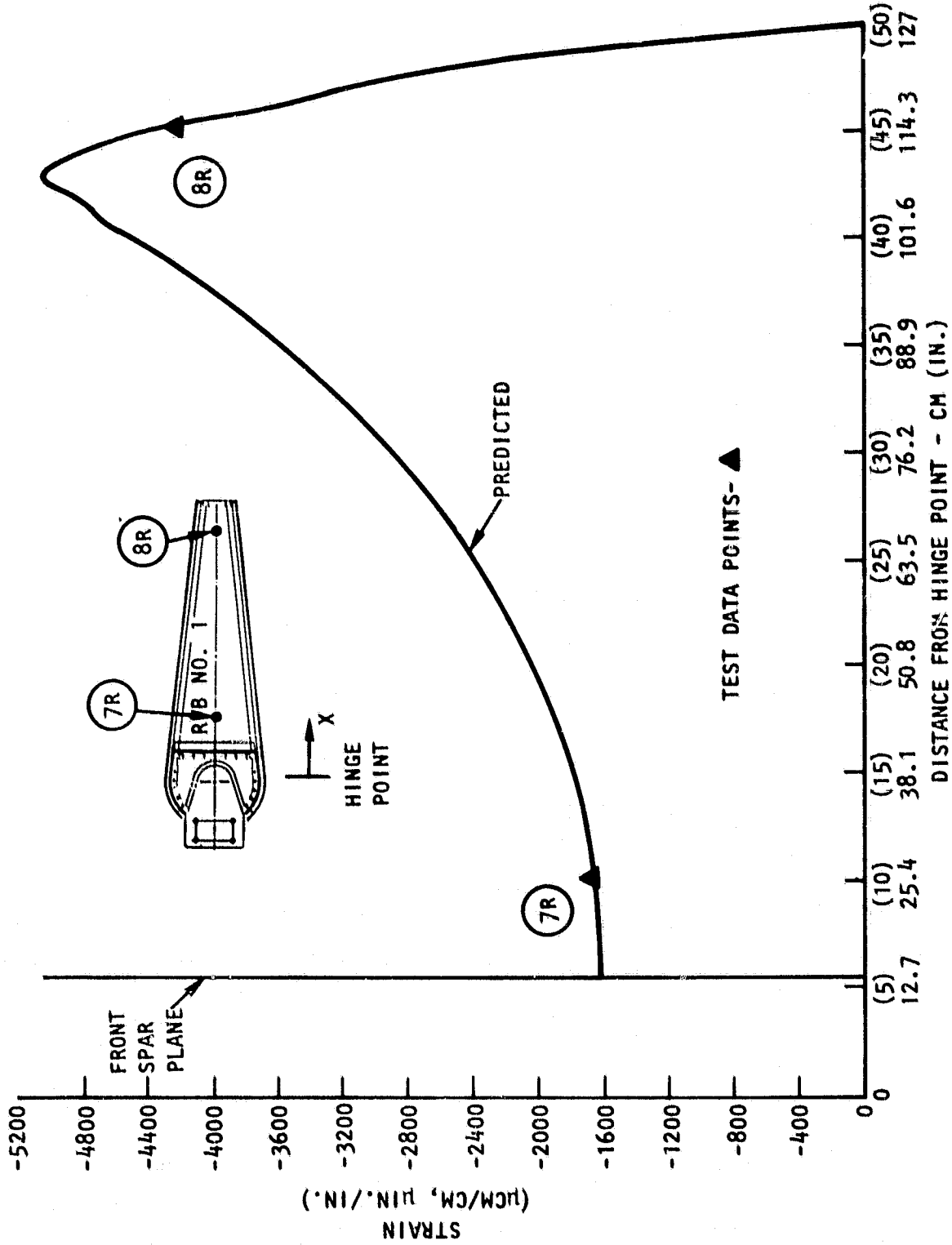
Figure 4-9. Shear Strain Distribution Along Rib No. 1 Web, Room Temperature
Ultimate Load Test

5. ELEVATED TEMPERATURE ULTIMATE MECHANICAL LOAD TEST

The graphite/polyimide (Gr/PI) technology demonstration segment (TDS) was successfully subjected to simulated ultimate mechanical load at 260°C (500°F). The orbiter body flap is subjected to ultimate load during a maneuver just prior to landing, when the projected body flap temperature is 260°C (500°F) during an abort-once-around (AOA) mission. However, the body flap is later subjected to 315°C (600°F) due to heat soak back after landing, when there are no loads.

5.1 ELEVATED TEMPERATURE ULTIMATE MECHANICAL LOAD TEST PROCEDURE

An ultimate load test was performed with the test article at a stablizied temperature of 260°C (500°F). The test loads shown in Figure 4-1 were applied in 10-percent increments, with data reading taken after each increment. The test instrumentation and test setup are described in Section 3.

While is was not a primary objective, it was desirable to subject the TDS to a 89°C (160°F) temperature delta across the cover panels to induce the corresponding thermal stresses. During the heating phase of the test, however, the maximum delta between the outer surfaces that could be achieved was 29°C (53°F), as limited by the capability of the test setup. This was accomplished by applying heat to the lower surface only. The maximum delta temperature between the lower surface inner and outer face sheets was 45°C (81°F).

While the TDS was being heated, the strain gages exhibited a temperature-induced resistance change, which erroneously registers on a recorder as strain. The indication is referred to as apparent strain to distinguish it from strain in the test part due to applied loads or thermally induced structural strain. The apparent strain magnitude varies with the temperature, the gage configuration and grid material, and the test part to which it is bonded. Due to the absence of apparent strain data on gages bonded to a Gr/PI composite structure, the thermally induced structural strain cannot be isolated from the total gage output while the test article is being heated. However, the delta strains recorded after temperature stabilization should accurately reflect load strain magnitudes. Similarly, thermally induced errors in the deflection readings result from thermal expansion of the connector between the test article and the deflection sensor. The use of quartz thread for the connector minimized the error for the thermal tests.

5.2 ELEVATED TEMPERATURE ULTIMATE LOAD TEST RESULTS AND DATA CORRELATION

The TDS responded to mechanical loads at 260°C (500°F) nearly identically to that at room temperature (Section 4). The deflection data for the elevated temperature test are compared with the analytical predictions in Table 5-1. As shown in Figure 5-1, the deflections were slightly larger than those at room temperature. The larger deflections are due to a reduction in the transverse elastic modulus of the cover panel laminate (Appendix B, Table B-1).

Table 5-1. TDS Deflections Under Ultimate Load
at 260 C (500°F)

Transducer No.	Prediction		Test Results	
	Centimeters	Inches	Centimeters	Inches
D1	-1.73	(-0.682)	-1.72	(-0.677)
D2	-1.19	(-0.468)	-1.19	(-0.468)
D3	-0.37	(-0.146)	-0.37	(-0.146)
D4	-0.47	(-0.187)	-0.45	(-0.177)
D5	-0.54	(-0.213)	-0.59	(-0.?34)
D6	-0.56	(-0.219)	-0.60	(-0.236)
D7	-0.47	(-0.185)	-0.51	(-0.202)
D8	-1.19	(-0.467)	-1.25	(-0.494)
D9	-1.18	(-0.466)	-1.23	(-0.484)
D10	-1.16	(-0.457)	-1.20	(-0.474)
D11	-1.15	(-0.453)	-1.20	(-0.474)
D12	-1.14	(-0.448)	-1.20	(-0.474)
D13	-1.89	(-0.743)	-1.94	(-0.762)
D14	-1.82	(-0.718))	-1.80	(-0.707)
D15	-1.73	(-0.681)	-1.72	(-0.679)
D16	-1.76	(-0.691)	-1.76	(-0.691)
D17	-1.80	(-0.710)	-1.84	(-0.724)
D18	-0.11	(-0.042)	-0.08	(-0.032)
D19	-0.24	(-0.065)	-0.17	(-0.065)
D20	-0.10	(-0.041)	-0.11	(-0.044)

The axial strain gage response is presented in Table 5-2. As shown in
Figure 5-2, there is little difference between the room temperature and 260°C
(500°C) mechanical response. As indicated by analysis, however, the thermal
stresses are quite significant. As shown in Figure 5-3, the thermal stresses
increase the rib cap tension stress and reduce the compressive stress by
52 MPa (7.5 ksi) or 53 percent. The rosette strain gage responses are presented
in Table 5-3. The test data and analytical correlation are similar to the
room temperature response presented in Section 4.2.3. Gages R1, R2, R4, and
R5, located near the split in the cover panels at the front spar, did not
agree well with the predicted values. Gages R3 and R6, located in the center
of the cover panels, showed better correlation. Rosettes located on the rib
webs (R7 and R8) provided excellent correlation between test response and
predictions. Thermal stresses tend to affect the cover panels somewhat. How-
ever, stresses remain low, The thermal effects on the stability rib web are
negligible, as shown in Figure 5-4.

5.3   NDE RESULTS AFTER ELEVATED TEMPERATURE ULTIMATE LOAD TEST

The TDS test article was subjected to a thorough NDE inspection after the
elevated temperature ultimate mechanical load test with the techniques
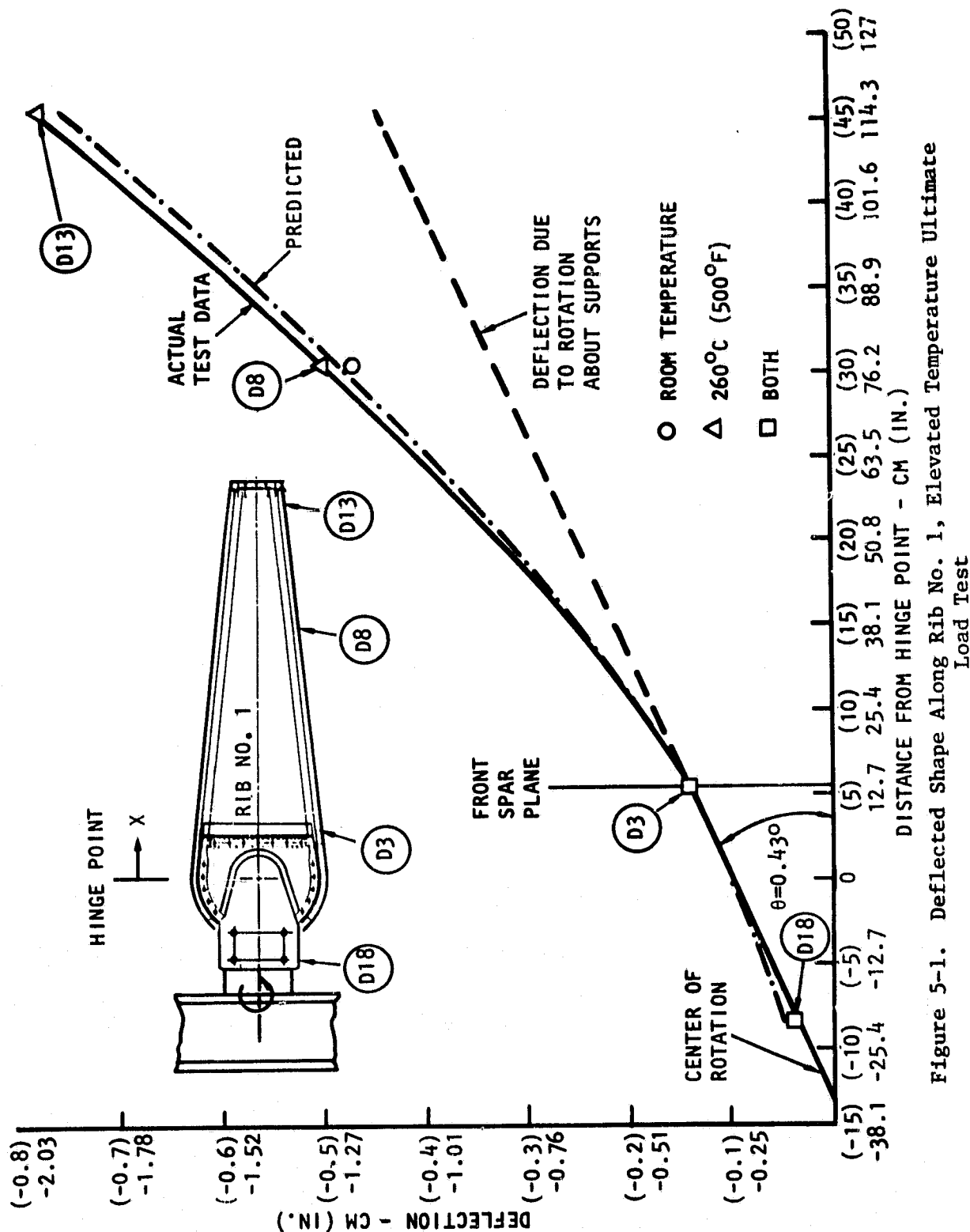
Figure 5-1. Deflected Shape Along Rib No. 1, Elevated Temperature Ultimate Load Test
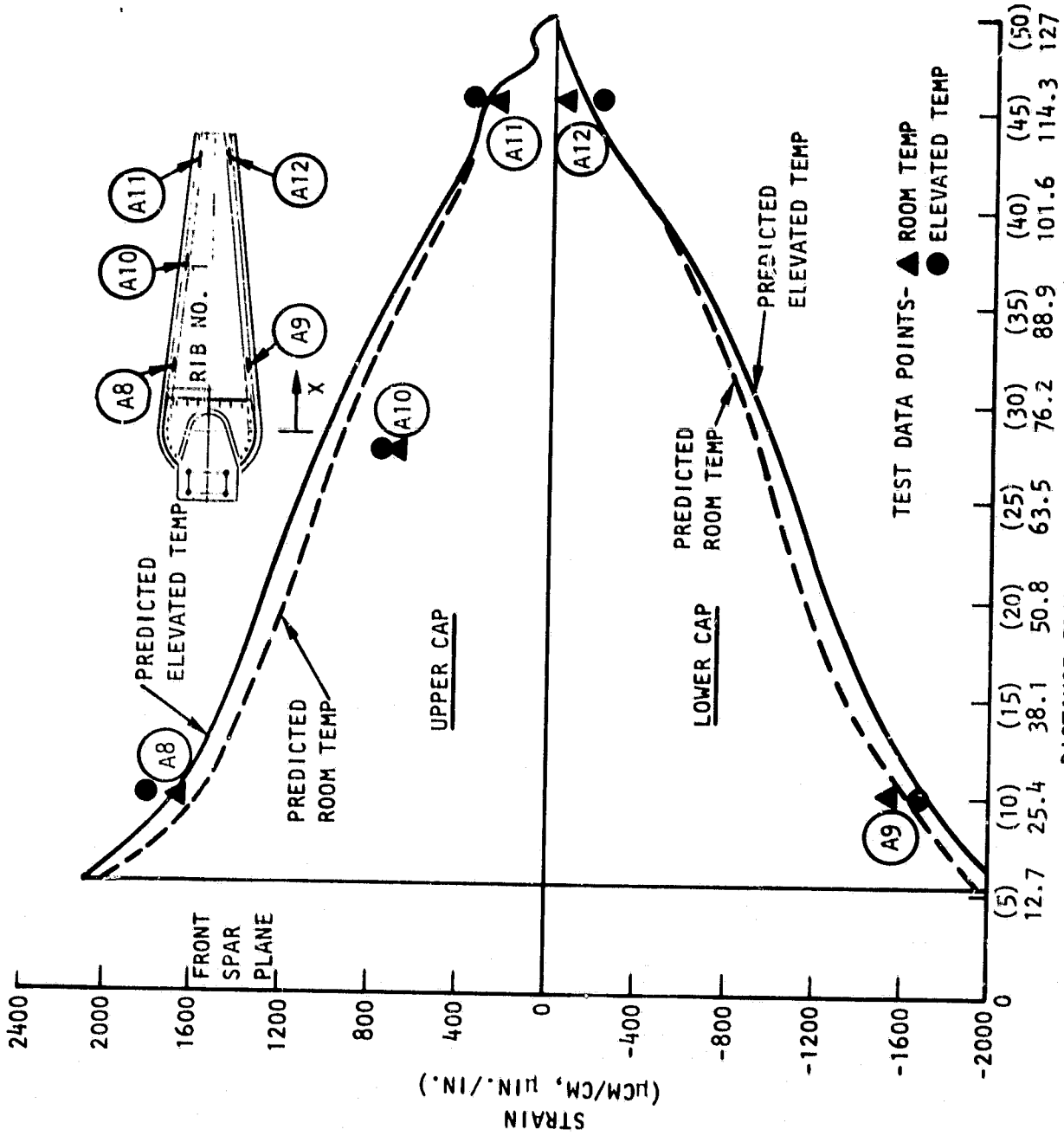
Figure 5-2. Strain Distribution Along RIB No. 1 Caps – Elevated Temperature Ultimate Mechanical Load Test

Table 5-2. Axial Strain Gage Response During 260 C (500°F) Ultimate Load Test

Gage No.	Mechanical Response			Temp + Mechanical	Mechanical Response			Temp + Mechanical
	Test Results Strain (μ in./in.)	Predicted Strain (μ in./in.)	Predicted Stress (psi)	Predicted Stress (psi)	Test Results Strain (μ cm/cm)	Predicted Strain (μ cm/cm)	Predicted Stress (MPa)	Predicted Stress (MPa)
A1	559	550	1,155	-1,268	559	550	7.96	-8.7
A2	2,050	1,766	4,590	2,838	2,050	1,766	31.6	19.6
A3	-884	-562	-1,195	-3,686	-884	-562	-8.24	-25.4
A4	-1,439	-1,595	-4,092	-5,828	-1,439	-1,595	-28.2	-40.2
A5	1,027	1,244	9,829	16,509	1,027	1,244	67.8	113.8
A6	-1,060	-1,245	-10,582	-3,453	-1,060	-1,245	-73.0	-23.8
A7[1]	-	-	-	-	-	-	-	-
A8	1,782	1,707	13,490	20,720	1,782	1,707	93.0	142.9
A9	-1,689	-1,731	-14,711	-6,849	-1,689	-1,731	-101.4	-47.2
A10	743	1,041	8,222	15,523	743	1,041	56.7	107.0
A11	332	313	2,473	6,283	332	313	17.0	43.3
A12	-227	-165	-1,400	4,704	-227	-165	-9.65	32.4
A13	1,462	1,448	-	-	1,462	1,448	-	-
A14[2]	-	-	-	-	-	-	-	-
A15	-1,717	-1,762	-14,974	-8,032	-1,717	-1,762	-103.2	-55.4

[1] Gage not installed
[2] Bad gage
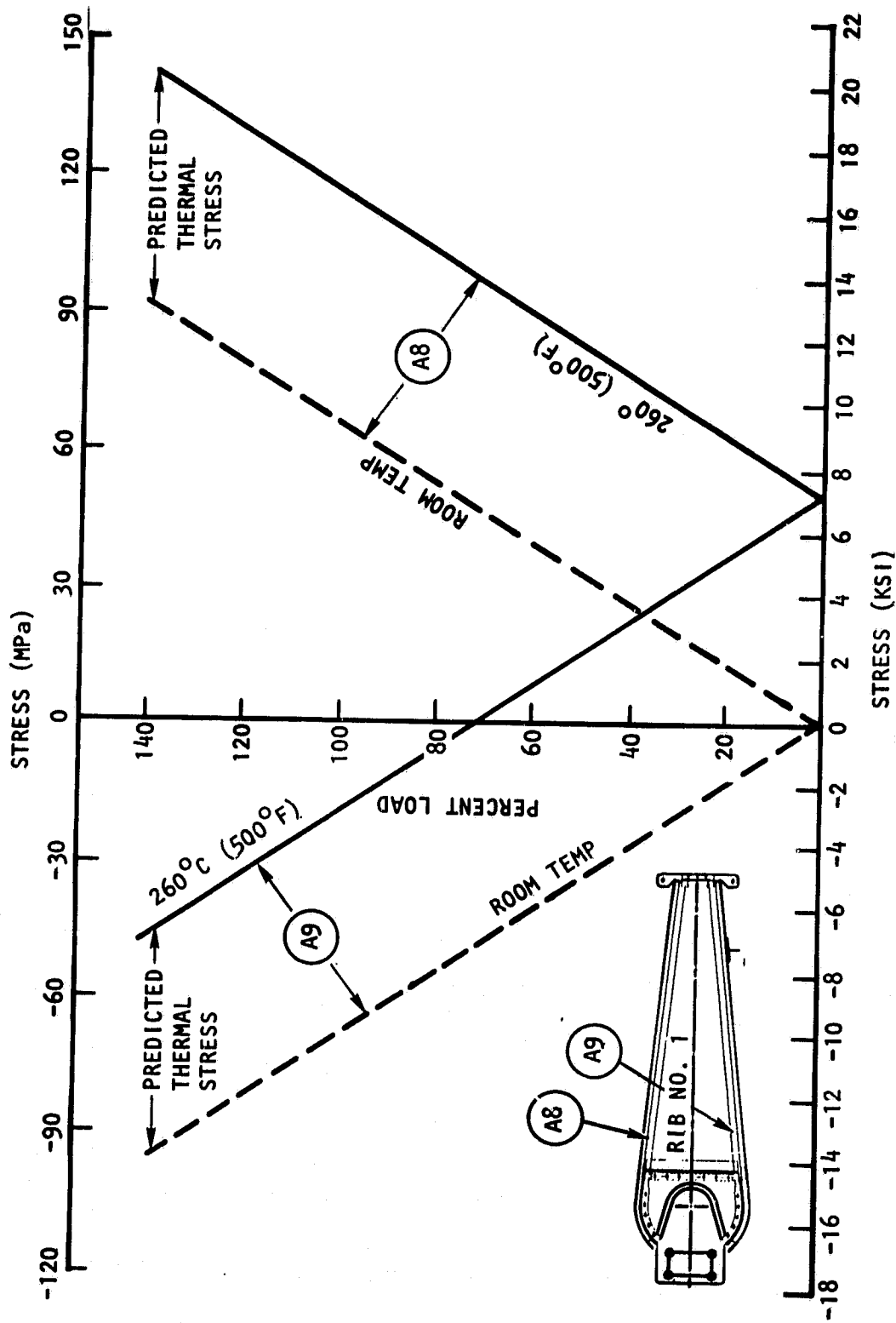
Figure 5-3. Predicted Mechanical and Thermal Stresses in Stability Rib Cap, Elevated Temperature Ultimate Load Test

Table 5-3. Rosette Response During Elevated Temperature Ultimate Load Test

Gage No.	Test Strains(1) (μ cm/cm, μ in./in.)			Predicted Strains (μ cm/cm, μ in./in.)			
	ε_1	ε_2	ε_3	ε_1	ε_2	ε_3	γ_{xy}
R1	665	400	-25	1,743	896	-8	57
R2	514	89	-358	1,460	610	-412	172
R3	608	698	-105	1,281	782	-135	417
R4	-747	-331	113	-1,941	-999	-134	-78
R5	-592	-77	412	-1,413	-422	405	-163
R6	-975	-206	144	-1,249	-352	134	-412
R7	-131	-821	-12	45	-802	-35	-1,614
R8	-948	-2,276	457	-1,134	-2,114	963	-4,057

(1)

$\varepsilon_x = \varepsilon_1$

$\varepsilon_y = \varepsilon_3$

$\gamma_{xy} = (2\,\varepsilon_2 - \varepsilon_1 - \varepsilon_3)$

described in Appendix C. The inspection found no evidence of blistering, cracks, delamination, skin-to-core debonds, or other forms of damage.

5.4 CONCLUSIONS

The 260°C (500°F) environment had minimal effect on the mechanical response of the TDS. The transverse elastic modulus of the $(0_2/\pm45/0)$ cover panel laminate appeared to be reduced by about eight percent. This resulted in slightly larger deflections, and transfer of load to the rib caps resulting in somewhat larger cap stresses. Thermal stresses in the rib caps were not measured during the test, but were predicted to be quite significant, increasing the tensile stress by 53 percent. Thermal effects on the rib web shear stress were negligible.

The analytical predictions were in good agreement with the experimental test results in the high strain areas of the rib caps and webs. As in the room temperature test, those strain gages in the vicinity of the split in the cover panels did not agree well with the predictions. However, the strains in this area were relatively low. The deflected shape of the TDS at elevated temperature was within 10 percent of that predicted. The primary test objective was achieved when the TDS survived ultimate mechanical loads at 260°C (500°F) with no evidence of failure.
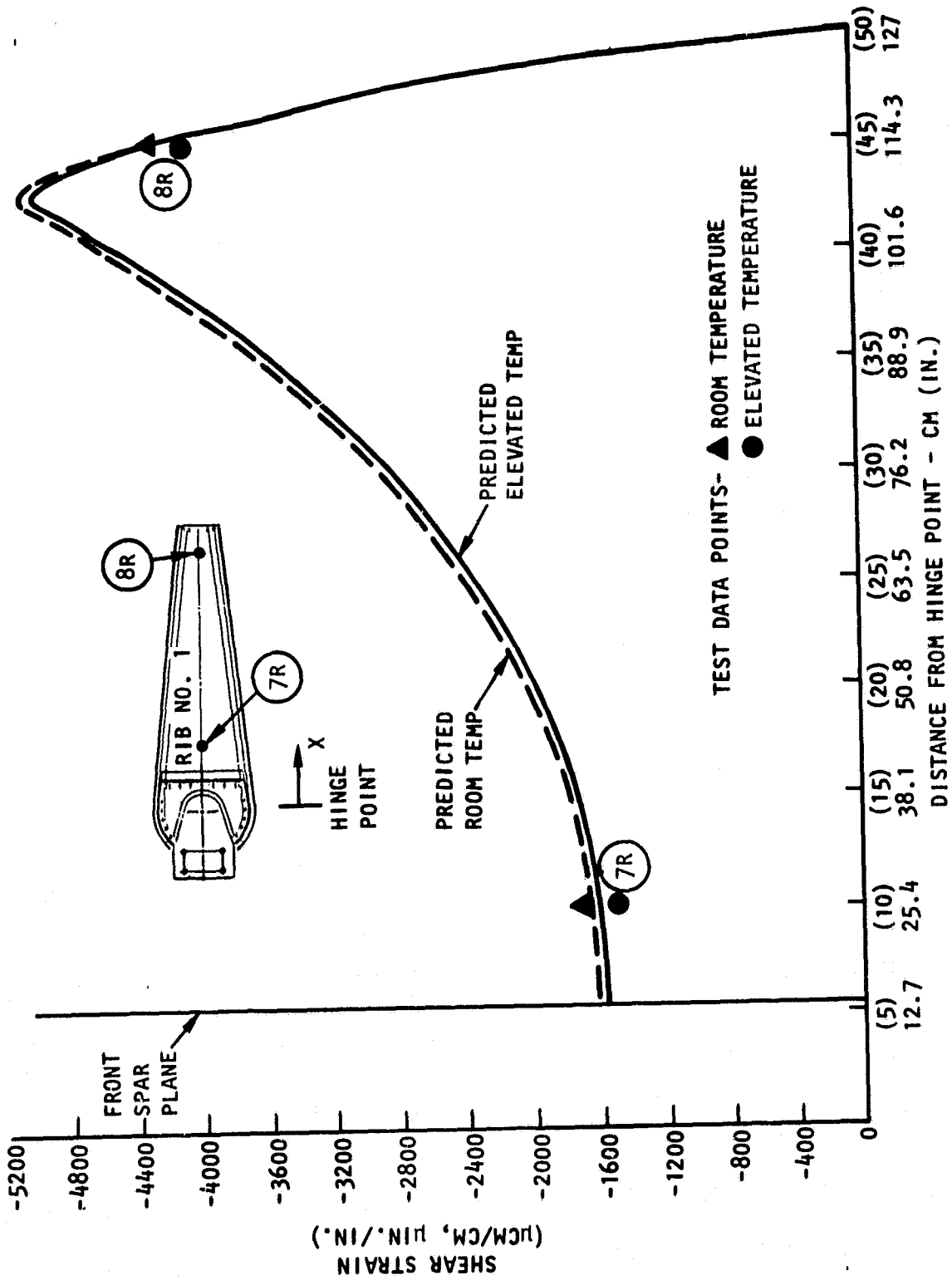
Figure 5-4.   Shear Strain Distribution Along RIB No. 1 Web, Elevated Temperature Ultimate Load Test

6. 400-CYCLE SIMULATED FATIGUE TEST

The Gr/PI body flap technology demonstration segment (TDS) was successfully subjected to 400 limit-load cycles at 260°C (500°F). The primary test objective was achieved; i.e., the TDS sustained mechanical loads simulating four orbiter lifetimes with no evidence of damage. The mechanical response of the TDS was nearly identical during each cycle, indicating no structural degradation because of the loads or temperature. Subsequent NDE inspection of the TDS revealed no anomalies.

The loads used during the previous elevated temperature mechanical load test (Section 5) were ultimate loads; the loads used during the fatigue test were limit loads (ultimate load is 1.4 times larger than limit load). Because the loads used during the fatigue test are proportional to the previous test, the analytical predictions and data correlation presented in Section 5 apply directly to the fatigue test.

6.1 SIMULATED FATIGUE TEST PROCEDURE

With the TDS stabilized at 260°C (500°F), 400 cycles of limit load were applied (Figure 6-1). The load was cycled from 5 percent to 100 percent of limit at the rate of one cycle per minute, with approximately a six-second dwell period at the upper and lower limits. The test data were recorded on the upper load limit on each cycle. The test instrumentation and test setup are described in Section 3.

6.2 SIMULATED FATIGUE TEST RESULTS

As shown in Figure 6-2, the mechanical response of a stability rib cap during the first and last cycle was nearly identical to the response during the previous elevated temperature mechanical load test. For the location of strain gage 8A, refer to Figure 3-6.

The response of the rib cap at gage 8A is shown in Figure 6-3 for all 400 cycles. Data points were taken as the load approached and passed the 100-percent level. Thus, not all data points were taken at precisely 100 percent load, and the curves tend to be erratic. The initial mechanical strain levels can be seen on the left portion of the curve for 0 to 100 percent of limit load, while the final strain levels are on the right portion of the curve.

Many of the strain gages tended to drift with time, as shown in Figure 6-4. The initial and final strain differentials between 0 and 100-percent limit load were similar, which indicates no time-dependent degradation of the structure.
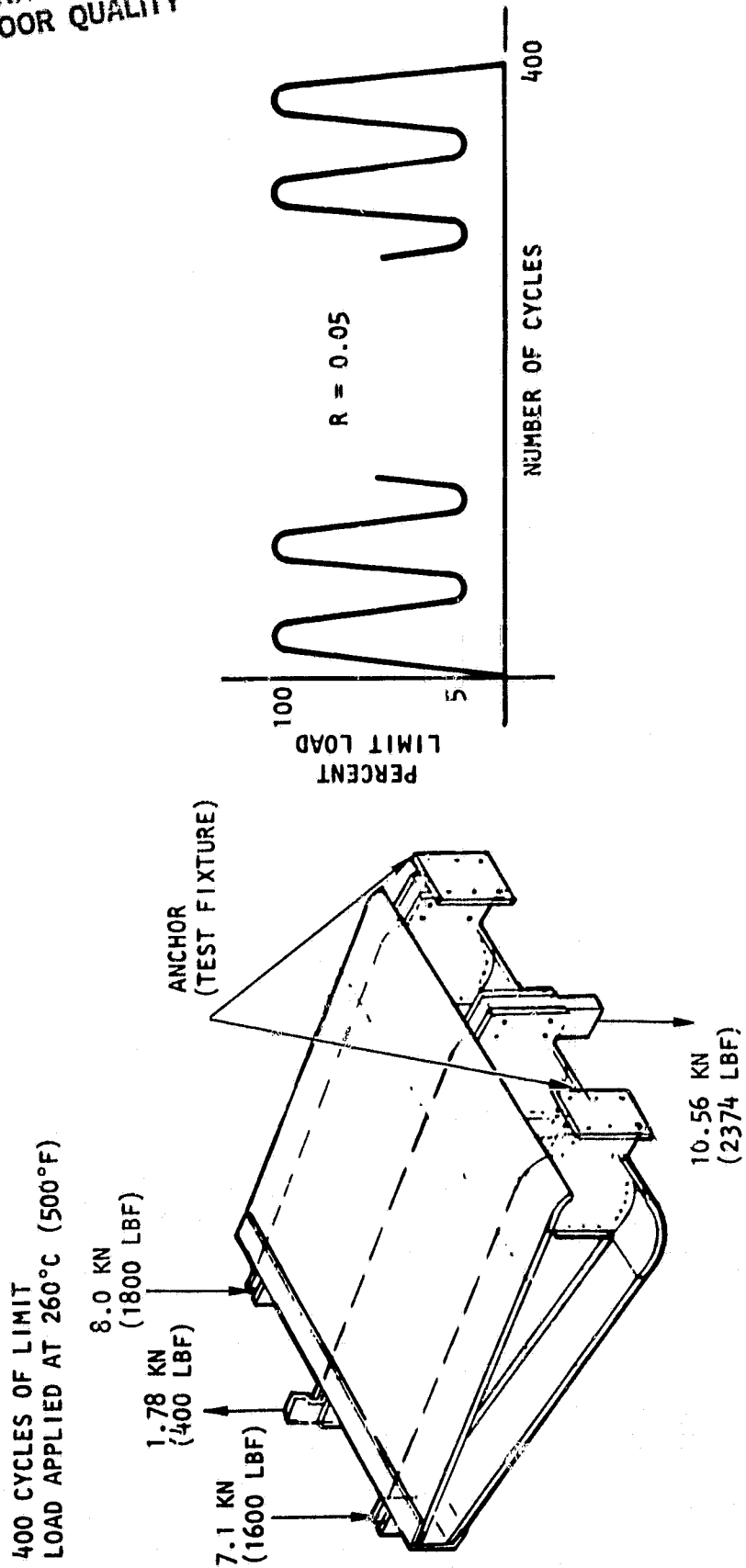
Figure 6-1. Simulated Fatigue Test Loads
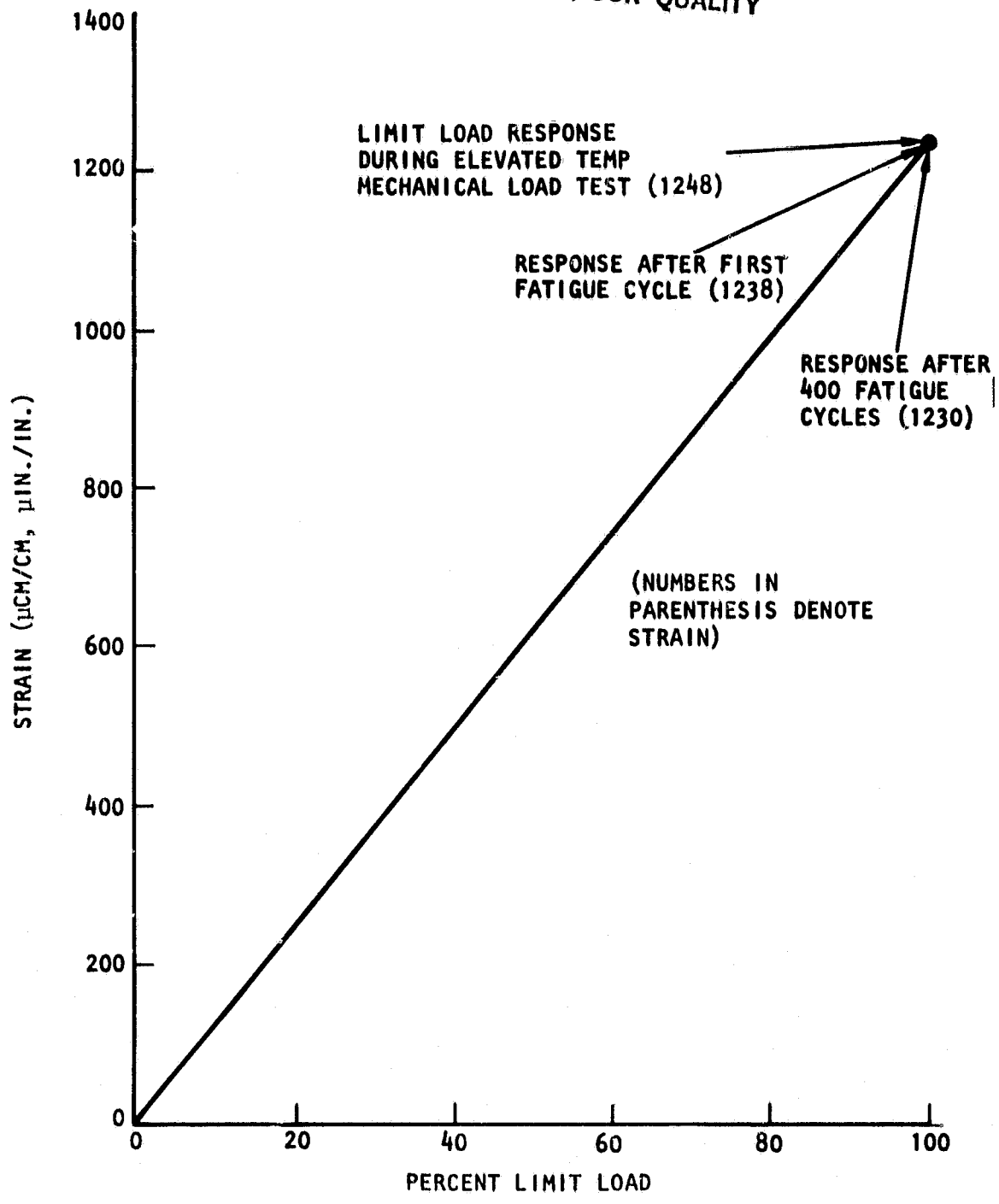
Figure 6-2. Comparison of Stability Rib Cap Response (Gage 8a) at
260°C (500°F) During Elevated Temperature Mechanical Load Test and
400-Cycle Fatigue Test
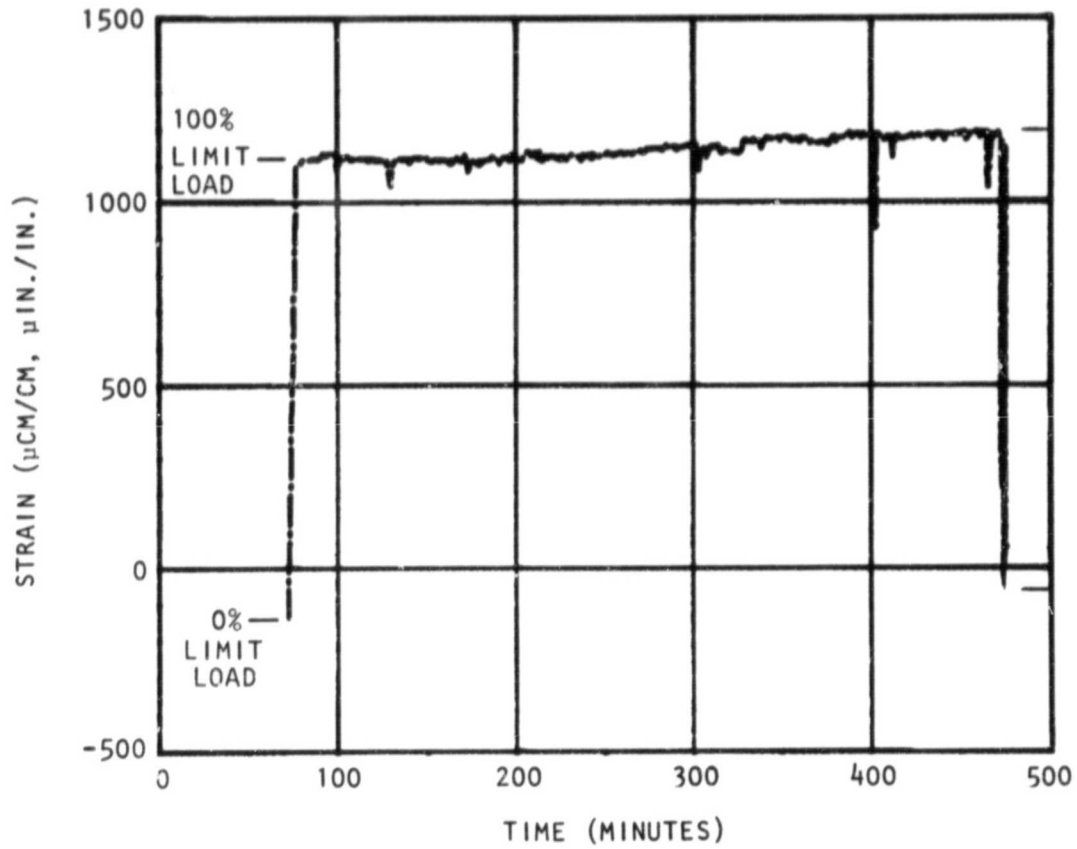
Figure 6-3.   Response of Stability Rib Cap (Strain Gage 8A)
During 400 Cycle Fatigue Test

68
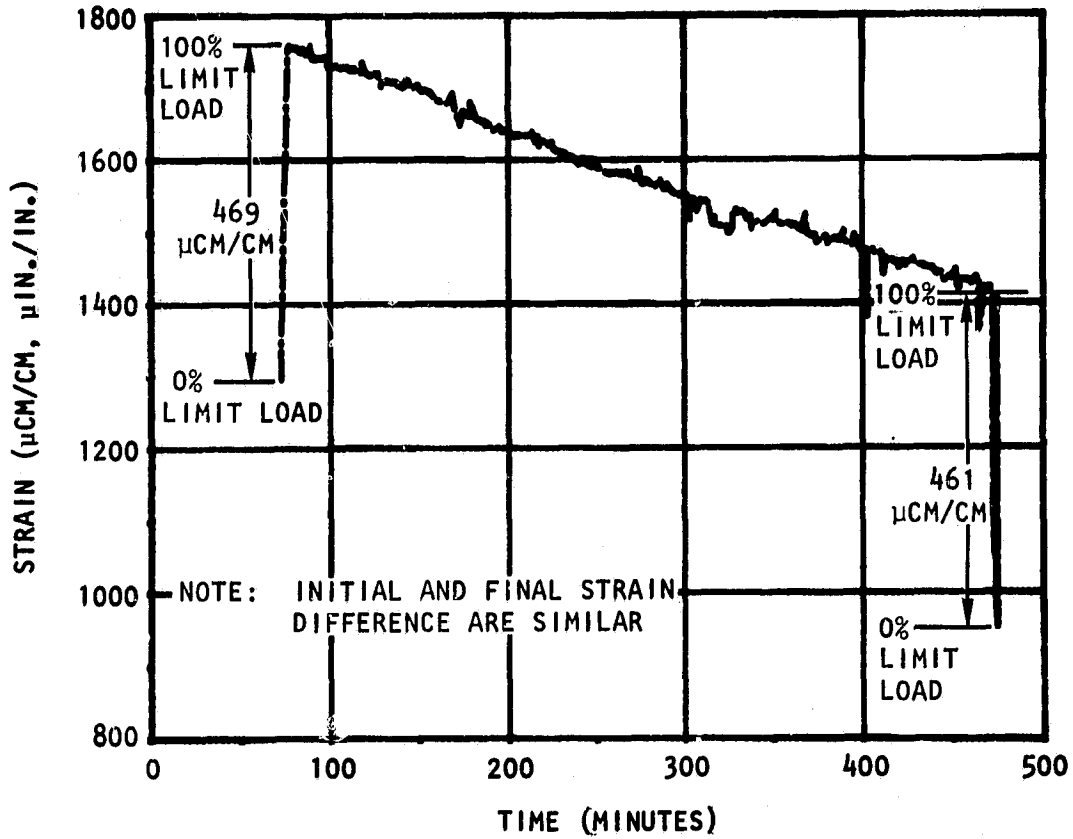
Figure 6-4. Time Dependence Drifting of Strain Gage 3R1 During
400 Cycle Fatigue Test

A typical deflectometer response is shown in Figure 6-5. Most of the deflectometer responses remained constant, while some drifted slightly with time. The deflected shape was identical to the previous test at 260°C (500°F) under limit load.

A typical load cell response is shown Figure 6-6. All load cell responses were constant and within a few percent of the desired load levels throughout the test.

6.3 NDE RESULTS FOLLOWING SIMULATED FATIGUE TEST

The TDS test article was subjected to a thorough NDE inspection after the simulated fatigue test, which used the techniques described in Appendix C. The inspection found no discrepancies due to the 400 limit load cycles at 260°C (500°F).

6.4 CONCLUSIONS

There was no evidence of structural degradation due to the 400 load cycles at elevated temperature. The mechanical response was similar during the first and last cycles, which were, in turn, similar to the previous elevated temperature mechanical load test at limit load (Section 5).
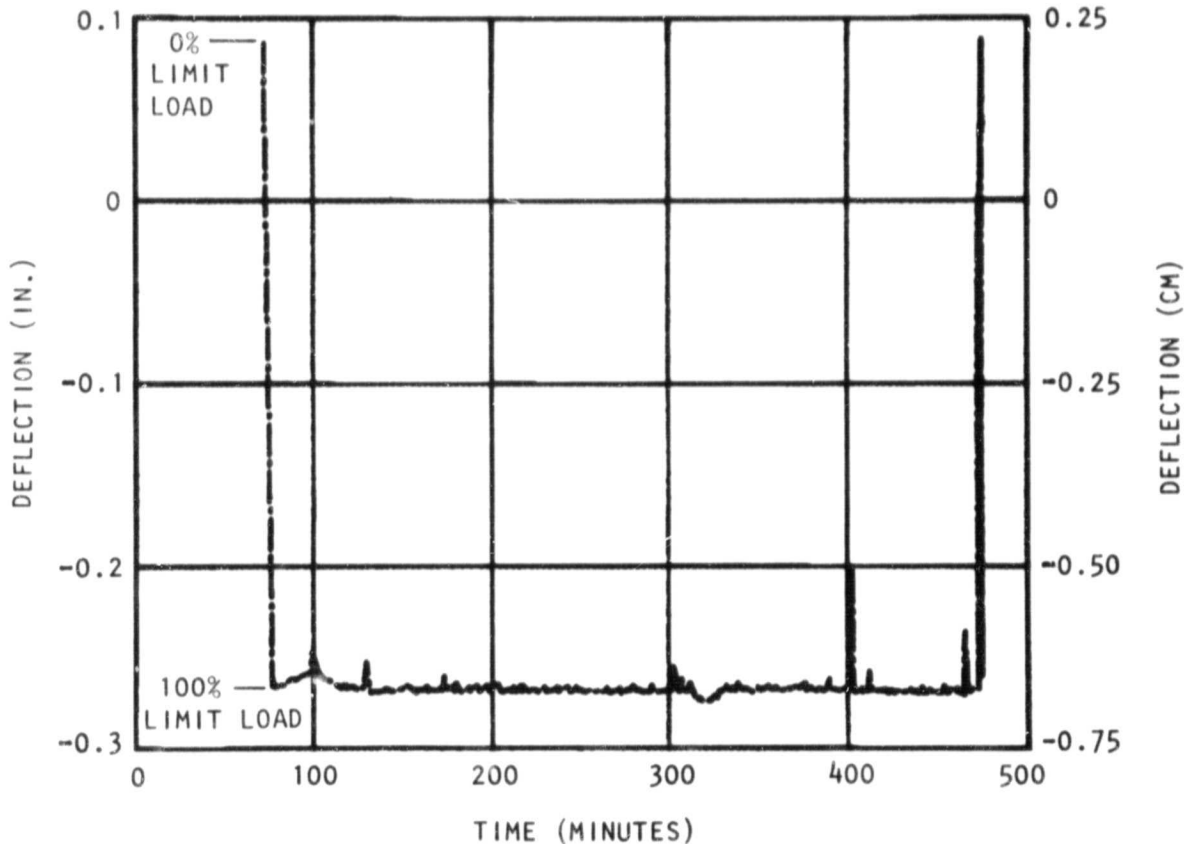
Figure 6-5.   Response of Deflectometer 011 During
400 Cycle Simulated Fatigue Test
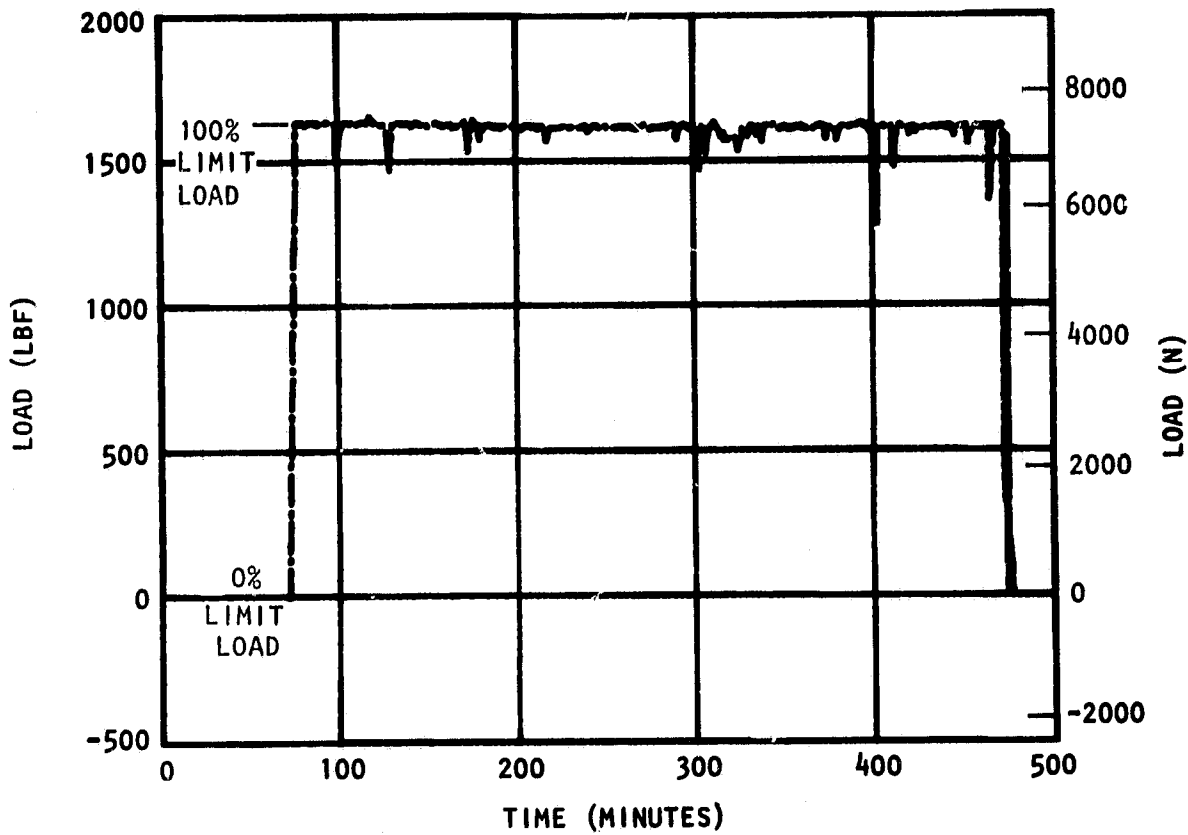
Figure 6-6.   Response of Load Cell No. 1 During
400 Cycle Simulated Fatigue Test

7. THERMAL-CYCLING TEST

The graphite/polyimide (Gr/PI) technology demonstration segment (TDS) was successfully subjected to 125 thermal cycles with temperature extremes from -107 to 315°C (-160 to 600°F). The objectives of the thermal cycling test were verification of the TDS structure under 125 thermal cycles and verification of the analytically predicted thermal response. All test objectives were achieved: there was no evidence of damage to the test article, and the thermal analysis was in excellent agreement with the test data.

The selected thermal cycle (Figure 7-1) was derived by combining two orbiter missions with extreme temperatures. The maximum temperature (315°C, 600°F) occurs only during an abort-once-around (AOA) mission. The minimum temperature (-107 C, -160°F) occurs during a long-cold-soak on-orbit mission. This implies that both limit temperatures are never attained during the same mission.

7.1 THERMAL-CYCLING TEST PROCEDURE

The TDS test article was subjected to 125 thermal cycles, with the temperatures ranging from -107 to 315°C (-160 to 600°F). The test setup is described in detail in Section 3. Nitrogen gas was piped through the spray-bar distribution system for cooling the structure. The initial four cycles were performed with only hot air through the spray bars for heating. The maximum temperature of 315°C (600°F) was attained; however, the time required would have substantially extended the test schedule and increased the cost. Quartz radiant heat lamps were added to the lower surface for thermal augmentation above 232°C (450°F), and the time required for a complete cycle was compressed to approximately 70 minutes. The thermal response of the outer face sheets of the upper and lower cover panels during a typical thermal cycle is shown in Figure 7-2. A maximum thermal gradient between the upper and lower panels of 27°C (80°F) was obtained when the quartz lamps were turned on.

Strain gage deflection and thermocouple data were recorded for all cycles. The structural response was identical during each of the 125 cycles, indicating no structural changes or degradation. However, few strain gages were still operable by the end of the test due to the 315°C (600°F) environment.

7.2 THERMAL MATH MODELS AND TEST DATA CORRELATION

Two different thermal math models (TMM's) were constructed to perform test data correlation for selected areas of the TDS. A one-dimensional cover-to-cover model was developed to predict the response of the cover panels between stability ribs. A two-dimensional cover-rib-cover model was developed to predict the response of the cover panels, including a stability rib. These models
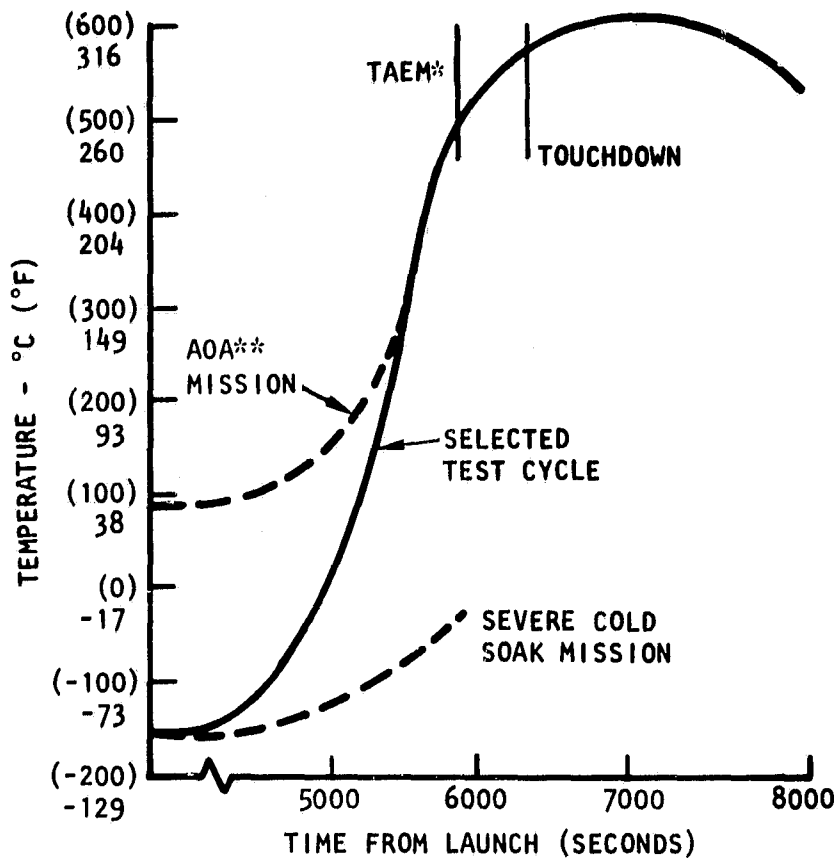
Figure 7-1. Body Flap Reentry Temperature Range
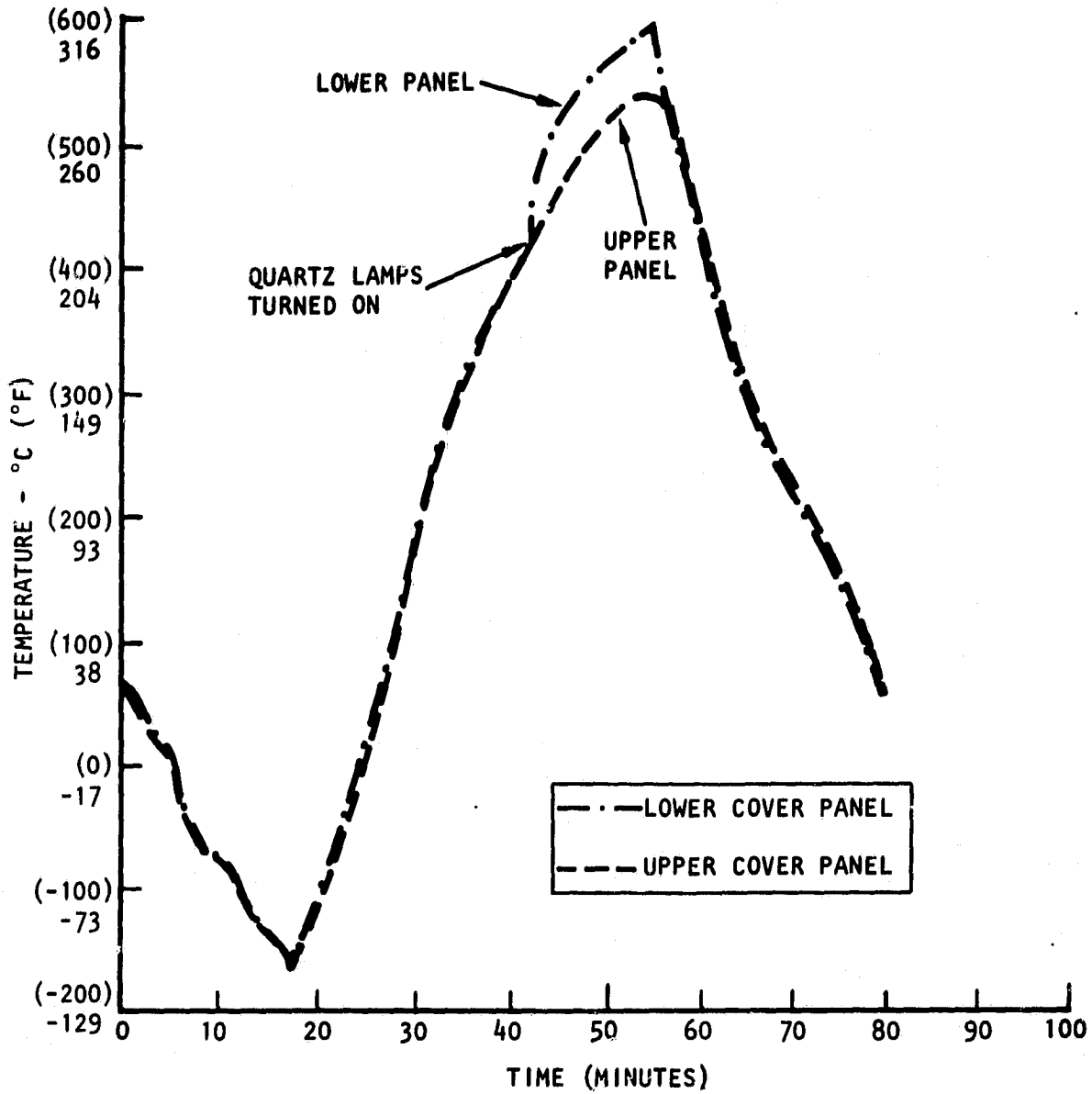
Figure 7-2.   Thermal Cycle Temperatures for Upper & Lower Cover Panels

are described in detail in Appendix D. The initial predictions of these models did not agree well with the test data. However, the actual thermal properties of the graphite/polyimide, glass/polyimide, and polyimide adhesives were not well known. An adjustment of the emissivity properties of the skin-to-core adhesive resulted in better modeling of the heat transfer between the sandwich panel face sheets.

The TMM's were used to correlate most of the 33 thermocouples placed on the TDS. Examples of these test correlations runs are shown in Figures 7-3 and 7-4. Figure 7-3 shows the predicted and actual response of thermo-couple T11, which is located on the inner face sheet of the upper cover panel (Figure 3-4). The one-dimensional cover-cover TMM was used for this example. Figure 7-4 shows the predicted and actual response of thermocouple T24, which is located on the stability rib web midway between the cover panels (Fig-ure 3-7). The two-dimensional cover-rib-cover TMM was used for this example, As can be seen from these examples, the analysis accurately predicted the tem-perature profiles.

7.3 NDE RESULTS AFTER THERMAL CYCLING TEST

The TDS test article was subjected to a thorough NDE inspection after the thermal cycling test. The techniques described in Appendix C were used. The inspection found no discrepancies or anomalies due to the 125 thermal cycles.

7.4 CONCLUSIONS

The primary goals of the thermal cycling test program were achieved, i.e., the TDS sustained the thermal environments with no evidence of damage, and the analytical predictions were in excellent agreement with measured response. However, the analytical models were based on estimated thermal properties. For future studies, tests should be run to determine the actual thermal con-ductivities and emissivities of the graphite/polyimide, glass/polymide, and face-sheet adheseive (FM-34). With these data, the models could become even more effective.
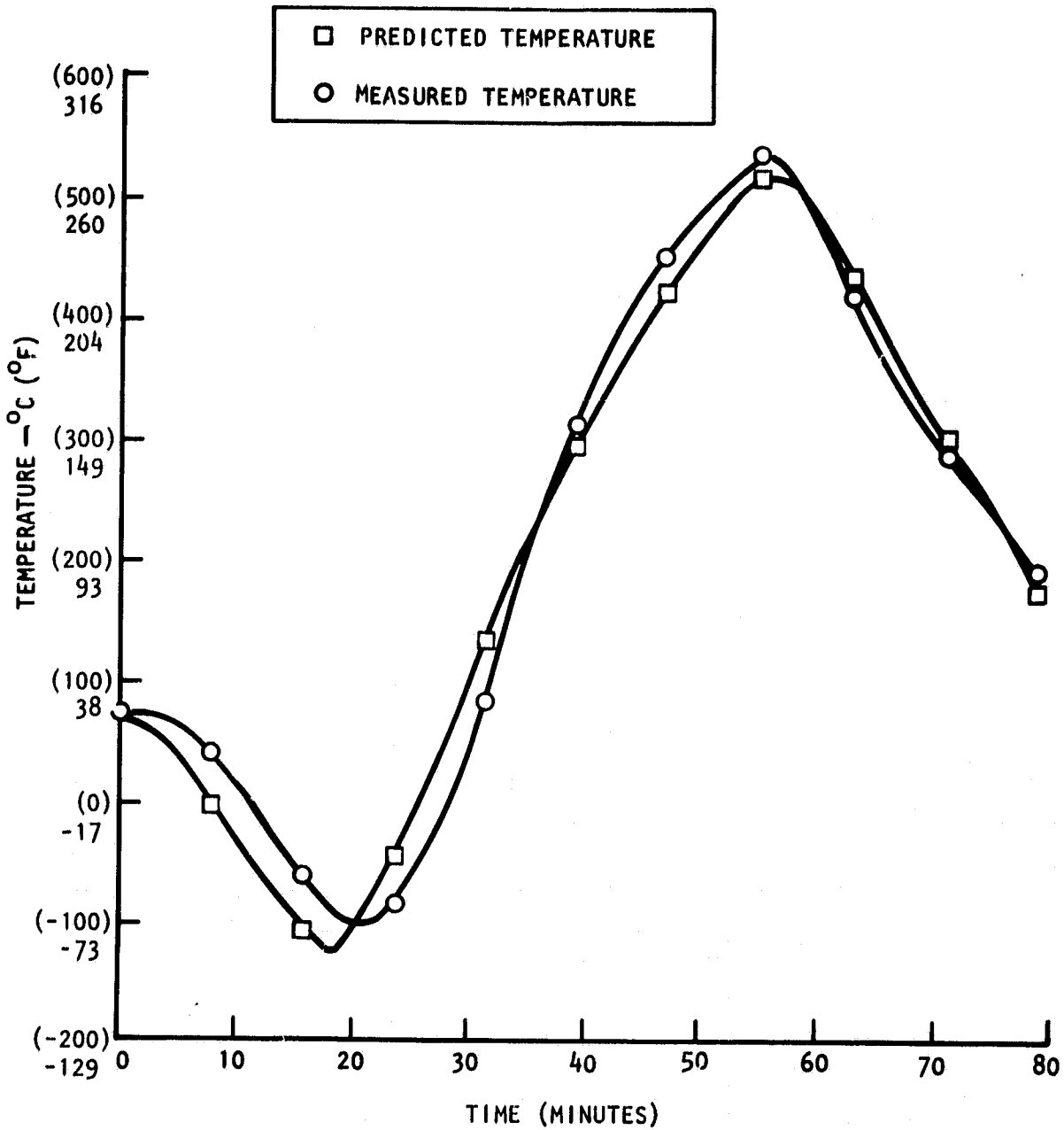
Figure 7-3. Comparison Between Predicted and Measured Temperature History at Thermocouple T11 (Refer to Figure 3-5)
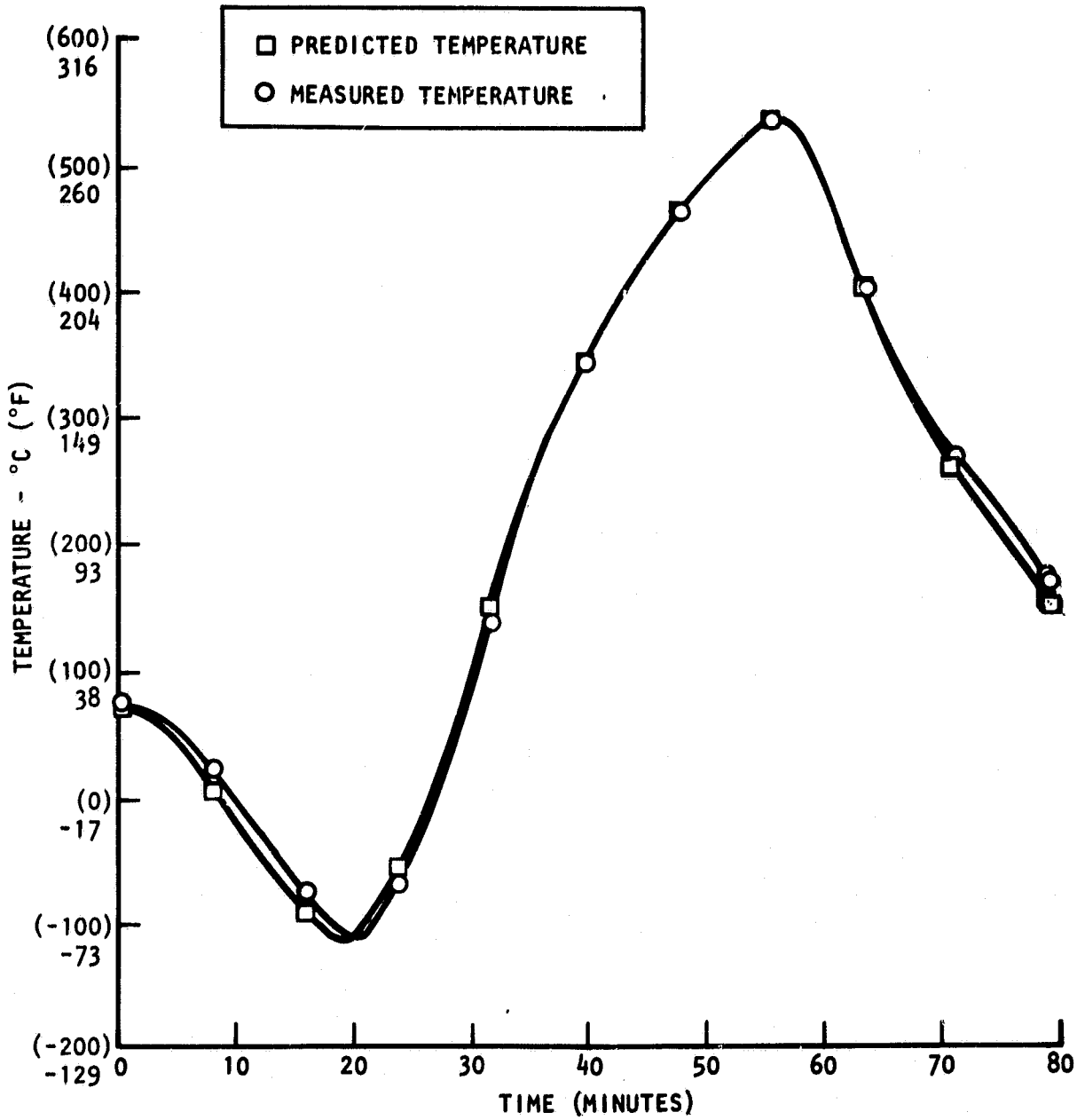
Figure 7-4. Comparison Between Predicted and Measured Temperature
History at Thermocouple T24 (Refer to Figure 3-7)

8. REPEATED ELEVATED TEMPERATURE ULTIMATE LOAD TEST

The graphite/polyimide (Gr/PI) technology demonstration segment (TDS) was
again successfully subjected to ultimate mechanical loads at 260°C (500°F). The
objective of the test was to ensure that the previous tests, namely the simulated
fatigue and thermal cycle tests, had not degraded the structure. The structural
response during this final test was nearly identical to that of the previous
elevated temperature ultimate load test. Thus there was no indication of
structural degradation from the 400 limit load cycles at 260°C (500°F) and 125
thermal cycles between -107 and 315 C (-160 and 600°F). After the test, NDE
inspection found no evidence of damage.

8.1 ELEVATED TEMPERATURE ULTIMATE LOAD TEST PROCEDURE

The TDS was heated to 260°C (500°F), and the temperatures were allowed to
stabilize. The test loads shown in Figure 4-1 were then applied in increments
to ultimate load or 140 percent of limit load. Instrumentation readings were
taken after each increment. The majority of the strain gages did not survive
the extended period at 315°C (600°F) during the thermal cycling test.

8.2 ELEVATED TEMPERATURE ULTIMATE LOAD TEST RESULTS

The response of the TDS to mechanical loads at 260°C (500°F) was nearly
identical to the previous elevated temperature ultimate load test (Section 5).
The deflection data for the initial and final tests are compared in Table 8-1.
As shown in Figure 8-1 and Table 8-1, the deflections were slightly larger
during the second test for most of the deflectometers.

The axial strain gage response is presented in Table 8-2. Only five of
the original 13 gages were in operation during the second test. The remaining
gages did not survive the 315°C (600°F) exposure during the thermal cycling
test. The surviving gages were in excellent agreement with strain response
during the first elevated temperature test (Figure 8-2). Of 24 strain channels
from the 8 rosette gages, only two channels survived. These channels were
also in agreement with the first test.

8.3 NDE RESULTS AFTER ELEVATED TEMPERATURE TEST

After this final test, the TDS was removed from the test fixture to allow
better access for NDE inspection. The test article was subjected to a rigorous
inspection with the techniques described in Appendix C. The inspection found
no evidence of damage.

Table 8-1. TDS Deflection Comparison--Elevated
Temperature Ultimate Load Tests

Transducer No.	Deflections First Test		Deflections Second Test	
	cm	inches	cm	inches
D1	-1.72	-0.677	-1.78	-0.699
D2	-1.19	-0.468	-1.24	-0.489
D3	-0.37	-0.146	-0.36	-0.143
D4	-0.45	-0.177	-0.46	-0.181
D5	-0.59	-0.234	-0.60	-0.235
D6	-0.60	-0.236	-0.60	-0.235
D7	-0.51	-0.202	-0.51	-0.199
D8	-1.25	-0.494	-1.23	-0.485
D9	-1.23	-0.484	-1.33	-0.523
D10	-1.20	-0.474	-1.14	-0.449
D11	-1.20	-0.474	-1.15	-0.453
D12	-1.20	-0.474	-1.24	-0.489
D13	-1.94	-0.762	-1.97	-0.774
D14	-1.80	-0.707	-1.86	-0.732
D15	-1.72	-0.679	-1.78	-0.702
D16	-1.76	-0.691	-1.79	-0.703
D17	-1.84	-0.724	-1.85	-0.729
D18	-0.08	-0.032	-0.069	-0.027
D19	-0.17	-0.065	-0.124	-0.049
D20	-0.11	-0.044	-0.089	-0.035

8.4 CONCLUSIONS

The TDS response during the final ultimate load test was nearly identical to the first elevated temperature ultimate mechanical load test. Thus, no structural degradation due to the endurance testing was indicated. Subsequent NDE inspection revealed no anomalies.

A significant increase in the confidence in large bonded graphite/polyimide structure resulted from the successful completion of the final elevated temperature ultimate load test.
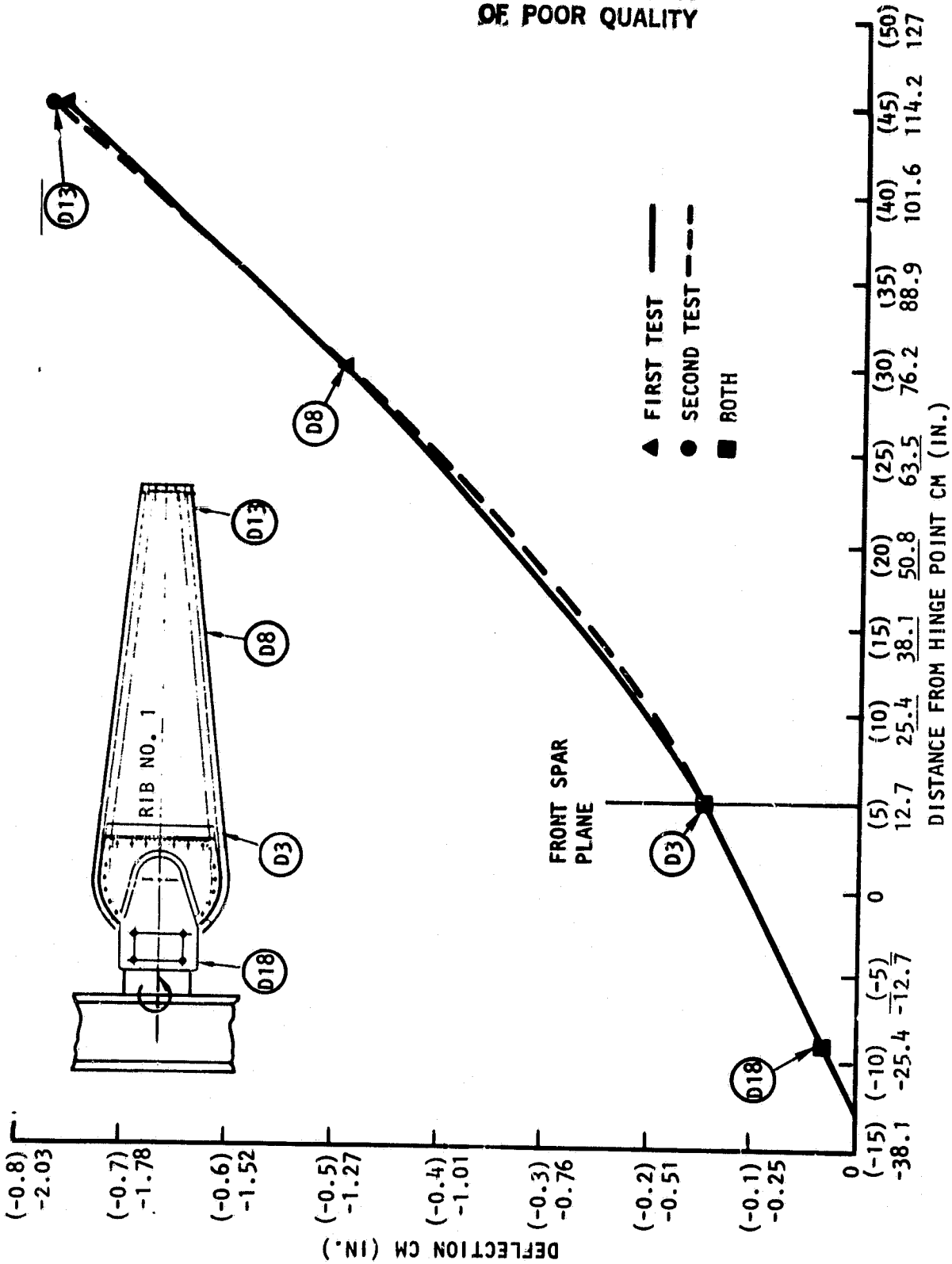
Figure 8-1. TDS Deflection Comparison — Elevated Temperature
Ultimate Load Tests

Table 8-2. TDS Axial Strain Gage Response
Comparison--Elevated Temperature
Ultimate Load Tests

Gage No.	First Test Strain (μ cm/cm, μ in./in.)	Second Test Strain (μ cm/cm, μ in./in.)
A1	559	443
A2	2,050	2,023
A3	-884	*
A4	-1,439	*
A5	1,027	*
A6	-1,060	*
A7[1]	-	-
A8	1,782	1,821
A9	-1,689	-1,805
A10	743	*
A11	332	*
A12	-227	*
A13	1,462	*
A14[2]	-	-
A15	-1,717	-1,812

[1]Not installed
[2]Bad gage
  *Gage did not survive thermal cycle test.
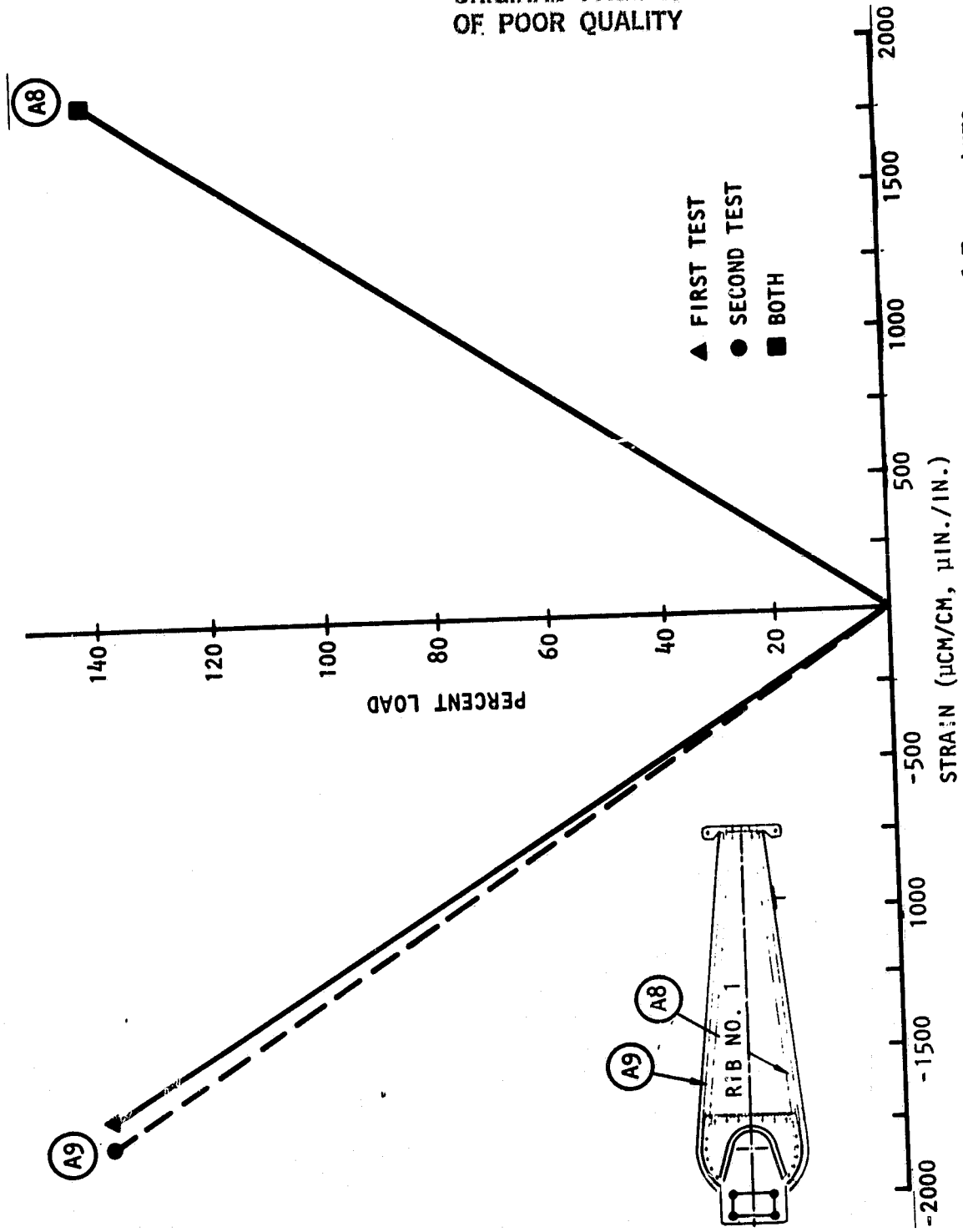
Figure 8-2. TDS Axial Strain Gage Response Comparison — Elevated Temperature
Ultimate Load Tests

83

9. CONCLUSIONS

Results of the graphite/LARC-160 technology demonstration segment (TDS) test program show that all test objectives were achieved. The TDS was successfully subjected to mechanical loads and thermal environments simulating 100 space Shuttle orbiter missions, demonstrating that Gr/PI composite technology readiness has been established. Analytical models, which provided good test data correlation, can now be used with confidence in the design of future Gr/PI composite structures. Ultrasonic and visual NDE techniques found no evidence of delamination, cracks, debonds, or other forms of damage in the TDS, demonstrating the ability of Celion/LARC-160 graphite/polymide to sustain simulated Space Shuttle orbiter thermal and mechanical loads. Specific conclusions from this test program are presented below.

1. Successful completion of the room temperature ultimate load test was the first major step toward verification of Gr/PI technology (design, analysis, and fabrication).

2. Successful completion of the ultimate load test at 260°C (500°F) verified the elevated temperature capability of bonded Gr/PI honeycomb structure.

3. Successful completion of the 400 limit load cycles at 260 C (500°F) verified the durability of Gr/PI and demonstrated the ability of bonded Gr/PI structure to withstand 100 orbiter missions.

4. Successful completion of 125 thermal cycles [-107 to 315°C (-160 to 600°F)] demonstrated the ability of Gr/PI structure to survive thermal extremes representing 100 orbiter missions and verified the thermal analysis methodology.

5. Successful completion of the repeated elevated temperature ultimate load test demonstrated that the previous endurance testing had not degraded the structure; hence, confidence in bonded Gr/PI materials and structure technology was increased.

10. REFERENCES

1. Morita, W.H., and S.R. Graves, Celion/LARC-160 Technology Overview and Space Shuttle Orbiter Applications. 14th National Technical Conference, Society for the Advancement of Materials and Process Engineering (October 1982).

2. Morita, W.H., and S.R. Graves. Feasibility of Direct-Bond Ceramic Thermal Protection System Tile on Graphite/Polyimide Structure. 26th National Symposium, Society for the Advancement of Material and Process Engineering (April 1981).

3. Morita, W.H., and S.R. Graves. The Shuttle Orbiter Structural Weight Reduction Potential and Advanced Composites Application. 40th Annual Conference, Society of Allied Weight Engineers, Inc. (May 1981).

4. Graves, S.R., and W.H. Morita. Analysis, Design and Test of a Graphite/ Polyimide Shuttle Orbiter Body Flap Segment. 14th National Technical Conference, Society for the Advancement of Materials and Process Engineering (October 1982).

5. Frost, R.K., et al. Development and Demonstration of Manufacturing Processes for Fabricating Graphite/LARC 160 Polyimide Structural Elements. NASA CR-165809 (January 1982).

6. Frost, R.K., and D.H. Wykes. Fabrication of Bonded Graphite/Polyimide Structures for Advanced Aerospace Applications. 14th National Technical Conference, Society for the Advancement of Materials and Process Engineering (October 1982).

APPENDIX A. COMPOSITE BODY FLAP ANALYSIS

The graphite/polyimide (Gr/PI) technology demonstration segment (TDS) is a full-scale segment of the composite body flap concept. The TDS test loads defined in Section 2 were based on actual body flap flight conditions and were meant to simulate the body flap stress state. This appendix presents the composite body flap loads and analysis that form the basis for the TDS test program.

State-of-the-art analysis techniques have been used to predict the composite body flap performance in projected aerodynamic, thermal, and acoustic environments. A NASTRAN finite element model was developed to determine the structural deflections and internal stress state induced by the aerodynamic and thermal loads. Incorporating more than 1,000 nodes, the NASTRAN model (Figure A-1) was updated from an aluminum body flap model to reflect the geometry and anisotropic properties of the composite body flap (Section 2). The body flap is designed to withstand the Space Shuttle sonic environment and to be compatible with the direct-bond RSI (reusable surface insulation) concept. Thus, the body flap is designed for minimum deflections under limit loads. Because of this deflection requirement, static stresses in the body flap are generally very low.

To model the temperature distribution in the body flap, a two-dimensional thermal model was developed to account for the 315°C (600°F) Gr/PI structural allowable and the anisotropic thermal characteristics of the composite material. Figure A-2 presents results of the thermal analysis at a point near the center of the composite body flap between two stability ribs. The upper surface is subjected to 649°C (1,200°F) during launch, and the 1.0-cm-thick (0.4-in.) HRSI (high-temperature reusable surface insulation) limits the structure temperature to 260°C (500°F). During reentry, the lower surface is subjected to 1,288°C (2,350°F), and the 6.1-cm (2.4-in.) HRSI limits the structure temperature to 315°C (600°F). This maximum structural temperature occurs due to heat soak back after the orbiter has landed.

Location of the body flap relative to the orbiter main engines (Figure A-3) makes acoustic fatigue a significant potential failure mode. An acoustic fatigue analysis methodology was developed to ascertain the suitability of various candidate designs to withstand the body flap sonic environment, where overall sound pressure levels during launch may be as high as 165 dB. A simplified theory for acoustic response was used in the main box cover sizing. It was assumed that, for a sonically excited system, a single mode, and corresponding resonant frequency, predominates in the frequency range of interest. In this case, it is the fundamental frequency of the body flap cover panel which is modeled as an orthotropic plate with clamped and simply supported edges.

PRECEDING PAGE BLANK NOT FILMED

NOTE: BODY FLAP AND LOADS ARE SYMMETRIC,
THEREFORE, ONLY HALF OF BODY FLAP
IS MODELED.
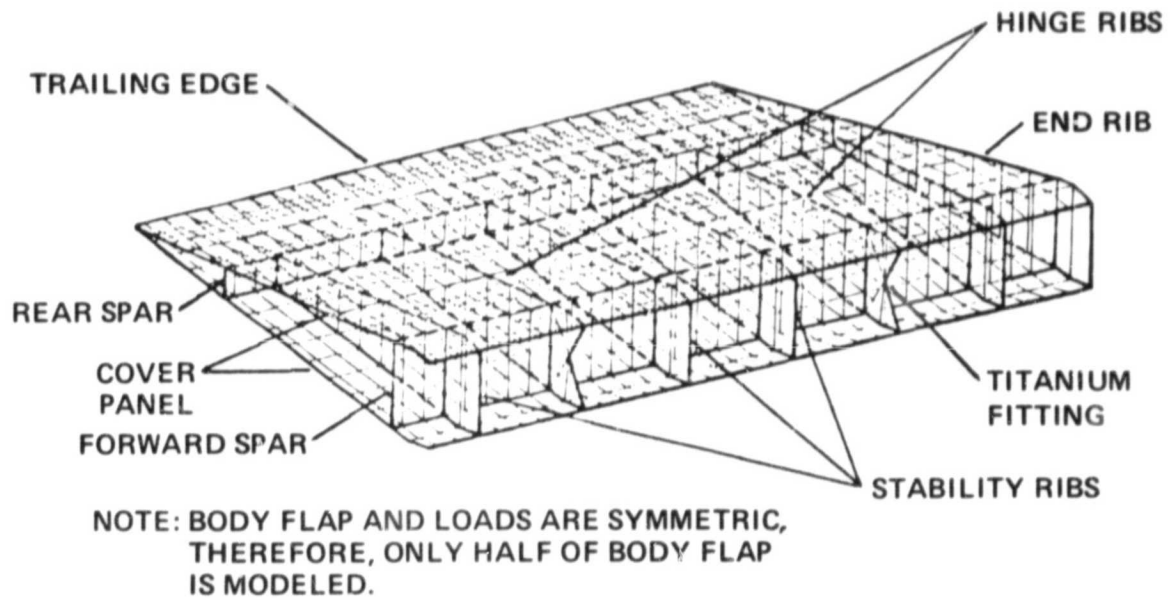
Figure A-1. Composite Body Flap NASTRAN Model

MAX TEMP = 649°C (1200°F) AT T = 5 SEC

0.4 IN.

1.0 CM

HRSI

UPPER HONEYCOMB COVER PANEL

OUTER FACE SHEET

TAEM

MAX TEMP 1288°C (2350°F) AT T = 5000 SEC

2.4 IN.

6.1 CM

HRSI

LOWER HONEYCOMB COVER PANEL

OUTER FACE SHEET

ENTRY

TOUCHDOWN

TEMPERATURE (°C)

TEMPERATURE (°F)

TIME (SECONDS)
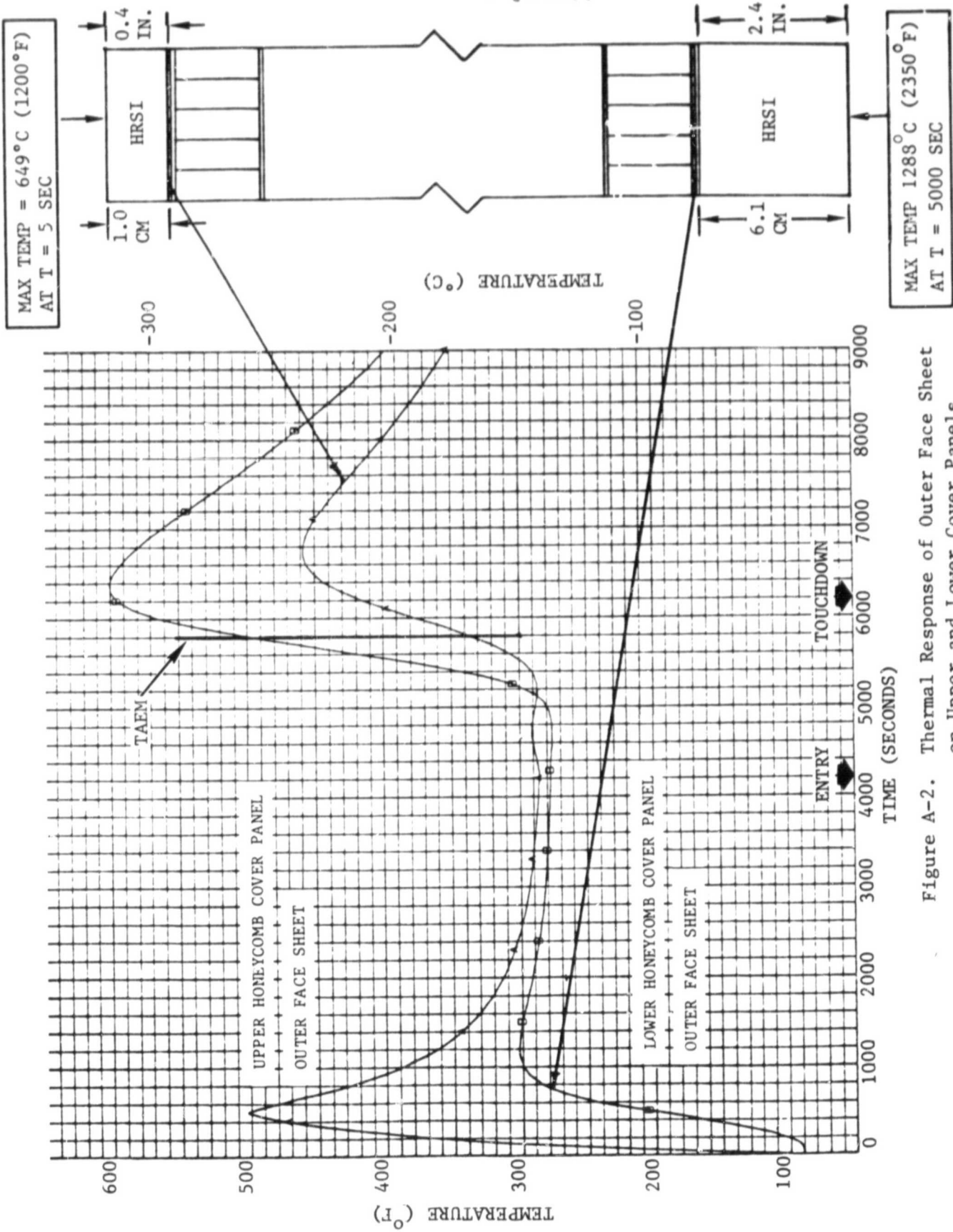
Figure A-2. Thermal Response of Outer Face Sheet on Upper and Lower Cover Panels
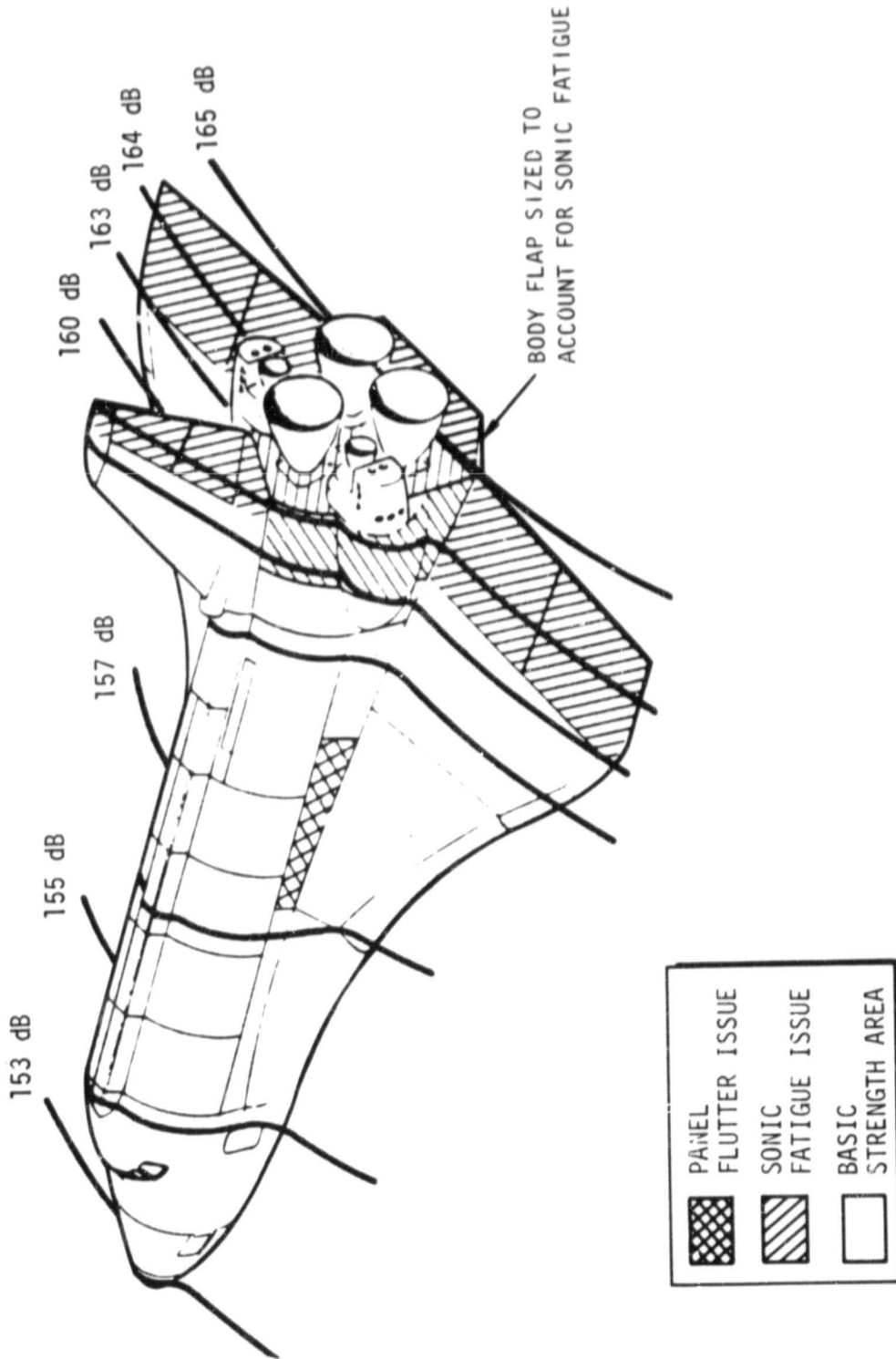
Figure A-3. Acoustically Driven Areas - Liftoff Critical

165 dB
164 dB
163 dB
160 dB
157 dB
155 dB
153 dB

BODY FLAP SIZED TO
ACCOUNT FOR SONIC FATIGUE

PANEL
FLUTTER ISSUE

SONIC
FATIGUE ISSUE

BASIC
STRENGTH AREA

A.1 COMPOSITE BODY FLAP LOADS AND STRESS ANALYSIS

The composite body flap NASTRAN model (Figure A-1) has been continually updated, refined, and revised since the preliminary analysis in 1979. In 1981, the NASTRAN model was updated to incorporate the latest design, material properties, and better modeling techniques. The analyses were based on the latest Shuttle Orbiter V5.4 loads. Out of the approximatlely thirty V5.4 loading conditions, a preparation-for-landing condition (No. 712516) is generally the most critical. It consists of air loads at TAEM (terminal area energy management) steady-state pitch condition TA251, a collapsing pressure of 14.271 kN/m^2 (2.07 psi), and temperature distribution T103. The resulting verification hinge support loads are shown in Figure A-4. The temperature profiles of the metal body flap (T103) were not applied to the composite body flap. Instead, new temperatures were calculated in which the thermal properties of the high-temperature Gr/PI composite were used.

The material properties used in the composite body flap analysis are presented in Appendix B. A comparison of the baseline aluminum body flap and composite body flap stress levels for the TAEM condition for selected components is presented in Table A-1, which illustrates that the static stress levels are very low in comparison with the material allowables. Thus, failure of the body flap under static loads is not anticipated.
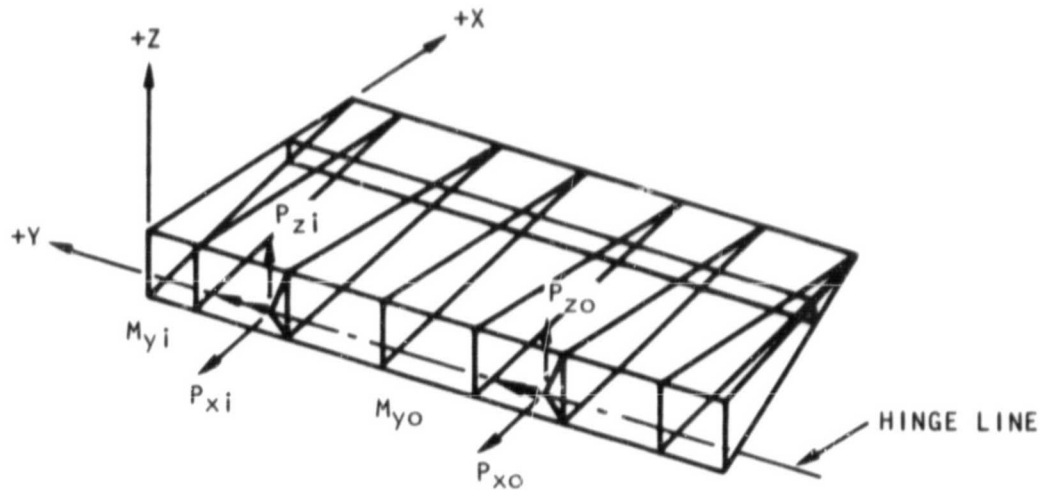
CONDITION NO.	P_{xi} KN (LB)	P_{zi} KN (LB)	M_{yi} NM (IN.-LB)	P_{xo} KN (LB)	P_{zo} KN (LB)	M_{yo} NM (IN.-LB)
712516	17.6 (3,950)	-55.3 (-12,432)	52,562 (465,240)	-15.3 (-3,447)	-76.2 (-17,136)	63,153 (558,982)

Figure A-4.   Space Shuttle Body Flap V5-4A Verification Support Loads

Table A-1. Predicted Body Flap Stress Levels Ultimate Load Condition 712516 - MN/m^2 (ksi)

Body Flap Component	Baseline Aluminum Design			Gr/PI Composite Design			Gr/PI Material Allowable			Composite Design Margin of Safety		
	σ_{max}	σ_{min}	τ_{max}	σ_{max}	σ_{min}	τ_{max}	σ^{tu}	σ^{cu}	τ_{max}	σ_{max} ms	σ_{min} ms	τ_{max} ms
Stability rib cap	21.3 (3.1)	-30.9 (-4.5)	--	137.1 (19.9)	-38.6 (-5.6)	--	614 (89)	558 (81)	--	3.5	13.5	--
Stability rib web	--	--	32.8 (4.8)	--	--	41.4 (6.0)	--	--	414 (60)	--	--	9.0
Hinge rib cap	130.3 (18.9)	-132.1 (-19.2)	--	287.6 (41.7)	-207.5 (-30.1)	--	614 (89)	558 (81)	--	1.1	1.7	--
Hinge rib web	--	--	84.0 (12.2)	--	--	141.0 (20.4)	--	--	414 (60)	--	--	1.9
Front spar cap	68.6 (9.9)	-116.8 (-16.9)	--	9.7 (1.4)	-24.1 (-3.5)	--	614 (89)	558 (81)	--	High	High	--
Front spar web	--	--	47.3 (6.9)	--	--	66.6 (9.7)	--	--	310 (45)	--	--	3.6
Rear spar cap	71.4 (10.4)	-91.7 (-13.3)	--	5.7 (0.84)	-18.3 (-2.7)	--	614 (89)	558 (81)	--	High	High	--
Rear spar web	--	--	69.4 (10.1)	--	--	69.4 (10.1)	--	--	310 (45)	--	--	3.5
Honeycomb covers*	209.4 (30.4)	-187.2 (-27.2)	102.3 (14.8)	176.7 (25.6)	-183.4 (-26.6)	110.0 16.0	1,000 (145)	758 (110)	275 (40)	4.7	3.1	1.5

*Maximum values at different points

APPENDIX B. TECHNOLOGY DEMONSTRATION SEGMENT NASTRAN MODEL

The TDS NASTRAN finite element model shown in Figure B-1 was used for the structural analysis. The analytical predictions made prior to the test did not agree with the test data. The original NASTRAN model was relatively simple, having less than 350 nodes. This simple NASTRAN model was reviewed and several changes were made, as follows:

a. The forward support area model was extended to the steel fixture.

b. The model was highly refined along Rib No. 1 where much of the test instrumentation was located.

c. Latest material properties data (Table B-1) was used.

d. The cut in the cover panel at the front spar was modeled.

e. All input data was reviewed and numerous small changes were made.

The final version of the model was relatively complex, having over 1,000 nodes. Good data correlation was achieved, as indicated in Sections 4 and 5. The TDS NASTRAN model is described in detail below.

A NASTRAN finite element analysis of the TDS structure was performed to characterize its behavior during the static mechnical testing as well as to ensure structural adequacy. The NASTRAN model was used to define the loading conditions that would subject the TDS to stress levels equivalent to those in the composite body flap. The loading scheme, shown in Figure B-1, consists of concentrated vertical loads applied at the aft end of each stability rib and at the forward end of the center rib. The outer ribs are cantilever-supported by attachment through Gr/PI load plates to the steel support fixture. The major thrust of the TDS NASTRAN analysis was to predict the deflection and strain during the static tests.

The TDS NASTRAN model has over 1,000 nodes and is highly refined along one rib where much of the test instrumentation is located. The cover panels are represented by QUAD1 and TRIA1 bending/membrane plate elements, which are specialized for orthotropic honeycomb sandwich panels. That is, the bending, membrane and transverse shear properties can be defined independently. The cover panels are not continuous structures. They comprise two segments: a main cover section extending from the rear spar to the front spar and a separate leading edge section extending from the front spar to the leading edge. This cover panel discontinuity is modeled by a refined mesh in which the QUAD1 elements are given reduced stiffness properties.

RIB 1
11.21 KN
(2520 LB)

RIB 2
2.49 KN
(560 LB)

RIB 3
9.96 KN
(2240 LB)

FRONT
SPAR

REAR
SPAR

COVER
PANELS

14.7 KN
(3324 LB)

ENDS FIXED
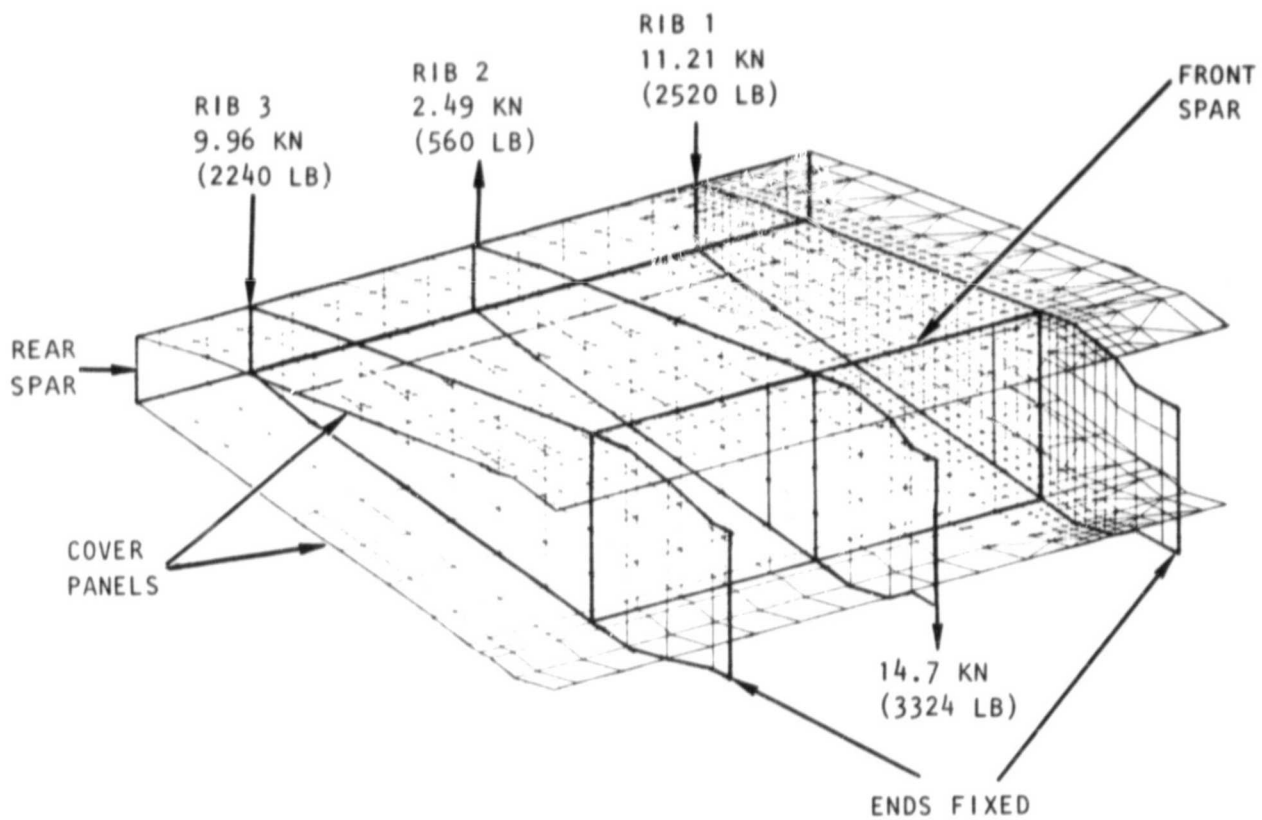
Figure B-1. Technology Demonstration Segment Nastran Finite Element Model

Table B-1. Typical Mechanical Properties of Selected Celion 3000/LARC-160 Laminates

Material Property	Laminate Orientation											
	|0/±45/90|				|0₂/±45/0|				|0/±45|			
	-168°C (-270°F)	RT	204°C (400°F)	316°C (600°F)	-168°C (-270°F)	RT	204°C (400°F)	316°C (600°F)	-168°C	RT	204°C (400°F)	316°C (600°F)
E^T_{11} GPa (Msi)	57.2 (8.3)	54.5 (7.9)	53.8 (7.8)	54.5 (7.9)	95.8 (13.9)	93.1 (13.5)	91.7 (13.3)	91.7 (13.3)	65.5 (9.5)	60.7 (8.8)	59.3 (8.6)	57.9 (8.4)
E^T_{22} GPa (Msi)	57.2 (8.3)	54.5 (7.9)	53.8 (7.8)	54.5 (7.9)	22.7 (3.3)	22.1 (3.2)	18.6 (2.7)	17.2 (2.5)	26.9 (3.9)	26.2 (3.8)	25.5 (3.7)	24.1 (3.5)
E^C_{11} GPa (Msi)	60.0 (8.7)	58.6 (8.5)	57.2 (8.3)	58.6 (8.5)	91.7 (13.3)	91.7 (13.3)	88.2 (12.8)	84.1 (12.2)	81.4 (11.8)	75.8 (11.0)	64.8 (9.4)	63.4 (9.2)
E^C_{22} GPa (Msi)	60.0 (8.7)	58.6 (8.5)	57.2 (8.3)	58.6 (8.5)	22.7 (3.3)	21.4 (3.1)	17.9 (2.6)	16.5 (2.4)	27.6 (4.0)	26.2 (3.8)	24.1 (3.5)	22.8 (3.3)
G_{12} GPa (Msi)	20.0 (2.9)	19.3 (2.8)	19.3 (2.8)	18.6 (2.7)	18.6 (2.7)	17.9 (2.6)	17.9 (2.6)	17.2 (2.5)	22.8 (3.3)	22.1 (3.2)	22.8 (3.3)	23.4 (3.4)
ν_{12}	0.32	0.31	0.31	0.30	0.652	0.655	0.658	0.64	0.72	0.71	0.70	0.70
ν_{21}	0.32	0.31	0.31	0.30	0.141	0.136	0.134	0.124	0.30	0.30	0.30	0.29
F^{TU}_{11} MPa (ksi)	554.3 (80.4)	592.2 (85.9)	605.3 (87.8)	576.4 (83.6)	937.6 (136)	1034.1 (150)	889.4 (129)	979.0 (142)	689.4 (100)	710.. (103)	689.4 (100)	663.2 (96.2)
F^{TU}_{22} MPa (ksi)	554.3 (80.4)	592.2 (85.9)	605.3 (87.8)	576.4 (83.6)	208.9 (30.3)	215.8 (31.3)	230.3 (33.4)	197.2 (28.6)	283.4 (41.1)	261.3 (37.9)	237.2 (34.4)	200.0 (29.0)
F^{CU}_{11} MPa (ksi)	689.4 (100.0)	597.1 (86.6)	514.3 (74.6)	464.0 (67.3)	1075.5 (156)	1013.5 (147)	730.8 (106)	566.0 (82.1)	730.8 (106)	710.1 (103)	481.2 (69.8)	437.1 (63.4)
F^{CU}_{22} MPa (ksi)	689.4 (100.0)	597.1 (86.6)	216.3 (74.6)	464.0 (67.3)	291.6 (42.3)	284.0 (41.2)	255.1 (37.0)	224.1 (32.5)	337.1 (48.9)	352.3 (51.1)	264.1 (38.3)	241.3 (35.0)
F^{SU}	310.2 (45)	227.5 (33)	220.6 (32)	206.8 (30)	275.8 (40)	220.6 (32)	213.7 (31)	206.8 (30)	344.7 (50)	310.2 (45)	262.0 (38)	241.3 (35)
α_{11} μcm/cm°C (μin./in.-°F)		1.667 (1.078)				0.453 (0.252)				0.5 (0.277)		
α_{22} μcm/cm-°C (μin./in.-°F)		1.667 (1.078)				8.86 (4.922)				4.55 (2.527)		

Each stability rib utilizes QDMEM1 elements to model the shear web and BAR elements to idealize the upper and lower rib caps. The QDMEM1 elements are quadrilateral membrane elements based on linearly varying strain shape functions. The centroids of the rib caps do not coincide with the midplane of the cover panels, where the grid points are located. Therefore, the BAR elements are given offsets from the honeycomb covers. The front and rear spars are modeled similar to the stability ribs; i.e., QDMEM1 elements are used for the webs, and offset BAR elements are used for the upper and lower caps.

The forward support area, which has two thick Gr/PI plates connected to the steel test fixture, is modeled by QUAD2 plate elements.

The materials properties used in the TDS NASTRAN model are given in Table B-1. These properties were derived from References B-1 through B-5. The analysis was found to be sensitive to the laminate mechanical properties. However, the available literature shows considerable variation in the reported properties. For example, the tensile modulus for an isotropic (0/±45/90) Celion/LARC-160 laminate has been reported as low as 40.4 GPa (6.0 Msi) and as high as 64.0 GPa (9.5 Msi). Test variables include specimen type (beam or coupon), instrumentation type (strain gage or extensometer), test type (tension or compression), fiber volume, and number of graphite filaments per tow (3,000 or 6,000). To resolve this problem, a spare stability rib cap was cut into four tensile specimens and tested at room temperature. However, these specimens also showed considerable variation, ranging from 47.8 GPa (6.94 Msi) to 57.5 GPa (8.34 Msi). A typical value of 54.5 GPa (7.9 Msi) was used in the analysis, which provided good test data correlation (see Sections 4 and 5). The variation in the stability rib cap properties is probably due to some misalignment of the $0°$ fibers as they are draped over the mold.

APPENDIX B. REFERENCES

B-1. Jones, J.S. Celion/LARC-160 Graphite/Polyimide Composite Processing Techniques and Properties, 14th National SAMPE Technical Conference (October 1982).

B-2. Ehret, R.M., et al. Development of Design Allowables Data for Celion 6000/LARC-160, Graphite/Polyimide Composite Laminates, NASA CR 165985, (November 1982).

B-3. Cashman, J.B. and S.F. McCleskey. Design Allowables Test Program, Celion 3000/PMR-15 and Celion 6000/PMR-15, Graphite/Polyimide Composites, NASA CR 165840 (June 1982).

B-4. Frost, R.K., et al. Development and Demonstration of Manufacturing Processes for Fabricating Graphite/LARC-160 Polyimide Structural Elements, NASA CR 165809 (January 1982).

B-5. Advanced Composites Design Guide. Third Edition, Air Force Flight Dynamics Laboratory, Wright-Patterson Air Force Base, Ohio (January 1977).

APPENDIX C. NONDESTRUCTIVE EVALUATION TECHNIQUES USED IN TDS FABRICATION AND TEST

Nondestructive evaluation (NDE) of the TDS consisted of three phases: an evaluation of the individual components of the subassemblies, i.e., skin panels for honeycomb structure, rib caps, and close-out channels (Phase 1); an evaluation of all subassemblies, i.e., honeycomb panels and ribs (Phase 2); and an evaluation of the completed structure (Phase 3).

C.1 PHASE 1. INSPECTION OF SOLID LAMINATE COMPONENTS

Solid laminate components such as face sheets, rib caps, and closeout channels were inspected under laboratory conditions to sensitivity "A" (see below). The technique used was the pulse-echo method with a reflector plate. A focused 1.27-cm-diameter (1/2-in.), 10-MHz transducer having a focal point, in water of 7.6 cm (3 in.) was focused on the front surface of the test component. The ultrasonic beam penetrated the part, and the echo from the reflector plate returned through the part and was picked up by the transducer. Any anomaly in the part would disrupt the round-trip sound path. Absence of a signal would result in an unrecorded (white area) on the C-scan recording.

C-scan sensitivity is one of the most important variables that must be considered in the quality assessment of laminates and bonded structures. Calibration sensitivity was optimized by fabricating comparative reference standards having internal defects of known type and size and using them for sensitivity settings. At the beginning of the NASA Graphite/Polyimide Design and Fabrication contract (NAS1-15183), personnel at Langley and Rockwell shared sample specimens of Gr/PI laminates having known defects. Ultrasonic C-scans and destructive correlative tests were made by both Langley and Rockwell personnel. Figure C-1 is a sample of the C-scan recording produced for sensitivity "A" on standard EX77.

C.2 PHASE 2. NONDESTRUCTIVE EVALUATION OF SUBASSEMBLIES

Subassemblies such as honeycomb sandwich structure with secondary-bonded components were inspected by the ultrasonic through-transmission technique with use of water squirters. NDE standards were designed for establishing ultrasonic sensitivity for the through-transmission tests. Several panels 15.24 by 15.24 cm (6 by 6 in.), representing particular sections of the composite body flap, were fabricated with built-in defects. The defects were made by including a strip of Teflon tape in the adhesive layer during assembly. The optimum sensitivity and frequency of the ultrasonic through transmission C-scan were then determined, which would show the greatest detail. The same frequency and sensitivity were then used to inspect similar components of a large structure. A typical NDE standard is shown in Figure C-2. A schematic
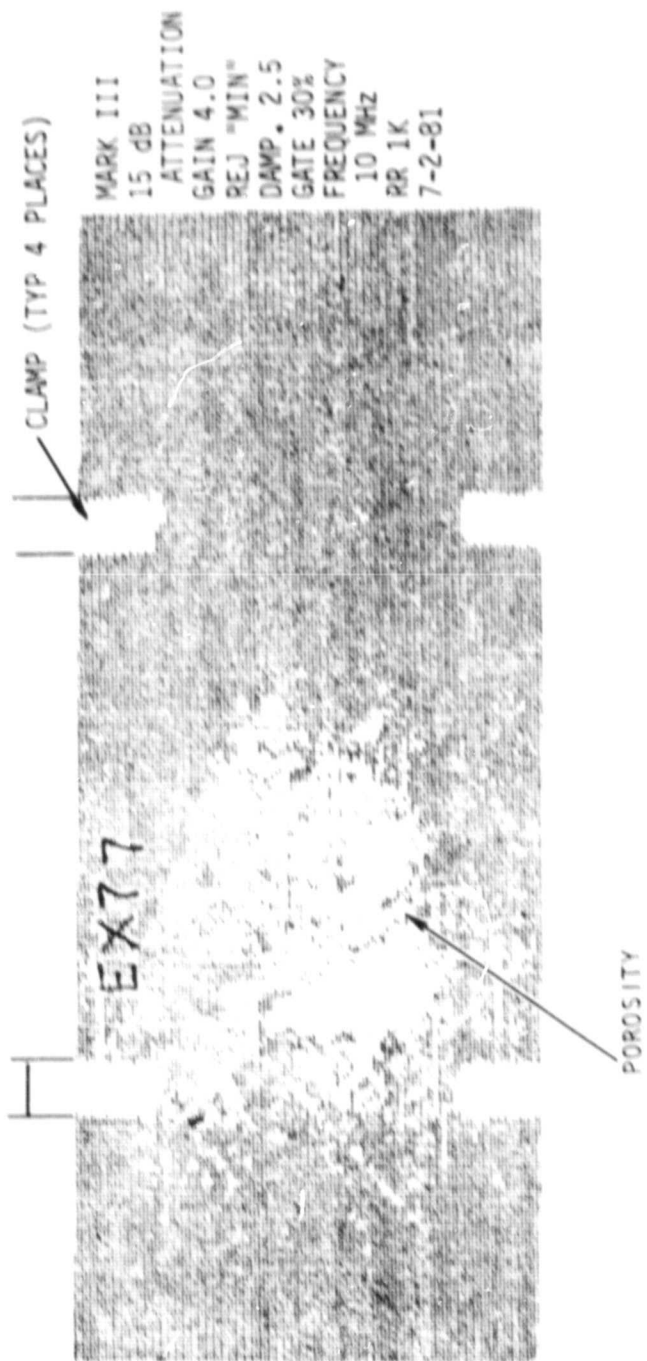
Figure C-1. C-Scan Recording of Solid Laminate Standard EX77
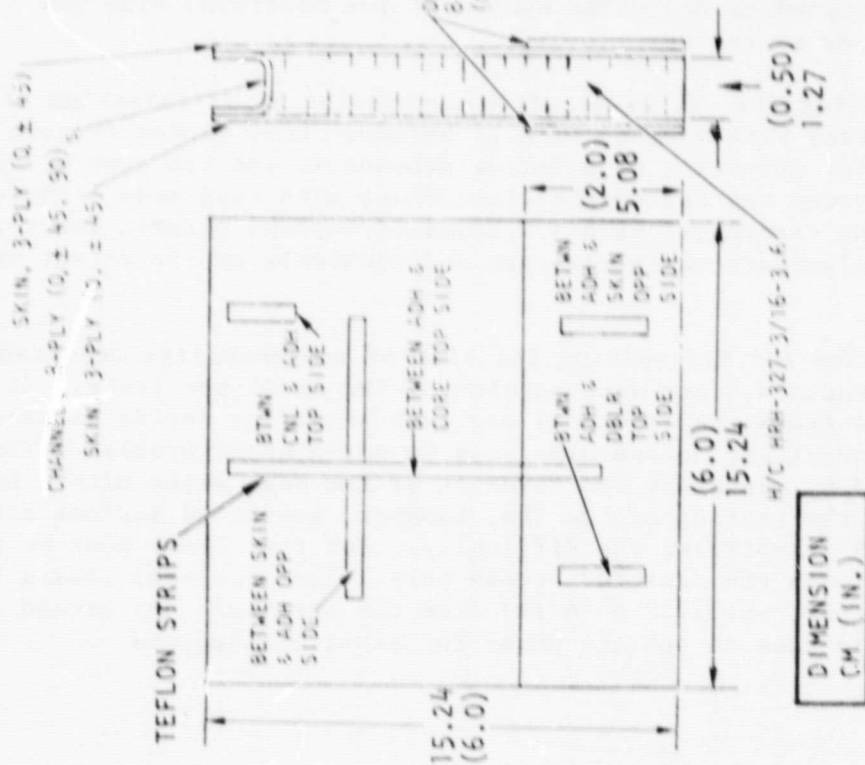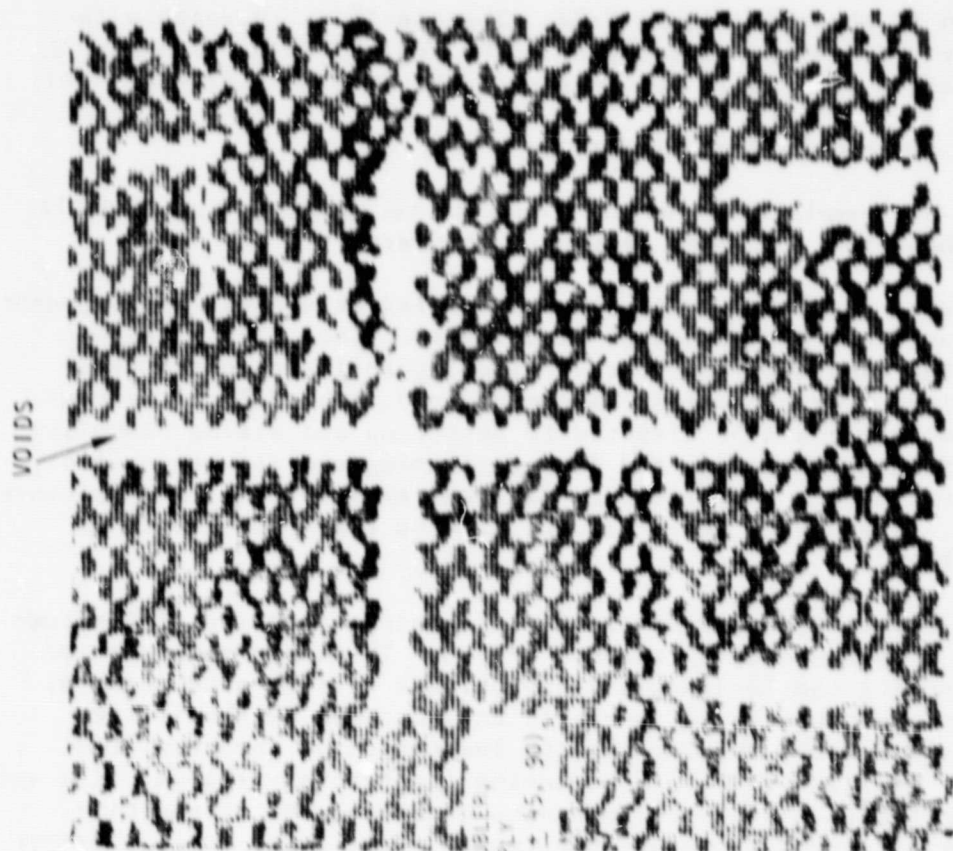
MARK III
15 dB
ATTENUATION
GAIN 4.0
REJ "MIN"
DAMP. 2.5
GATE 30%
FREQUENCY
10 MHz
RR 1K
7-2-81

CLAMP (TYP 4 PLACES)

POROSITY

EX77

Figure C-2. Ultrasonic Inspection Honeycomb Sandwich Standard GP4 - Stability Rib Assembly

103

of NDE specimen GP4 is shown in Figure C-2a. The specimen represents the body flap stability rib design. Locations of the Teflon strips shown in Figure C-2a are readily visible in the C-scan of the specimen (Figure C-2b).

C.3 PHASE 3. NDE OF COMPLETED TDS STRUCTURE

Evaluation of the completed structure required techniques and rationale that differ from those for component testing. They are:

1. The techniques and sensitivity (size anomalies detected) for components of the structure are intended to find imperfections that might be caused by the manufacturing process (i.e., porosity or small voids caused by lay-up or processing discrepancies). The NDE of the completed structure would be directed to detecting and sizing anomalies caused by flexing, heating, and fatigue-testing and structure (i.e., skin-to-core debond, adhesive bond failure, crushed core, and fractured laminates). Inspection would also be used to track the growth of existing flaws.

2. The method for recording results of ultrasonic evaluation of the components is to produce an ultrasonic C-scan. This is a plan view of the part showing the location and approximate size of each anomaly. This C-scan equipment is not portable and, because of the limited access, could not be used for <u>in-situ</u> inspection of the completed structure. If flaws were located during the testing program, size and position information would be needed to determine the propagation effects during subsequent endurance tests. Therefore, special effort had to be directed to designing equipment for obtaining size and position of any anomalies.

The methods selected for detection of any unbonding or delamination of face sheets was sonic testing with a model Mark II harmonic bond tester (Figure C-3). The method selected for detection of adhesive debonds in the rib caps or close-out sections to honeycomb was pulse-echo ultrasonics with hand-scan techniques (Figure C-4). A 5-MHz transducer with a 0.64-cm (1/4-inch) plastic delay shoe was used to detect delaminations in rib caps and closeouts and to detect voids in adhesive bonds.

A method was needed for determining the size of any anomalies detected during NDE of the structure after each portion of the endurance tests. It would be necessary to track the growth of any such anomalies during subsequent testing. Where the areas are accessible, this is not a major problem. The size can be estimated by measuring the movement of the test probe with a hand-held scale. Much of the testing of the TDS, however, presented serious access problems. Figure C-5 illustrates the difficulty. The test probe must be positioned on an area through the depicted access port. The test area toward the trailing edge of the part was 1.22 m (4 ft) from the opening. Any method for sizing the flaws would have to operate under the above limitations.
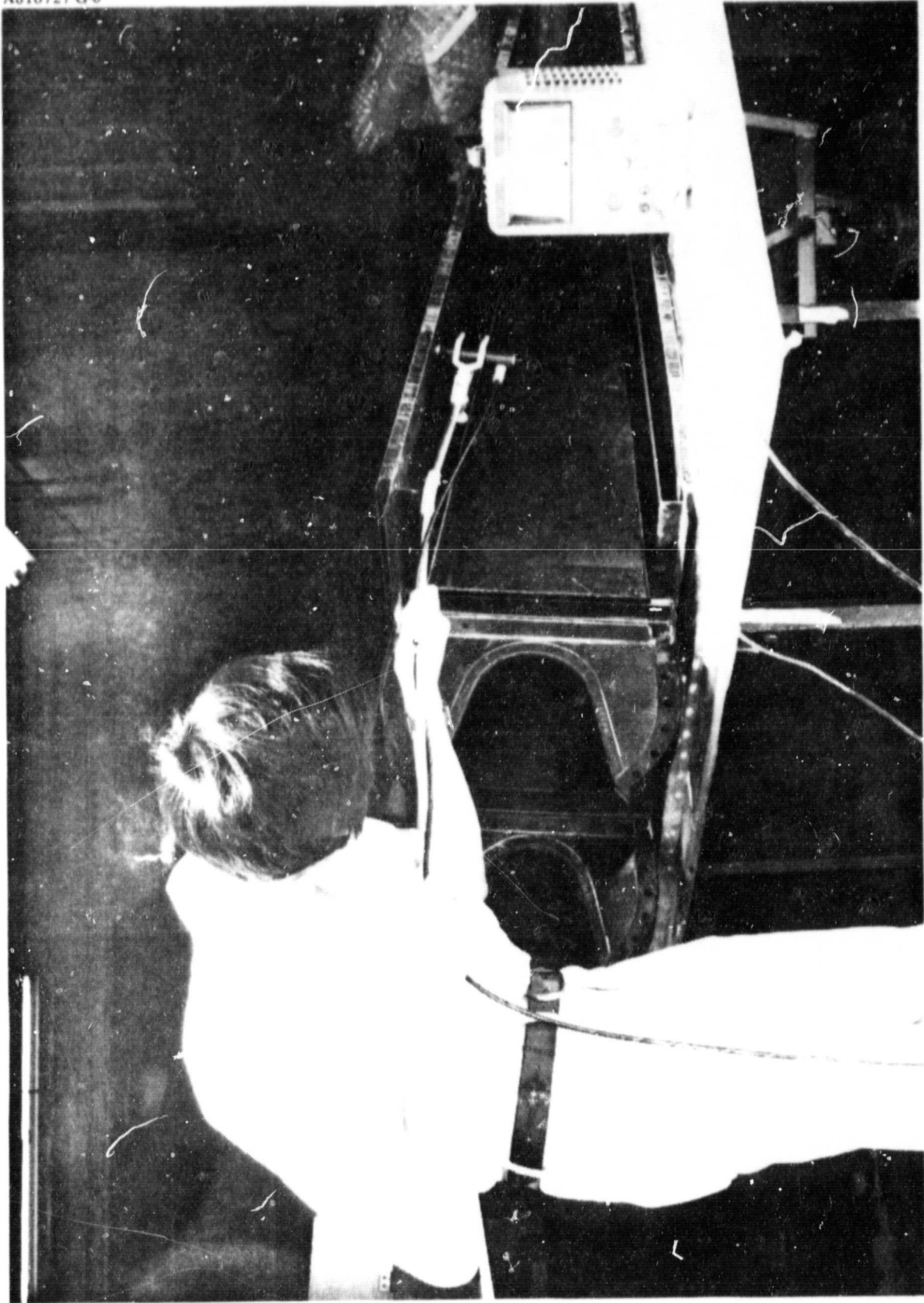
A810727 G-6

Figure C-3. Harmonic Bond Test – Face Sheet to Core Debond

A810727 G-4V
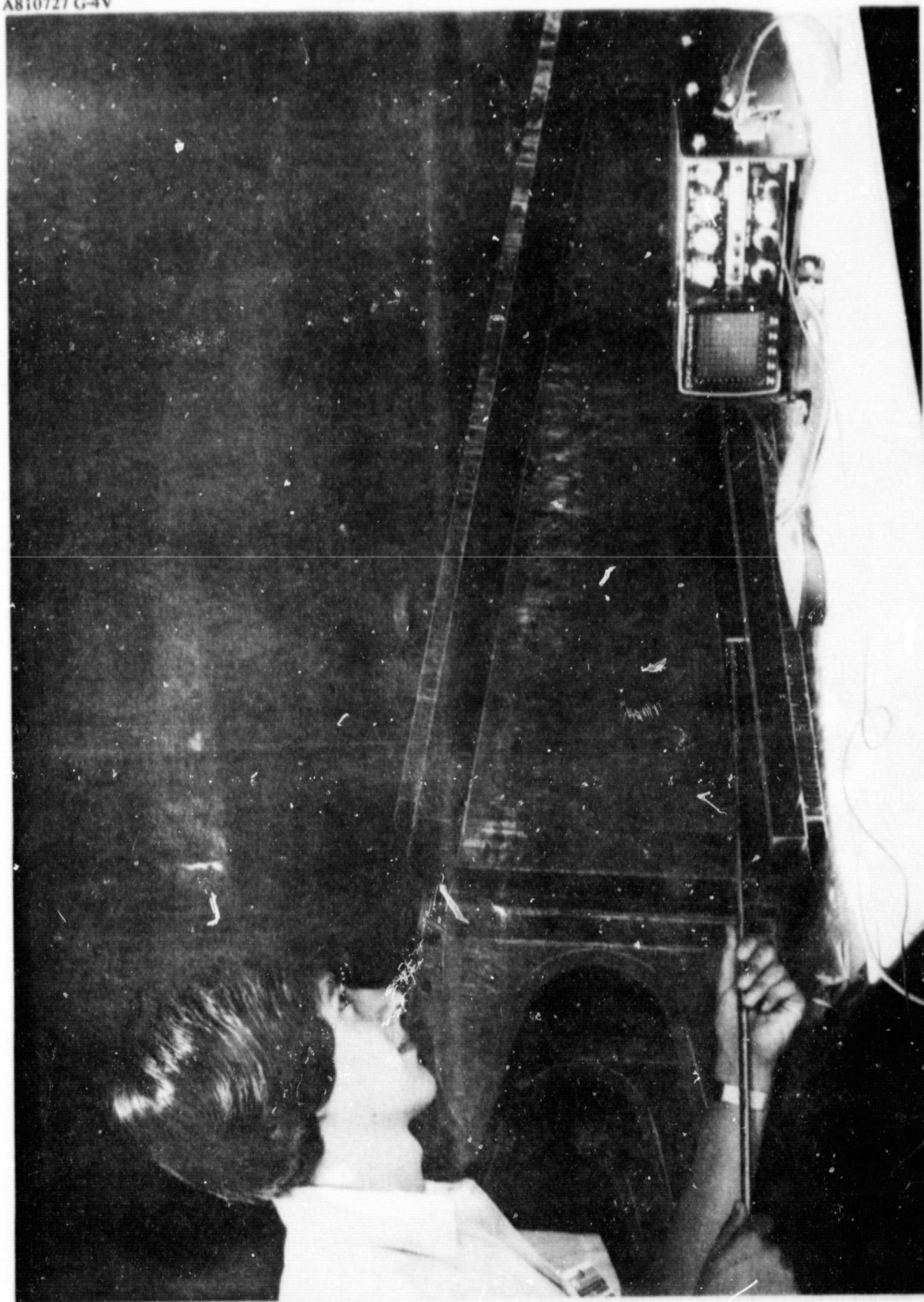
Figure C-4. Ultrasonic Pulse Echo Contact Testing – Rib-to-Cover Adhesive Bond
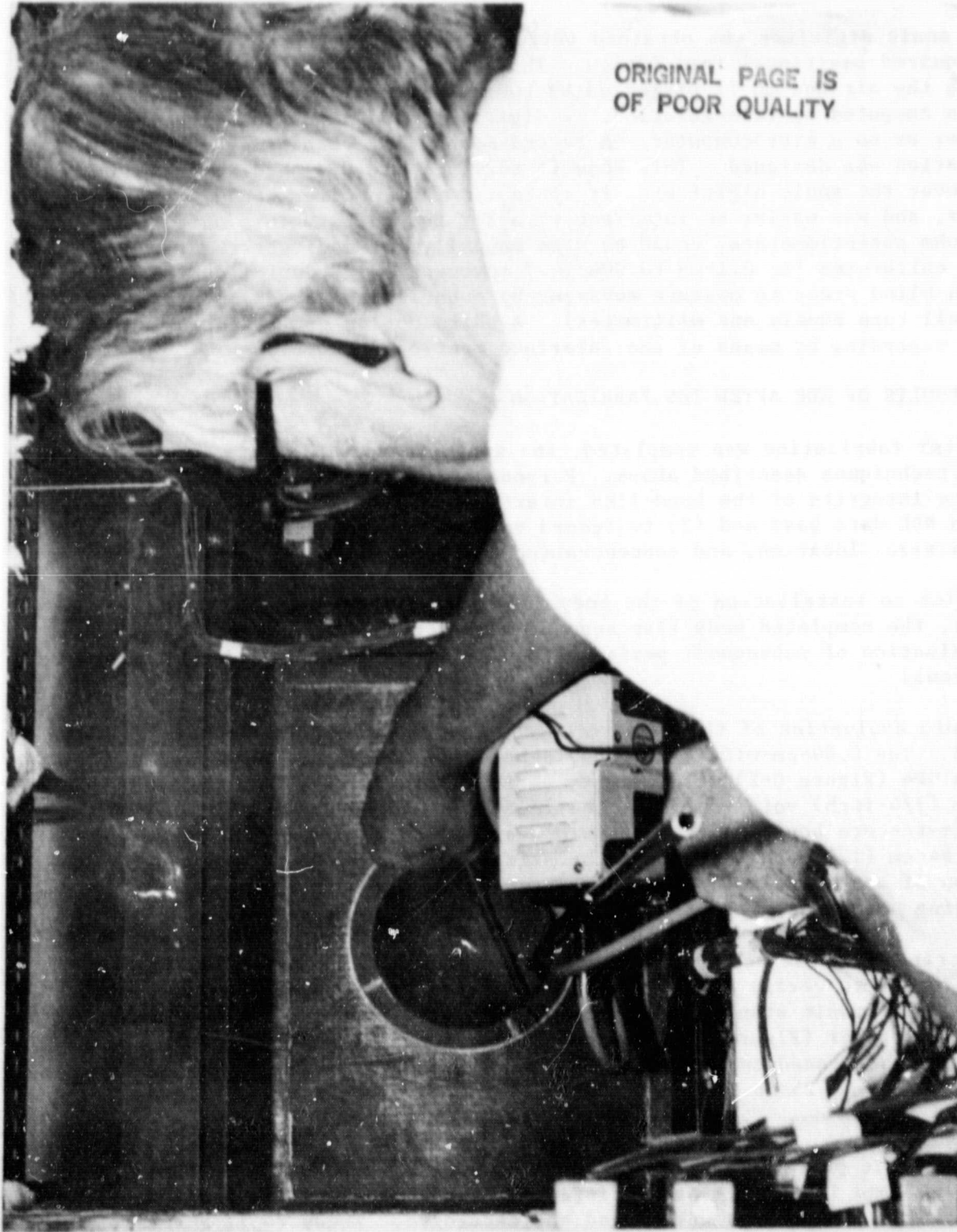
Figure C-5. Access to Interior of TDS for NDE

A sonic digitizer was obtained (Figure C-6) and evaluated for recording the required positional information. This unit sends a ultrasonic signal through the air and it is picked up by two receivers. Position information is then computed by triangulation, is digitized, and input to either an X-Y recorder or to a microcomputer. A second method for obtaining X-Y position information was designed. This Roje fixture (Figure C-7) had several advantages over the sonic digitizer: it could fit into smaller space, it was less complex, and was easier to interface with X-Y recorders. This unit, with two 50-kilohm potentiometers, could be used manually for a direct reading on scales calibrated for 0.1-mm (0.004-in.) movement. The device could also be used in blind areas to measure movement by counting the turns on the pinion (one full turn equals one millimeter). A third option permitted making a C-scan recording by means of the interface mentioned above.

C.4 RESULTS OF NDE AFTER TDS FABRICATION

After fabrication was completed, the graphite/polyimide TDS was inspected by the techniques described above. Purpose of the inspection was (1) to evaluate the integrity of the bond-line interfaces of the TDS structure and establish an NDE data base and (2) to record various parameters of suspect areas such as size, location, and concentration for subsequent analysis.

Prior to installation of the body flap into the environmental test chamber, the completed body flap segment was inspected to provide a data base for evaluation of subsequent periodic inspections. These data base tests were as follows:

Sonic evaluation of the skin-to-core bond was performed as shown in Figure C-3. The 0.64-cm-wide (1/4-inch) debonds in ultrasonic standards GP1 through GP4 (Figure C-2) were used to verify a sensitivity that will detect a 0.64-cm (1/4-inch) void in either the face-sheet-to-adhesive bond or in the adhesive-to-core bond. A grid pattern was used to ensure two passes across each 0.64-cm (1.4-inch) square on the skin surface. A sketch showing the location of any anomalies was made. These data were used as a baseline for evaluating sonic inspections of the body flap segment after each test.

Ultrasonic pulse-echo evaluation of laminates to honeycomb (rib caps, etc.) was performed to verify adhesive bond integrity. The procedure was developed by using ultrasonic standards GP1 through GP4 with a sonic instrument Mark I ultrasonic tester (Figure C-4). Rockwell-developed Gel 3000 was used as a couplant. The transducer was a 10 MHz 1.1-cm-diameter (0.44-in.) transducer with a 0.64-cm (0.25-in.) plastic delay. Results of this inspection are discussed below.

Ultrasonic pulse-echo hand-scan techniques revealed that all rib cap-to-face-sheet bond interfaces had satisfactory bond integrity, even through seven insignificant indications were found and cataloged. These small anomalies were used as references for subsequent inspections to help verify ultrasonic test settings and accuracy of mapping techniques. The Roje transducer fixture

A810722 G-2
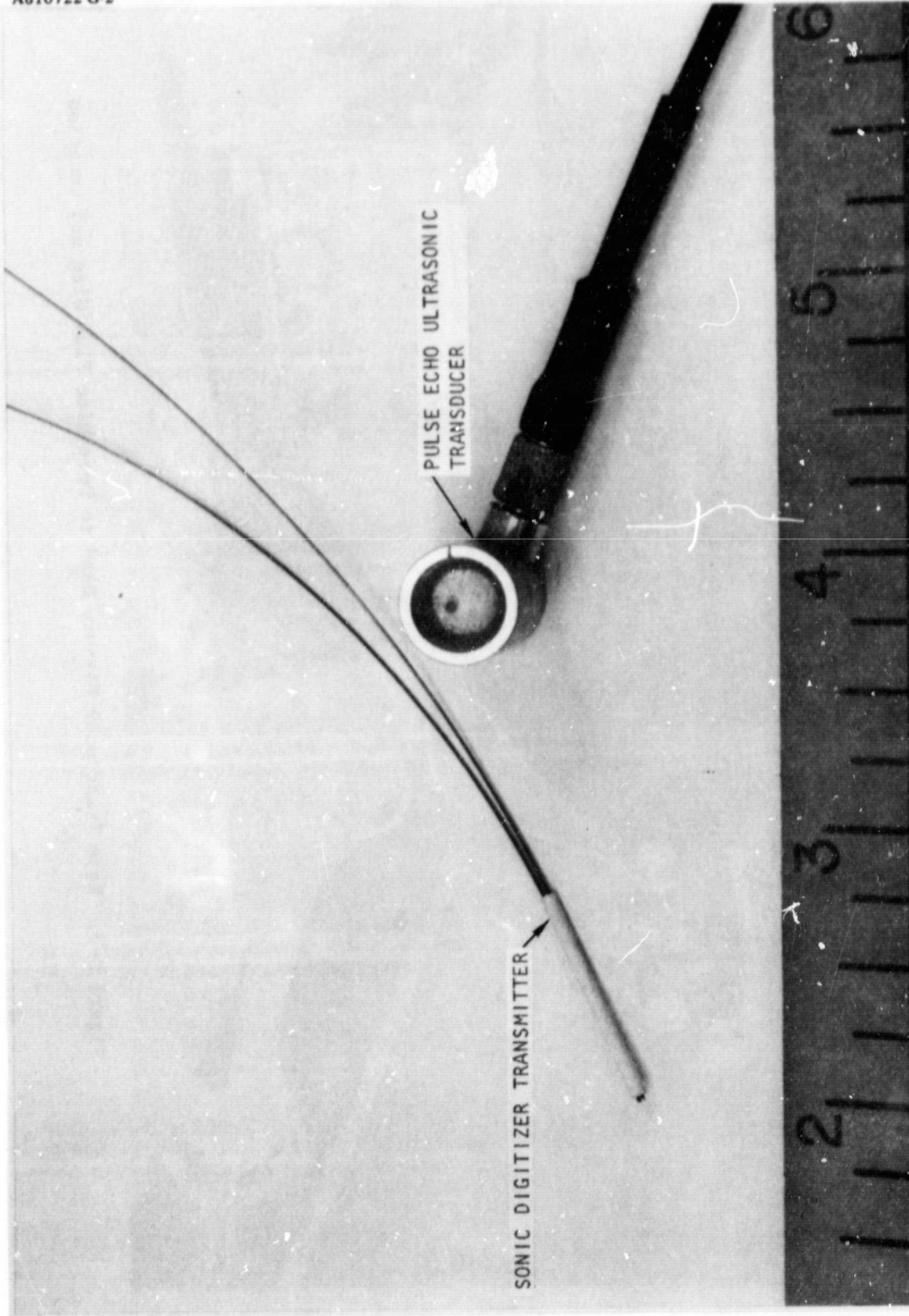
Figure C-6. Sonic Digitizer Transmitter (left) and Pulse
Echo Ultrasonic Transducer

A810727 G-3
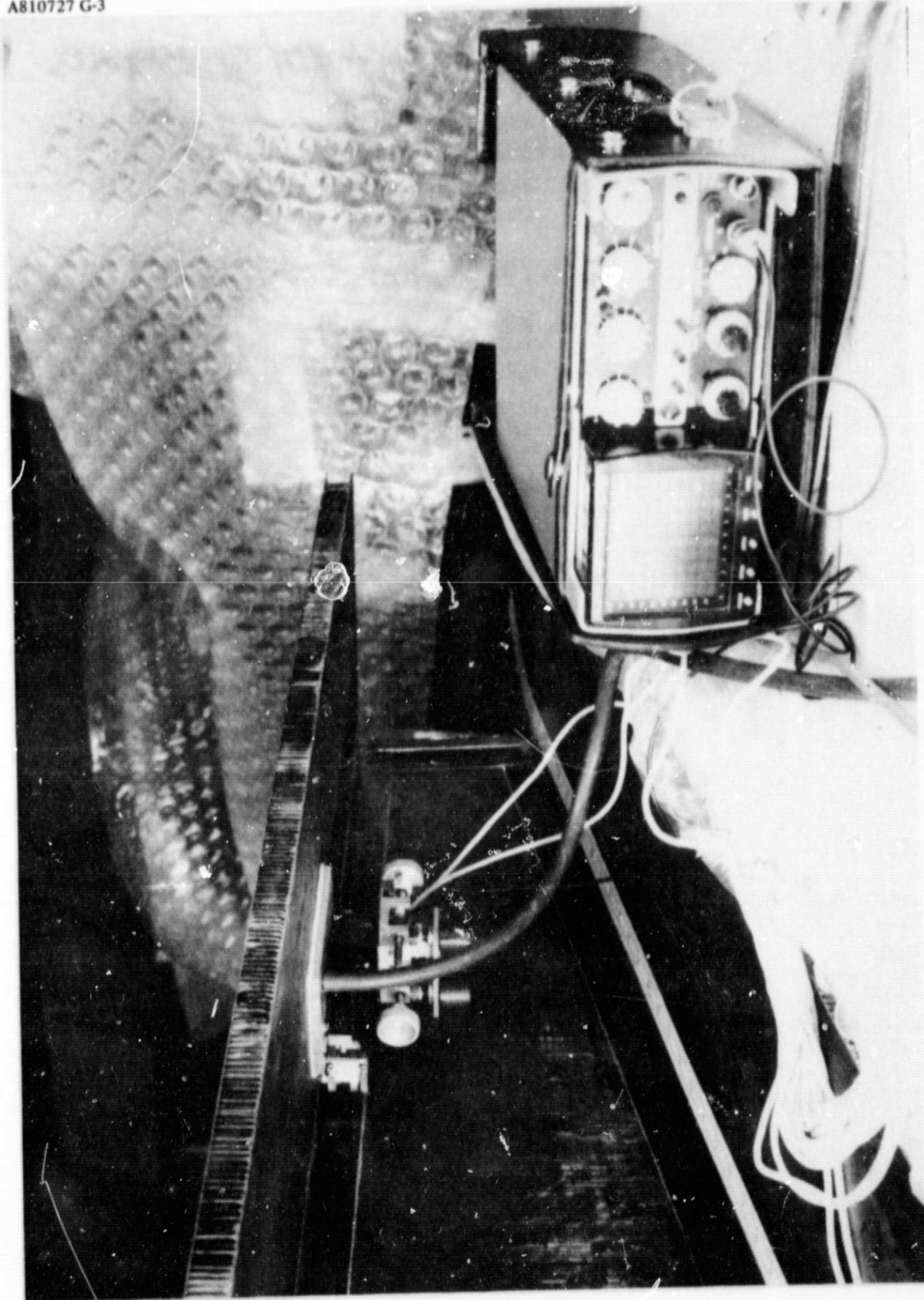
Figure C-7. Roje Transducer Fixture Used to Determine Flaw Size and Location

was used to measure the size of the largest indication, which is located on the left side of the upper cap of rib No. 1, 71 cm (28 in.) aft of the leading edge end of the cap. It measured 0.15 by 0.18 cm (0.059 by 0.069 in.). Any significant indication should measure 0.64 by 0.64 cm (0.25 by 0.25 in.).

Harmonic bond (sonic) inspection revealed that all face-sheet-to-core bond interfaces had satisfactory bond integrity. There are, however, many insignificant pinpoint indications. None of these small anomalies exhibits any readily measurable length or width insofar as any movement of the inspection probe resulted in loss of indication signal. All sonic indications, however, were mapped by marking each location on the test article and each was traced on paper. These tracings can be used, if needed, to correlate with any significant indications that may develop after subsequent physical testing.

C.5 NDE RESULTS SUBSEQUENT TO EACH STRUCTURAL TEST

The TDS article was subjected to rigorous NDE after each structural test, (1) room-temperature mechanical load test, (2) elevated temperature mechanical load test, (3) simulated fatigue test, (4) thermal cycle test, and (5) elevated temperature mechanical load test.

For each NDE, a thorough visual examination was made to verify absence of surface blisters, cracked skin, or distortion of structural members. When direct visual examination was restricted by instrumentation lines or test fixtures, a flexible fiber optics unit was employed.

Ultrasonics and sonics inspection were performed as described earlier, and the reported results define no deviations from the baseline NDE results.

APPENDIX D. TECHNOLOGY DEMONSTRATION SEGMENT THERMAL MATH MODELS

The thermal math models described below were used to perform the data correlation for the thermal cycling test (Section 7). The thermal math models (TMM) of the TDS were constructed by modeling core sections through the TDS at selected locations. The one-dimensional cover-to-cover thermal math model is a cross section between ribs. The geometry is shown in Figure D-1 with the TMM components listed in Table D-1. The two-dimensional "cover-rib-cover" model is a core section through a stability rib. Because of thermal symmetry, only half of the stability rib core section was modeled. Figure D-2 shows the TMM network. Its components are listed in Table D-2.

Although the cover-to-cover TMM is simple, it takes into account radiative exchange between the inner-most cover face sheets (nodes 2 and 4). In the honeycomb, the modes of heat transfer considered were thermal radiation between cover face sheets, conduction through the honeycomb itself, and conduction through the intervening gas (usually air) in the honeycomb.

The basic equation used for calculating solid conduction between nodes "i" and "j" was

$$COND_{ij} = \frac{2[K_i(T_i)][K_j(T_j)]V_{ij}W_{ij}}{12\left\{2[K_j(T_j)]l_j + [K_i(T_i)]l_j\right\}}$$

where K_i and K_j were the conductivities of nodes i and j, respectively, V_{ij} W_{ij} defined the conduction area, and l_i and l_j were the conduction path lengths through section i and j, respectively.

For gas conductors, the equation used was

$$COND_{ij} = \frac{K_{air}[(T_i + T_j)/2](1-a)V_{ij}W_{ij}}{l_{core}}$$

where V and W were the same as above, a was the ratio of the honeycomb core to the total cross-sectional area, K_{air} was the conductivity of the air within the honeycomb, and l_{core} was the effective path length through the core.

Radiation in both models was calculated by using the overall interchange factor (F_{ij}) defined in the equation:

$$F_{ij} = \frac{1}{\left(\frac{1}{e_i} + \frac{1}{e_j}\right) - \left(\frac{2 F_{ij}}{1 + F_{ij}}\right)}$$

113

Table D-1.   Cover-to-Cover Conductor Descriptions

Conductor	Node I	Node J	Description
12	1	2	Gas conduction-cover panel honeycomb
13	1	3	Solid conduction-cover panel face sheet/honeycomb
23	2	3	Solid conduction-cover panel face sheet/honeycomb
28	2	8	Gas conduction-cover panel face sheet/air node
48	4	8	Gas conduction-cover panel face sheet/air node
45	4	5	Gas conduction-cover panel honeycomb
46	4	6	Solid conduction-cover panel face sheet/honeycomb
56	5	6	Solid conduction-cover panel face sheet/honeycomb

NODE	DESCRIPTION
1	UPPER COVER PANEL OUTER FACE SHEET
2	UPPER COVER PANEL INNER FACE SHEET
3	UPPER COVER PANEL HONEYCOMB
4	LOWER COVER PANEL INNER FACE SHEET
5	LOWER COVER PANEL OUTER FACE SHEET
6	LOWER COVER PANEL HONEYCOMB
8	AIR NODE
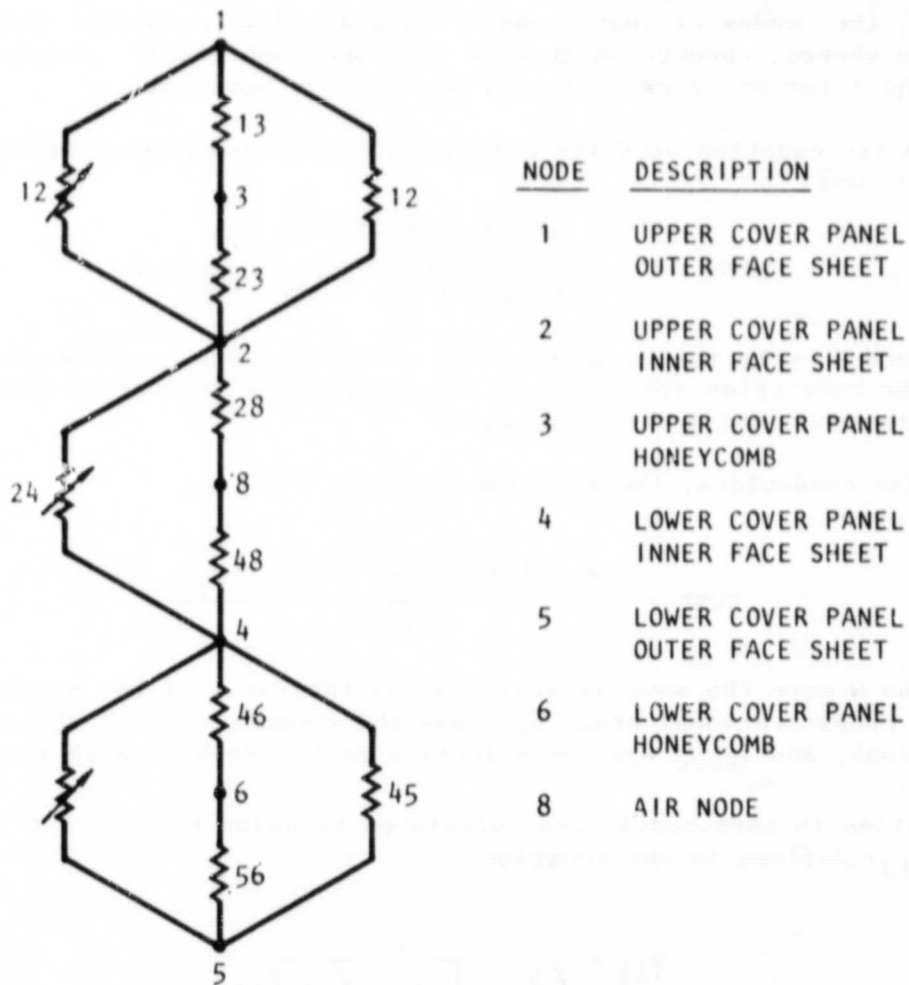
Figure D-1.   Cover-to-Cover Thermal Math Model

114

NODE | DESCRIPTION

1 — UPPER COVER PANEL OUTER FACE SHEET

2 — UPPER COVER PANEL INNER FACE SHEET

3 — UPPER COVER PANEL HONEYCOMB

4 — UPPER CAP PLATE

5 — UPPER ANGLE, DOUBLER AND CHANNEL

6,8,28,48, 38,18,16 — WEB FACE SHEET

50,7,9,29,49, 39,19,17.60 — WEB HONEYCOMB

15 — LOWER ANGLE, DOUBLER AND CHANNEL

14 — LOWER CAP PLATE

13 — LOWER COVER PANEL HONEYCOMB

12 — LOWER COVER PANEL INNER FACE SHEET

11 — LOWER COVER PANEL OUTER FACE SHEET

Figure D-2. Cover-Rib-Cover Thermal Math Model

115

Table D-2. Cover-Rib-Cover Descriptions

Conductor	Node i	Node j	Description
12	1	2	Gas conduction-cover panel honeycomb
13	1	3	Solid conduction-cover panel face sheet/honeycomb
23	2	3	Solid conduction-cover panel face sheet/honeycomb
24	2	4	Solid conduction-face sheet/cap plate
45	4	5	Solid conduction-cap plate/angle, doubler, channel
46	4	6	Solid conduction-cap plate/web face sheet
450	4	50	Solid conduction-cap plate/rib honeycomb
451	4	50	Gas conduction-cap plate/rib honeycomb
56	5	6	Solid conduction-angle, doubler, channel/web face sheet
67	6	7	Solid conduction-web face sheet/honeycomb
68	6	8	Solid conduction-web face sheet
750	7	50	Solid conduction-web honeycomb
751	7	50	Gas conduction-web honeycomb
79	7	9	Solid conduction-web honeycomb
80	7	9	Gas conduction-web honeycomb
89	8	9	Solid conduction-web face sheet/honeycomb
828	8	28	Solid conduction-web face sheet
929	9	29	Solid conduction-web honeycomb
930	9	29	Gas conduction-web honeycomb
2848	28	48	Solid conduction-web face sheet
2829	28	29	Solid conduction-web face sheet/honeycomb
2949	29	49	Solid conduction-web honeycomb
2950	29	49	Gas conduction-web honeycomb
4849	48	49	Solid conduction-web face sheet/honeycomb
3839	38	39	Solid conduction-web face sheet honeycomb
3848	38	48	Solid conduction-web face sheet
3949	39	49	Solid conduction-web honeycomb
3950	39	49	Gas conduction-web honeycomb
1939	19	39	Solid conduction-web honeycomb
1940	19	39	Gas conduction-web honeycomb
1819	18	19	Solid conduction-web face sheet/honeycomb
1838	18	38	Solid conduction-web face sheet
1719	17	19	Solid conduction-web honeycomb
1720	17	19	Gas conduction-web honeycomb
1760	17	60	Solid conduction-web honeycomb
1761	17	60	Gas conduction-web honeycomb
1617	16	17	Solid conduction-web face sheet/honeycomb
1516	15	16	Solid conduction-angle, doubler, channel/web face sheet
1415	14	15	Solid conduction-cap plate/angle, doubler, channel
1416	14	16	Solid conduction-cap plate/web face sheet
1460	14	60	Solid conduction-cap plate/rib honeycomb
1461	14	60	Gas conduction-cap plate/rib honeycomb
1213	12	13	Solid conduction-cover panel face sheet/honeycomb
1214	12	14	Solid conduction-face sheet/cap plate
1112	11	12	Gas conduction-cover panel honeycomb
1113	11	13	Solid conduction-cover panel face sheet/honeycomb

116

where e_i and e_j were the emissivities of nodes i and j, respectively, and F_{ij} was the view factor from node i to node j.

Capacitances of all nodes was calculated using the basic equation of

$$CAP_i + \rho V_i C_p(T_i)$$

where the specific heat (C_p) was a function of temperature and equaled 1.52 grams/cm^3 (0.055 lb/in.^{3}) for the graphite/polyimide face sheets, and was equal to 0.61 grams/cm^3 (0.022 lb/in.^{3}) for the glass/polyimide honeycomb. The material properties used in the TMM are presented in Tables D-3 and D-4. Table D-3 presents the thermal properties of graphite/polyimide; Table D-4 presents the properties of glass/polyimide.

For determining the thermal conductivity of a laminated composite based on unidirectional properties, the following formulas are employed. The conductivity for a single ply "i" at any arbitrary angle "theta" is

$$K_{\theta_i} = K_{0°} \cos^2\theta_i + K_{90°} \sin^2\theta_i$$

The conductivity for any general laminated composite with individual ply thickness "t_i" is

$$K \text{ composite} = \frac{\Sigma K_{\theta_i} t_i}{\Sigma t_i}$$

Table D-3. Thermal Properties of Graphite/Polyimide Used in Thermal Analysis

Temperature °C (°F)	Thermal Conductivity K Parallel		Thermal Conductivity K Transverse		Specific Heat C_P	
	$\frac{Btu}{Hr\ Ft\ °F}$	$\frac{W}{M\ °C}$	$\frac{Btu}{Hr\ Ft\ °F}$	$\frac{W}{M\ °C}$	$\frac{Btu}{Lbm\ °F}$	$\frac{KJ}{Kg\ °C}$
-129 (-200)	6.0	10.38	0.46	0.80	0.08	0.34
-73 (-100)	8.3	14.36	0.50	0.87	0.12	0.50
-18 (0)	10.6	18.35	0.55	0.95	0.16	0.67
38 (100)	12.9	22.32	0.59	1.02	0.20	0.84
93 (200)	15.2	26.31	0.63	1.09	0.22	0.92
149 (300)	17.5	30.29	0.68	1.18	0.25	1.05
204 (400)	19.8	34.27	0.72	1.25	0.28	1.17
260 (500)	22.1	38.25	0.77	1.33	0.30	1.26
316 (600)	22.4	38.77	0.81	1.40	0.33	1.38

Table D-4. Thermal Properties of Glass/Polyimide
Used in Thermal Analysis

Temperature °C (°F)	Thermal Conductivity K Parallel		Thermal Conductivity K Transverse		Specific Heat C_P	
	$\frac{Btu}{Hr\ Ft\ °F}$	$\frac{W}{M°C}$	$\frac{Btu}{Hr\ Ft\ °F}$	$\frac{W}{M°C}$	$\frac{Btu}{Lbm\ °F}$	$\frac{KJ}{K_g °C}$
-129 (-200)	0.09	0.16	0.05	0.09	0.1	0.42
-73 (-100)	0.12	0.21	0.08	0.14	0.17	0.71
-18 (0)	0.155	0.27	0.105	0.18	0.22	0.92
38 (100)	0.183	0.32	0.117	0.20	0.26	1.09
93 (200)	0.210	0.36	0.136	0.24	0.275	1.15
149 (300)	0.238	0.41	0.146	0.25	0.28	1.17
204 (400)	0.265	0.46	0.155	0.27	0.285	1.19
260 (500)	0.280	0.48	0.162	0.28	0.288	1.20
316 (600)	0.300	0.52	0.169	0.29	0.29	1.21